3-22-2007

Design of a Rear-Wheel After-Market Suspension System for Manual Wheelchairs

Rick Daniel Bierworth
University of South Florida

Design of a Rear-Wheel After-Market Suspension System for Manual Wheelchairs

by

Rick Daniel Bierworth

A thesis submitted in partial fulfillment
of the requirements for the degree of
Master of Science in Mechanical Engineering
College of Mechanical Engineering
University of South Florida

Major Professor: Stuart Wilkinson, Ph.D.
Nathan Crane, Ph.D.
Craig Lusk, Ph.D.

Date of Approval
March 22, 2007

Keywords: Disabled Mobility, Modified Wheel, Shock Reduction, Vibration Reduction, Finite Element Analysis

Table of Contents

List of Figures iii

List of Nomenclature vii

Abstract viii

1. Introduction 1

2. Suspension Wheelchair Technology 3
    2.1 Current Suspension Designs 3
        2.1.1 Elastomers 5
        2.1.2 Steel Springs 6
        2.1.3 Composite Springs 9

3. Structural Failure of Wheelchairs 12
    3.1 Failure of Non-Suspension Wheelchairs 12
    3.2 Failure of Suspension Wheelchairs 14

4. After-Market Suspension for Wheelchair 19
    4.1 Design Process 20
    4.2 Materials Used 25

5. Finite Element Analysis (FEA) 28
    5.1 Setting Up the FEA Models 30
    5.2 Simulation of the Fork 33
    5.3 Simulation of the Inner Hub and Pin 34
    5.4 Simulation of the Inner Hub and the 4'' Ball Bearings 42
    5.5 Simulation of the Outer Hub and the Spokes 44

6. FEA Results 46
    6.1 Fork and Bolt Results 47
    6.2 Inner Hub and Pin Results 51
    6.3 Inner Hub and Ball Bearing Results 53
    6.4 Outer Hub and the Spokes Results 56

7. Prototype 58
7.1 Machining and Assembly Process 58
7.2 Wheelchair Testing - Modifications 59
7.2.1 Wheel Wobble 59
7.2.2 Polyurethane Issues 61

8. Conclusions 66

References 67

Appendices 69
Appendix A: Detailed Drawings of the Fork, Inner Hub, and Outer Hub 70
Appendix B: Rubber and Foam Chart From McMaster-Carr 77
Appendix C: Fork and Bolt Analysis – 20 Degree Camber 78
Appendix D: Fork and Bolt Analysis – 3 Degree Camber 89
Appendix E: Inner Hub and Pin Analysis – 3 Degrees Camber 101
Appendix F: Inner Hub and Pin Analysis – 3 Degree Camber – With Local Mesh Refinement 114
Appendix G: Inner Hub and Pin Analysis – 20 Degrees Camber 128
Appendix H: Inner Hub and Pin Analysis – 6 Degrees Camber 141
Appendix I: Inner Hub and Ball Bearing Analysis 154
Appendix J: Outer Hub and Spoke Analysis 165

List of Figures

Figure 1: Non-Suspension "Rigid Mount" of the Rear Wheels on a Wheelchair 3

Figure 2: "Frog Legs"™ Suspension for Caster Wheels 4

Figure 3: Suspension on an Invacare A6-S™ 5

Figure 4: Coil Compression Spring Suspension of a Quickie XTR™ 7

Figure 5: Tension Spring Suspension of a Permobil Colours Boing™ 8

Figure 6: Composite Spring Suspension System Mounted on a Rigid Frame Wheelchair 9

Figure 7: Failure of the Right Castor Pin of the Permobile Colours Boing™ Chairs 14

Figure 8: Failure of the Telescoping Tube on the Invacare A-6S™, Chair 1 and 3 15

Figure 9: Failure of the Invacare A-6S™ Along the Frame of Chair 2 16

Figure 10: Failure of Quickie XTR™ Chair 1, Where the Mount is Welded to the Frame 16

Figure 11: Failure of the Right Caster Mount on the Quickie XTR™ Chair 3 17

Figure 12: Regular Wheelchair Wheel 20

Figure 13: Color Code for Wheel Suspension 21

Figure 14: Assembly of the Inner Hub, Outer Hub, and Ball-Race Bearings 22

Figure 15: Assembly of Needle Roller Bearing and Fork 23

Figure 16: Assembly of Fork and 3/8'' Pin 24

Figure 17: Assembly of Bolt and Set Screw 24

Figure 18: Urethane Rubber (Green), Which Reduces the Shock Loads and Vibrations That Are Transmitted to the User 25

Figure 19: Free-Body Diagram of the Wheelchair 32

Figure 20: FEA Model of the Fork and Bolt 33

Figure 21: First Model of Interaction Between the Inner Hub and the Pin/Needle Roller Bearing 34

Figure 22: The Constraints Applied to the First Model 35

Figure 23: The Contact Areas of the First Model, and the Applied Loads 36

Figure 24: Second FEA Model of the Inner Hub 37

Figure 25: Third (Simplified) Model – Inner Hub and Pin Only 38

Figure 26: Third Model - Translational and Rotational Constraints 39

Figure 27: Third Model - Contact Areas Between Inner Hub and Pin 40

Figure 28: Third Model - Transverse Load Applied to the Lower Extension, Which Represents the Rim of the Wheel 41

Figure 29: FEA Model of the Inner Hub, Cut in Half 42

Figure 30: The Load that the Ball-Race Bearings Transmit to the Inner Hub is Depicted by the Red Arrows 43

Figure 31: FEA Model of the Outer Hub and Spoke Analysis 44

Figure 32: The Model Was Cut in Half and a Symmetric Constraint Was Applied to the Cut Surface 45

Figure 33: The Max Von-Mises Stress of 33,040 psi, for the 3 Degree Camber Fork and Bolt Analysis 48

Figure 34: Convergence Graphs 50

Figure 35: Close-up of the Max Von-Mises Stress of 31,455 psi for the Inner Hub and Pin Analysis..... 53

Figure 36: The Max Von-Mises Stress of 20,380 psi, for the Inner Hub and Ball Bearing Analysis Legend Values Are Set Between 2,040 psi and 18,340 psi 54

Figure 37: Using a Range of 0 to 40,000 psi for the Legend, the Stress Contour Shows that the Inner Hub Experiences Very Little Stress..... 55

Figure 38: The Max Von-Mises Stress of 37,231 psi, for the Outer Hub Spoke Hole Analysis, is Located at the Top of the Upper Spoke Hole..... 57

Figure 39: Over-all Von-Mises Stress Contour for the Outer Hub Analysis..... 57

Figure 40: Inner Hub Re-Design - With Hardened Stainless Steel Bushing, and a Second Cut-Out for the Silicone Rubber 60

Figure 41: Fork Re-Design - Needle Roller Bearings are Inserted Into Either Side of the Fork..... 60

Figure 42: The Polyurethane Causes the Fork to Rotate Upward When there is No One in the Wheelchair..... 61

Figure 43: Suspension System with Someone Sitting in the Wheelchair..... 62

Figure 44: Re-Designed Suspension System 63

Figure 45: Overall Picture of After-Market Suspension System..... 64

Figure 46: After-Market Suspension System on Author's Wheelchair..... 65

Figure 47: Fork Drawing– Isometric View..... 70

Figure 48: Fork Drawing– Front View 71

Figure 49: Fork Drawing– Top View 71

Figure 50: Inner Hub Drawing– Isometric View..... 72

Figure 51: Inner Hub Drawing– Front View 73

Figure 52: Inner Hub Drawing– Side View 73

Figure 53: Outer Hub Drawing– Isometric View 74

Figure 54: Outer Hub Drawing– Front View 75

Figure 55: Outer Hub Drawing– Side View 76

Figure 56: Outer Hub Drawing– Top View 76

Figure 57: Comparison of Rubber and Foam Chart 77

List of Nomenclature

h	Height
P	Dynamic Load
W	Static Load
δ_m	Dynamic Deflection
δ_s	Static Deflection

Design of a Rear-Wheel After-Market Suspension System for Manual Wheelchairs

Rick Daniel Bierworth

ABSTRACT

The objective of this study was to design and build an after-market suspension for the rear wheels of a manual wheelchair. Suspension for wheelchairs is important because it has been reported that the International Organization for Standards' requirements for vibration loads on wheelchair users (ISO 2631-1), are not meet by today's standard wheelchairs. Today's wheelchairs need to be able to absorb everyday shock loads, thereby minimizing the energy transmitted to the user.

The chosen design is based around the concept of adding shock reduction material between the hub of the wheel, and the axel bolt that connects the wheel to the frame of the chair. The approach taken was to design a suspension system that resides between an oversized wheel bearing, and the axle. To do this, ball-race bearings with an inner diameter of 4" were chosen, and polyurethane rubber was used as the shock absorbing material.

Pro-Mechanica, a finite element analysis program, was used to analyze the suspension system. Since the most common camber/tilt for wheelchair wheels is three degrees from the vertical, the anticipated loads were applied to the wheel at this angle. A prototype of the suspension system was constructed to verify that the design would work, but no tests were performed on it.

This analysis showed that the suspension system should not fail when subjected to 10 times the static load. This load was considered large enough to encompass the forces that a wheelchair chair wheel is typically subjected to. There is room for further work in the area of weight reduction, and in the use of the suspension system on steeper wheel cambers.

1. Introduction

Up until modern times, wheelchairs were typically made primarily from wood, but in the 1930's, Everest and Jennings made the first steel wheelchair. After World War II, veterans were given this one size fits all (depot) wheelchair, the kind typically used by hospitals, airports, and nursing homes today. They were not designed for optimum performance, but were simply meant to allow an individual to be moved from place to place. These generic wheelchairs are not suitable for active wheelchair users, who need a light-weight, custom fit wheelchair. In the 1970's, wheelchair users started to modify their own chairs, and the concept of light-weight, and ultra-light-weight adjustable wheelchairs was born [1].

Today, over 20 million people use a wheelchair as their primary source of mobility [1]. Wheelchair users that are more active need a chair that is not only light-weight, but is also able to decrease the shock and vibration loads that are transmitted to the user. Studies have shown that the human body is unable to absorb these repeated shock loads, which cause increased pain, and also increases the chance of secondary spinal cord injury. It has also been reported that the International Organization for Standards' requirements for vibration loads on wheelchair users, (ISO 2631-1), are not meet by today's standard wheelchairs [2]. The same way in which a modern car is designed to absorb a majority of the energy resulting from pot holes, speed bumps and

debris, today's wheelchairs need to be able to absorb everyday shock loads, thereby minimizing the energy transmitted to the user.

2. Suspension Wheelchair Technology

On non-suspension wheelchairs, both the rear wheels and the castor wheels of the chair are mounted rigidly to the frame. Figure 1 shows the typical mounting of the rear wheels of a wheelchair. The shock loads are transmitted directly from the wheel to the frame of the chair.

Figure 1: Non-Suspension "Rigid Mount" of the Rear Wheels on a Wheelchair

2.1 Current Suspension Designs

Suspension can be added to the rear wheels, the castor wheels, or both. Three common methods used to achieve this include using elastomers, springs, and spring / damper combinations [2]. "Frog Legs" ™, a product that is currently on the market,

provides after-marker suspension for the castor wheels by using an elastomer damper to decrease the vibration and shock transmitted from the ground to the wheelchair and user. The elastomer that they use for their suspension is polyurethane with a 60 shore-A durometer. On their website, "Frog Legs"™ claims that 80% of a wheelchair's vibrations come through the front castors [3]. This shows how important castor fork suspension is for the active wheelchair user. Figure 2 below shows a picture of the "Frog Legs"™ suspension system, which replaces the factory installed castor wheels by retrofit. The arrow on the left is pointing to the black polyurethane that is used to absorb the shock and vibration forces.

Figure 2: "Frog Legs"™ Suspension for Caster Wheels

Suspension is also added to wheelchairs through rear-wheel suspension. At the time of this research, no after-market suspension was available to the rear wheels of a

manual wheelchair. The suspension chairs available had the suspension incorporated into their design. Within the category of rear suspension wheelchairs, there are typically two design styles: the use of elastomers, and the use steel springs. Composite springs have also been used for wheelchair suspension.

2.1.1 Elastomers

A rear suspension wheelchair that uses elastomers as a shock absorber is the Invacare A6-S™, which is shown in Figure 3. This system absorbs the shock and damps the system at the same time, effectively replacing a spring and damper with a single element.

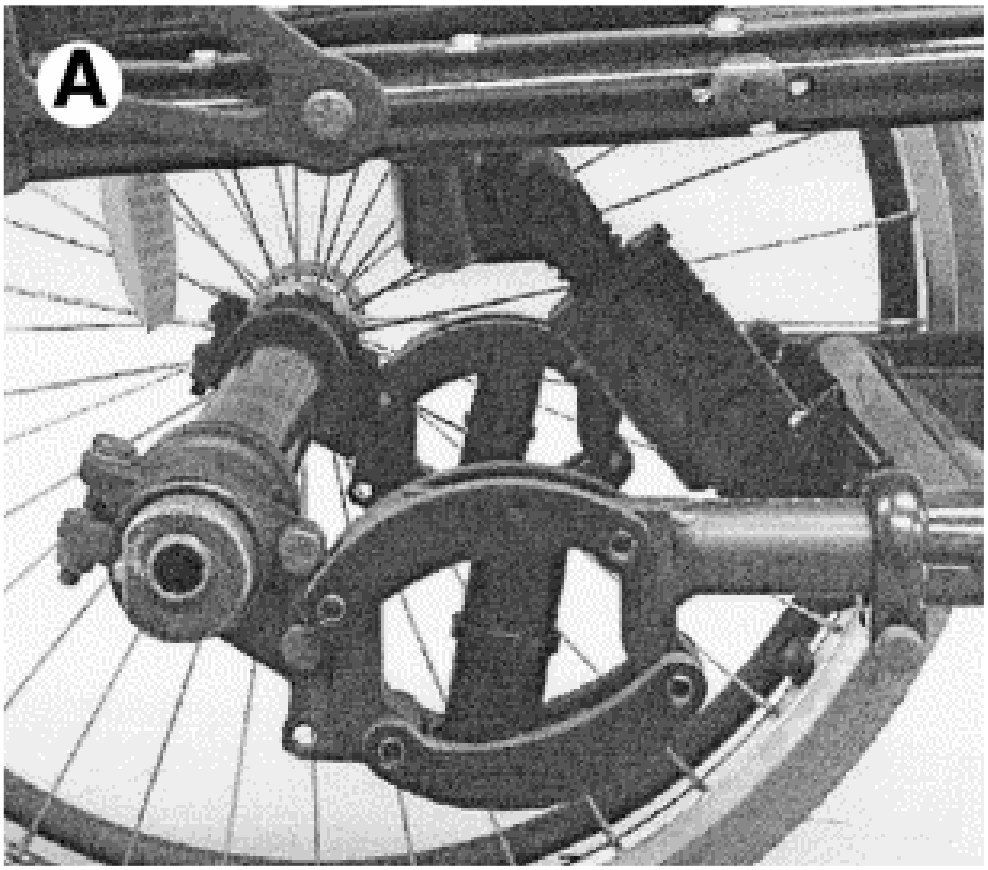

Figure 3: Suspension on an Invacare A6-S™

Low damping elastomers are used for shock absorption because they quickly recover the energy that it took to deform them. They also help to damp out unwanted oscillations. An elastomer is able to behave in this manner due to the arrangement of its molecules. They have long polymer chains that are made up of many carbon atoms. Various other atoms, like hydrogen, nitrogen, chlorine, etc., are then linked to the chain. The bonds within the chain are very strong, but the bonds connecting all the chains together are considerably weaker. To enable the chains to return to their original position after a load is applied and then removed, the polymer has to be cured, during which strong bonds are made between chains at various points. The curing process can only be done once, therefore, the rubber can not be recycled [4].

When designing with polymers, consideration has to be made as to how they will interact with their surroundings. Polymers are adversely affected by oil, UV radiation, strongly oxidizing environments, and various chemicals. They tend to creep at room temperatures, and to be brittle at low temperatures. However, most polymers resist water, acids, and alkalis. When carbon black is added to them, polymers obtain protection from UV rays. To add a degree of chemical stability, some of the hydrogen molecules are replaced with chlorine or fluorine molecules. Polymers also provide excellent electrical resistance [4].

2.1.2 Steel Springs

The Quickie XTR™, shown in Figure 4, uses the kind of "rock shock" suspension system that can be seen on most mountain bikes today. It consists of a shock absorber inside a coil compression spring. This system is able to absorb shock, and damp oscillations at the same time. Figure 5 shows the coil spring system of the Permobil

Colours Boing™. It uses an A-Arm suspension system that consists of two tension springs. Coil springs are made from typical spring steel. Spring steel is made by bending the steel into the desired shape, and then heat treating it to the desired hardness.

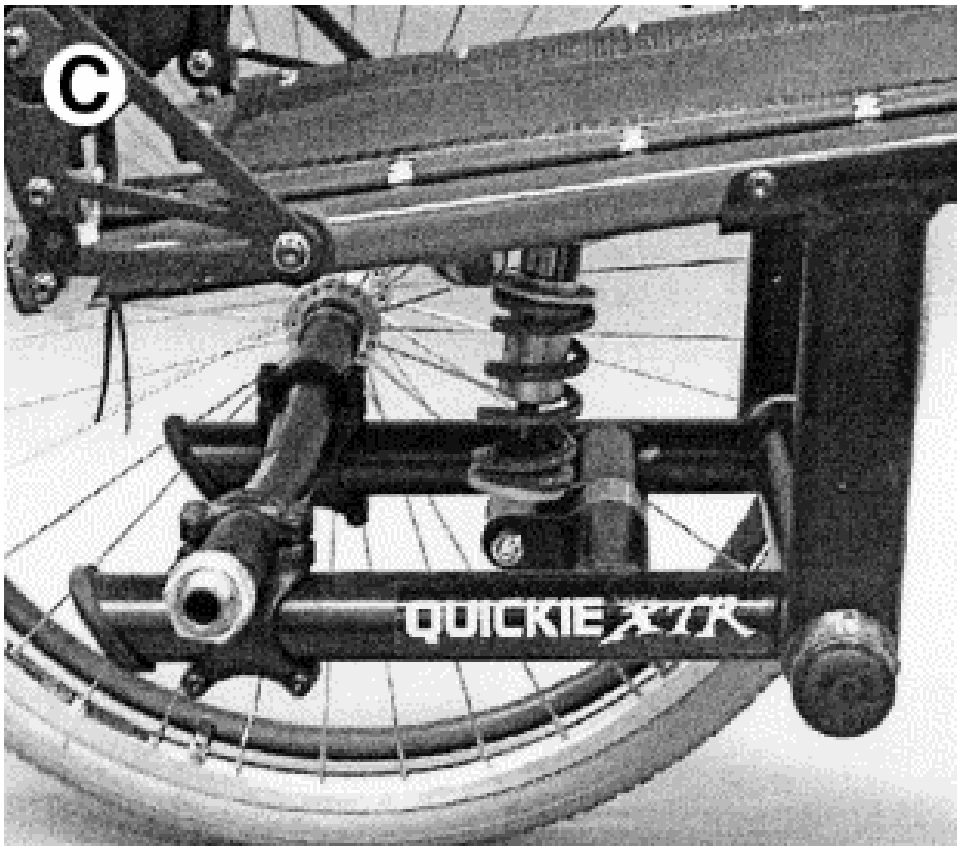

Figure 4: Coil Compression Spring Suspension of a Quickie XTR™

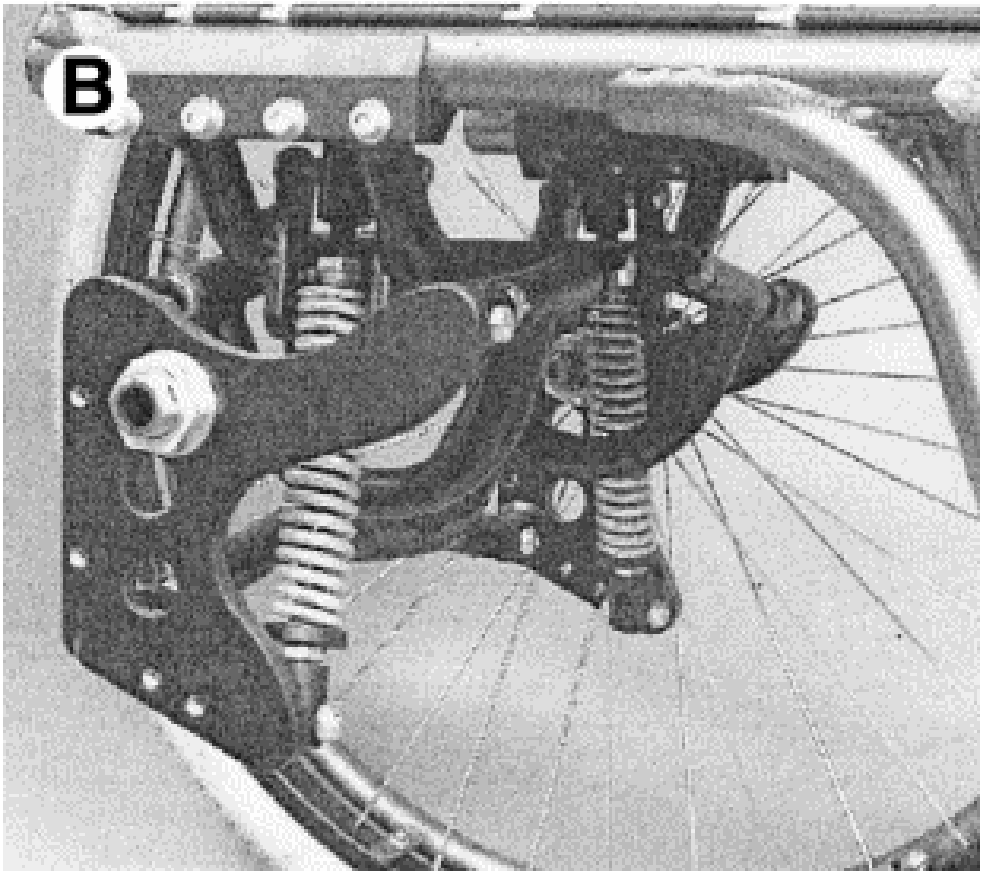

Figure 5: Tension Spring Suspension of a Permobil Colours Boing™

2.1.3 Composite Springs

As part of the Capstone Design class at the University of South Florida, the use of composite springs for wheelchair suspension was researched. The design focused around the concept of an after-market suspension for standard rigid frame wheelchairs. It involved the use of a glass fiber reinforced polymer (GFRP) composite leaf spring mounted between the frame and the rear wheels. Normally the axle is hard mounted to the frame of the chair. With this design, one end of the spring is attached to the frame of the wheelchair with a mount, and the other end of the spring attached to the axle of the wheels. This results in a cantilevered leaf spring that is able to absorb the shock loads experienced by the wheels. To damp the oscillations, a rubber strap was wrapped around the frame and the end of the leaf spring. Figure 6 shows the suspension system added to an Invacare Terminator ^{TM} wheelchair.

Figure 6: Composite Spring Suspension System Mounted on a Rigid Frame Wheelchair

When researching the use of composites for springs, the following was uncovered. Composites are made from polymers in the form of thermosetting resins like polyester or epoxy. These polymers, referred to as the matrix, are commonly mixed with glass fiber, carbon fiber, or Kevlar fiber to produce reinforced polymers (GFRP, CFRP, KFRP respectively). Polyester-GFRP is the cheapest composite, while epoxy-CFRP and epoxy-KFRP are more expensive. To obtain high stiffness and strength, continuous fibers are used, as compared to chopped fibers. The fibers used in the creation of these composites have been through a drawing process that aligns their chains with one another, giving them a strength-to-weight ratio that exceeds steel. The fibers carry the load, while the polymers act to transmit the loads throughout the fibers, as well as to protect the fibers from environmental damage. Combining the high stiffness and strength of glass, carbon, or Kevlar fibers, with the ductility and durability of polymers, has created a class of materials that has a strength-to-weight ratio better than many types of metals. Factors that affect the performance of composites include: moisture, fatigue, and heat [4].

Other factors that affect the properties of composites include choice of fiber, choice of matrix/ resin, fiber-resin ratio, fiber length, fiber orientation, and laminate thickness. Glass fibers are cheap, but are not as strong as the more expensive carbon or Kevlar fibers, which are stronger, stiffer, and have a lower density than glass. Kevlar fibers are also fire retardant and, unlike carbon, allow radio waves to pass through them. A unique feature about carbon fibers is that they are electrically conductive. As for the matrix, polyester has relatively low cost and is the most widely used. Epoxy matrices provide better properties at elevated temperatures than do polyesters, but they cost more

than polyester. Increasing the fiber to resin ratio, increasing the fiber length, and running the fibers in the same direction, all act to increase the strength of the composite. Contrary to what one may think, decreasing the laminate thickness increases the strength, because the chance of having entrapped air is decreased [4].

Because they are made from oil and do not bio-degrade, polymers are seen by many as environmentally unfriendly. However, there is on-going research into using recyclable materials, like sugar and starch, as a basis for the synthesis of polymers [4].

3. Structural Failure of Wheelchairs

When redesigning a wheelchair to incorporate suspension, it is important that the structural integrity of the frame is not compromised. It has been reported that 80% of injuries to people in wheelchairs occur because of engineering factors associated with the wheelchair design [5]. Therefore, before engaging in the design of a new kind of suspension for manual wheelchairs, it is important to understand how both suspension and non-suspension wheelchairs have previously failed when subjected to testing.

3.1 Failure of Non-Suspension Wheelchairs

A test was done on 3 styles of wheelchairs: depot wheelchairs (DW), light-weight wheelchairs (LW), and ultra-light-weight wheelchairs (UW). The UWs generally weigh less than 30 lbs, while the LWs generally weight between 30 and 35 lbs [5]. Depot wheelchairs are the heaviest and cheapest. The chairs were constructed from steel, aluminum, titanium, or composite materials. A majority of the UW's were constructed from 6061 (aircraft) aluminum, while some were made from titanium. The DW's were all made from steel, and the LW's were made from either steel, or composites [5].

The wheelchairs were subjected to a series of double-drum test and curb-drop tests. A double-drum test consists of two metal cylinders that the wheelchair rides on. These cylinders have slats that are positioned 180° apart, and are supposed to simulate the everyday forces that a wheelchair is subjected to, such as sidewalk cracks, and door

thresholds. The curb-drop test is supposed to simulate bumping down off a curb, and consists of repeatedly dropping a wheelchair from a height of 5 cm. The double-drum test is run for 200,000 cycles, and if catastrophic failure has not occurred, the chair is subjected to 6666 cycles of the curb-drop test. To meet ISO requirements, a chair has to survive one complete set of double-drum and curb-drop tests [2].

After being subjected to a double-drum test and a curb-drop test, it was found that the UW lasted the longest, and that the DWs had the worst results . Some of the modes of failure that took place include:

- Class 3 Wheelchair frame cracking, caster stem breakage. Chair is deemed unusable at this point
- Class 2 Repairs that need to be made by a technician, like fixing flat tires or performing wheel alignments.
- Class 1 Repairs that can be done by the user, like tightening of loose screws and bolts [5].

All of the wheelchairs made from fiberglass experienced failure, and 76% of the chairs that were made from low-strength steel tubing experienced failure. However, none of the titanium chairs had a class 3 failure. It was found that the UW's performed the best overall. These results confirmed the findings from previous tests which stated that the UW's perform better than the LW or DW wheelchairs [5].

3.2 Failure of Suspension Wheelchairs

It is obvious that incorporating suspension into manual wheelchairs will create a soother, safer, more comfortable ride for the user. With that in mind, it would also make sense that adding suspension to a manual wheelchair should result in more durable, longer lasting wheelchairs. However, three suspension wheelchairs that are currently on the market, the Quickie XTR™, the Invacare A-6S™, and the Permobile Colours Boing™, were subjected to a series of double-drum and curb-drop tests, and the results showed otherwise [2].

In the study of the Quickie XTR™, Invacare A-6S™, and Permobile Colours Boing™, each chair was tested until failure. Three Permobile Colours Boing™ chairs were tested, and all of them experienced fracture of the right caster stem, as shown in Figure 7. It was suggested that the casters failed because their quick release system decreased their strength, and because part of the threaded section of the stem was exposed, resulting in a stress concentration.

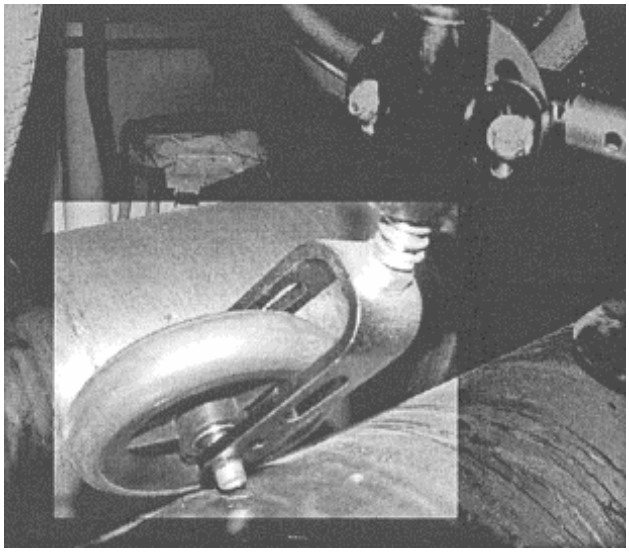

Figure 7: Failure of the Right Castor Pin of the Permobile Colours Boing™ Chairs

Because the chair was not able to complete the double-drum test, it was not subjected to any curb-drop tests [2].

When the three Invacare A-6S™ chairs were tasted, all of them completed one cycle of double-drum and curb-drop tests. The failure in chairs 1 and 3 occurred in the telescoping tube of the suspension system. The failure took place in the heat affected zone of a weld, as shown in Figure 8. The failure of the second chair was caused by a stress concentration at a screw hole in the seat part of the frame, as shown in Figure 9 on the next page [2].

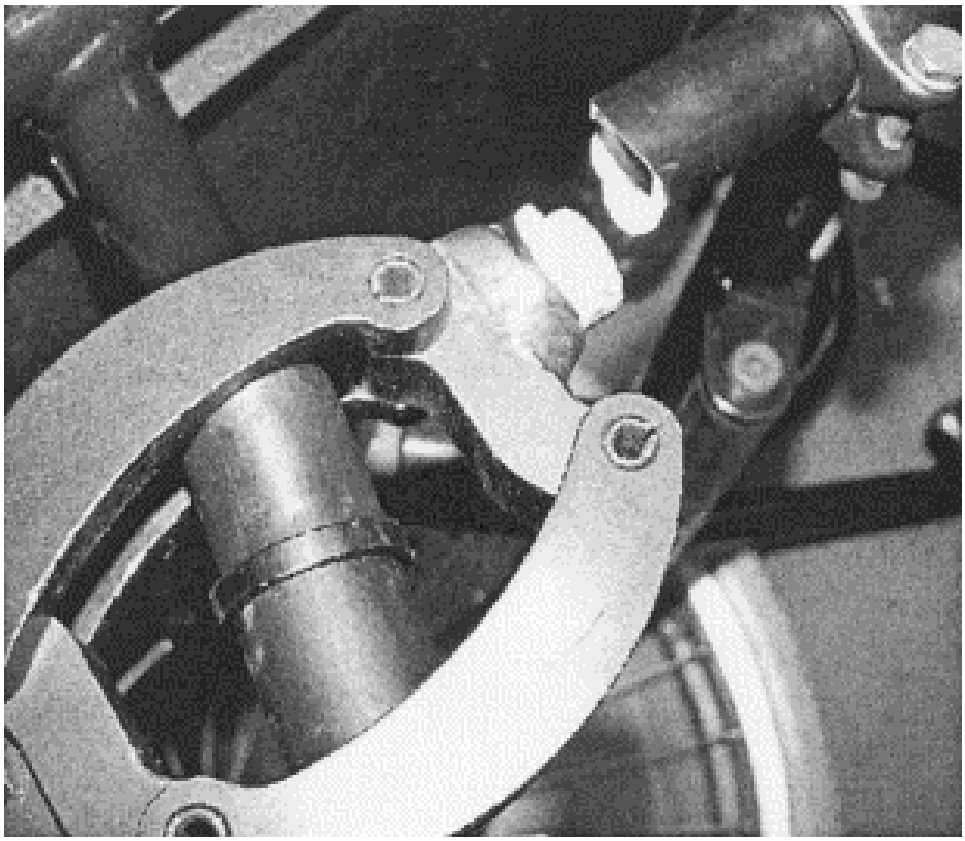

Figure 8: Failure of the Telescoping Tube on the Invacare A-6S™, Chair 1 and 3

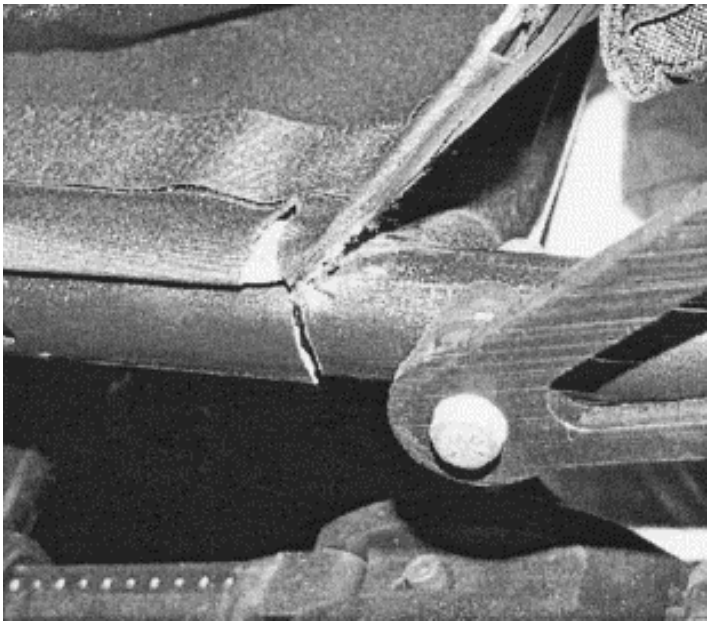

Figure 9: Failure of the Invacare A-6S™ Along the Frame of Chair 2

The three Quickie XTR™ chairs outlasted all the others, with chair 1 lasting 1,000,000 double-drum cycles and 33,330 curb-drop cycles, before experiencing fracture where the mount was welded to the lower part of the frame, as show in Figure 10.

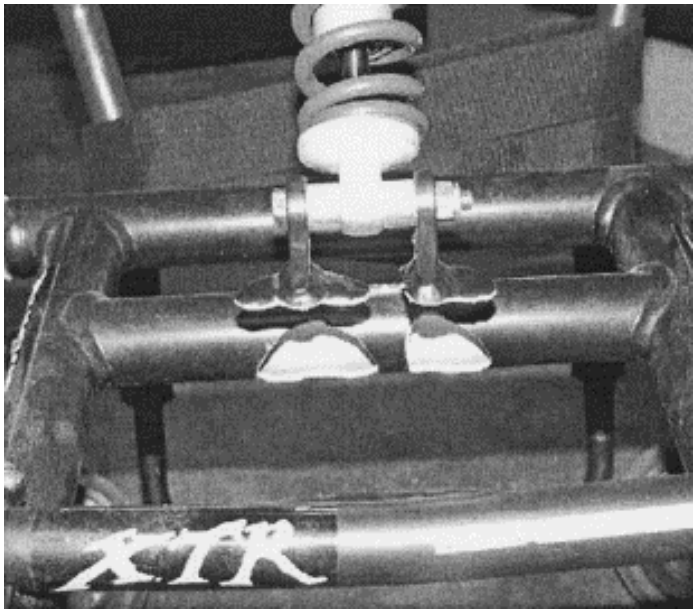

Figure 10: Failure of Quickie XTR™ Chair 1, Where the Mount is Welded to the Frame

Chairs 2 and 3 had similar durability, but failed in different ways. Chair 2 experienced a fracture at a screw hole in the right side of the seat part of the frame, while chair 3 experienced a fracture in the mount for the right caster wheel as shown in Figure 11. The caster mount for chair three was considered substandard [2].

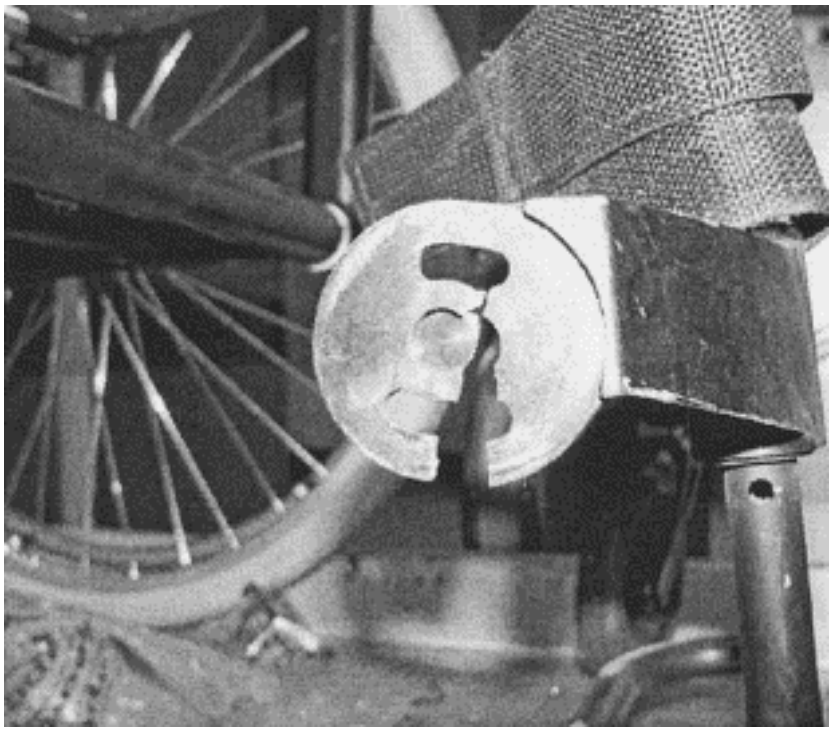

Figure 11: Failure of the Right Caster Mount on the Quickie XTR™ Chair 3

The results from the suspension wheelchair test were compared with the results obtained from a test of four different ultra light-weight wheelchairs (12 wheelchairs total). It was found that the suspension wheelchairs did not show any significant improvement over ultra-light-weight wheelchairs, in the area of durability. However, the suspension wheelchairs were shown to be more durable than the light-weight wheelchairs. Because the Permobile Colours Boing™ had problems with its castor pins failing, the results for the whole group were unfavorable. When this chair was removed

from the analysis, the number of cycles for the Quickie XTR™ and the Invacare A-6S™ were 911,394, which outlasted the 187,362 cycles of the light-weight wheelchairs. However, they were still below the 1,092,441 cycles for the ultra-light-wheelchairs [2].

This study of suspension wheelchairs has shown that there is room for improvement in the area of rear suspension for manual wheelchairs. In the next section, the design of the after-market suspension system that was developed during this thesis will be discussed.

4. After-Market Suspension for Wheelchair

There is a need for an after-market suspension system for manual wheelchairs that will allow the users of regular / non-suspension wheelchairs to add rear-wheel suspension to their wheelchairs. During the previous mentioned USF senior design project, after-market rear-wheel suspension was attempted through the addition of leaf spring suspension between the wheels and the frame the chair. However, it was found that wheelchair frames are too diverse to permit a retrofit of one single suspension design to all frames.

To design a more universal suspension system, this thesis has focused on the design of a wheel that has suspension incorporated into it. This approach will allow the addition of suspension to most wheelchairs by simply buying new wheels. This approach will also take advantage of the proven durability of ultra light-weight wheelchairs, allowing the wheelchair user to take a tried and true ultra light-weight wheelchair, and then add suspension wheels to it. The suspension can also be used on other wheelchairs besides ultra light-weight wheelchairs.

4.1 Design Process

A typical wheelchair wheel either has a quick-release pin or a bolt, which passes through a set of ½" inner diameter ball-race bearings, and is then inserted into the frame of the chair. For simplicity, a quick-release pin will be referred to as a bolt for this paper. Figure 12 below shows a typical wheelchair wheel.

Figure 12: Regular Wheelchair Wheel

The ball-race bearings of a regular wheelchair wheel have a ½" inner diameter, and the quick-release pin / standard bolt, passes through the middle of the ball-race bearings and is then attached to the frame of the chair. The design for this thesis is based around the concept of adding shock absorbing material between the spokes of the wheel, and the bolt that connects the wheel to the frame of the chair. The approach taken was to design a suspension system between the inner diameter of the ball-race bearings, and the bolt. To do this, ball-race bearings with an inner diameter of 4" were chosen. Figure 13

on the following page is a picture of the suspension system designed for this thesis. The green rectangle represents the shock absorbing material that absorbs the shock load that would normally be transmitted from the wheel to the frame of the chair.

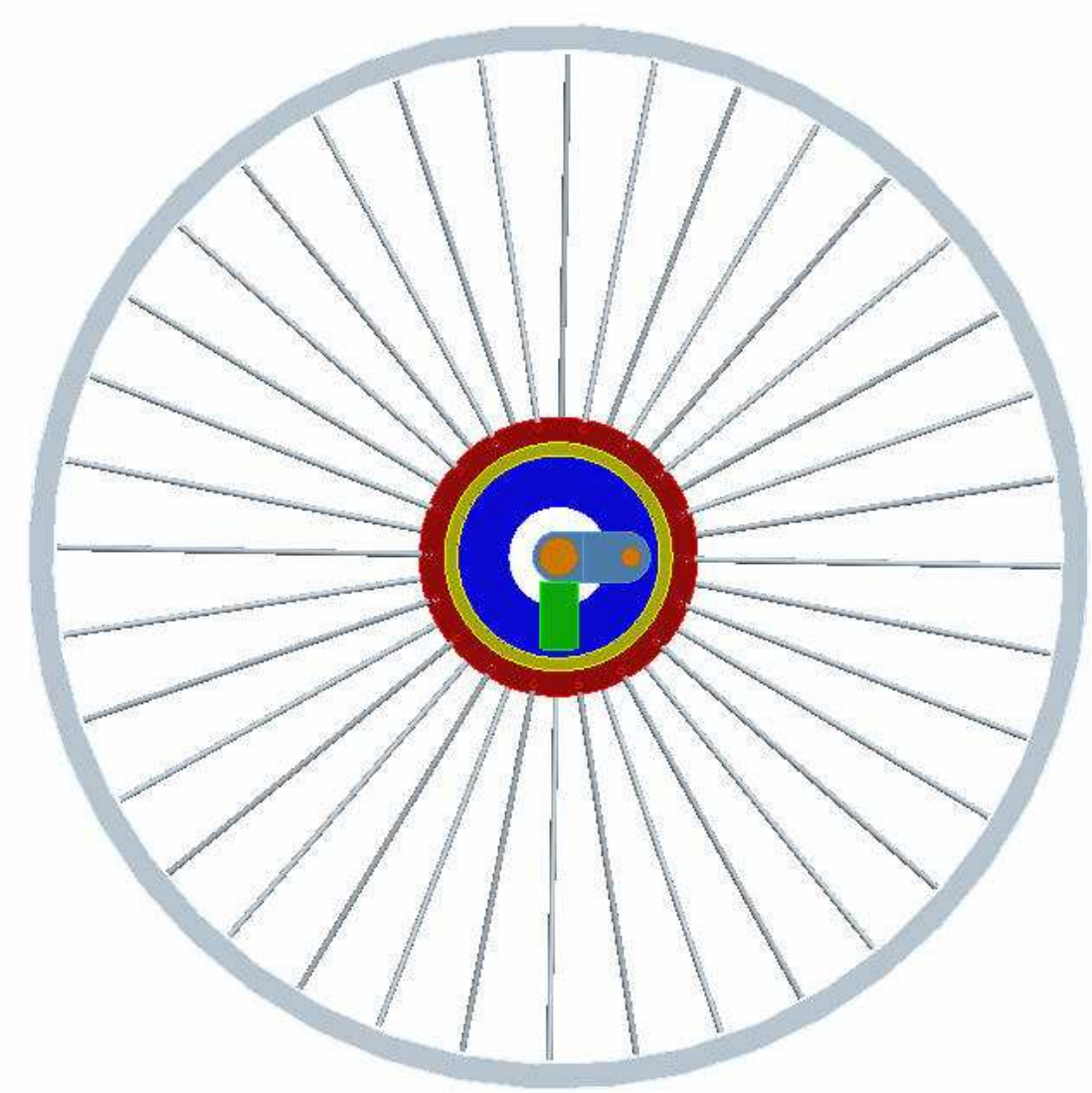

Figure 13: Color Code for Wheel Suspension

Red = Outer Hub; Yellow = 4" inner diameter ball bearing;
Dark Blue = Inner Hub; Light Blue = Fork; Gold = ½" quick-release pin / standard bolt, and 3/8" pin; Green = Urethane

The procedure for constructing the suspension wheel will now be covered. There is no direct contact between the outer hub and the inner hub. They are connected by way of the ball-race bearings being press fitted into the space between the inner and outer hub. The use of a retaining ring was considered, but they were too large for this application. See Figure 14-a through 14-d below for a description of the assembly process.

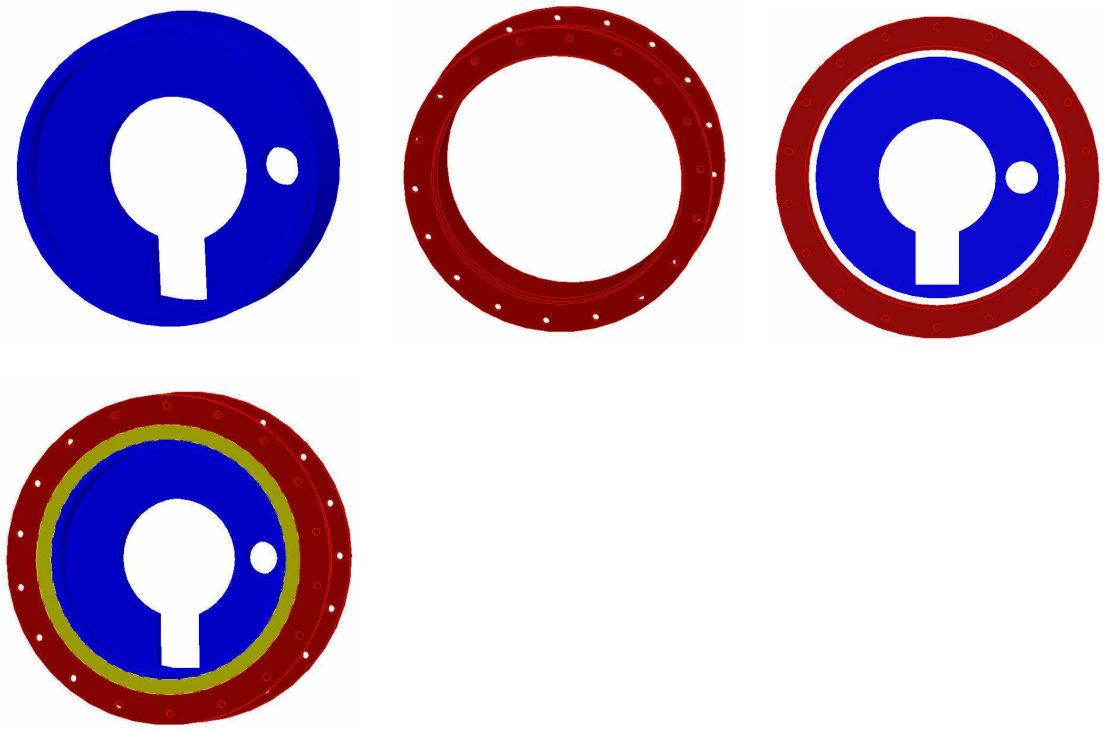

Figure 14: Assembly of the Inner Hub, Outer Hub, and Ball-Race Bearings

a. **(top left) Inner hub**
b. **(center) Outer hub**
c. **(right) Inner hub is placed inside the outer hub**
d. **(bottom left) The ball-race bearings (yellow) are press fitted between the outer and inner hub, and hold the two together.**

Next, a 3/8" inner diameter, 9/16" outer diameter, needle roller bearing is pressed into the 9/16" diameter hole in the inner hub. In Figure 14-d, this is the small hole. Then the fork is inserted through the circular and square opening in the inner hub, and aligned so that the 3/8" holes in both sides of the arms of the fork, line up with the 3/8" needle roller bearing. See Figure 15-a and 15-b below for further description of the assembly process.

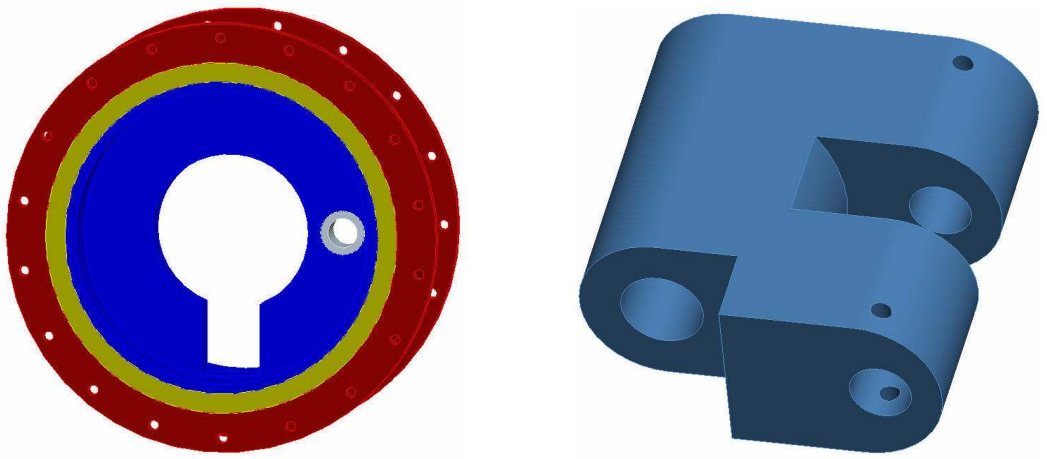

Figure 15: Assembly of Needle Roller Bearing and Fork

a. **(left) The needle roller bearing (gray) pressed into the hole in the inner hub.**
b. **(right) The fork with a ½" hole for bolt that attaches the wheel to the chair, and two 3/8" holes for the pin that connects the fork to the inner hub.**

The fork is attached to the inner hub with a 3/8" diameter pin that passes through the holes in the fork, and the needle roller bearing. 3/8" washers, not shown, are used between the fork and the inner hub so that they do not bind. Two set screws are used to keep the 3/8" pin from coming out of the fork. Loctite™ can be used to keep the set screws from loosening over time. See Figure 16-a and 16-b below.

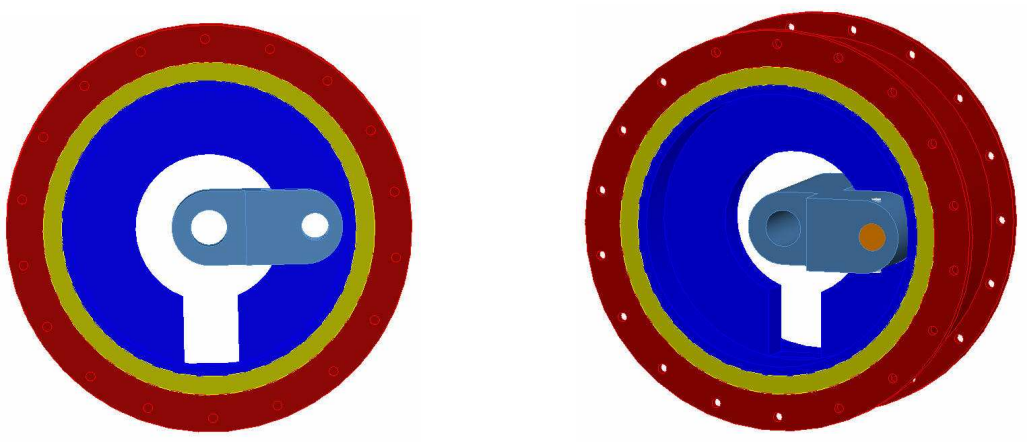

Figure 16: Assembly of Fork and 3/8'' Pin

a. **(left) The fork inserted through the inner hub, and aligned with the needle roller bearing.**
b. **3/8 inch pin (gold color) that connects the fork to the inner hub**

Then, a ½" diameter bolt that attaches the wheel to the frame of the wheelchair is inserted into the ½" hole in the fork. No bearings are required at this interface because there is no relative motion between the fork and the ½" bolt during operation. Figures 17-a and 17-b show the assembly of the outer hub, ball-race bearings, inner hub, fork, pin, and bolt.

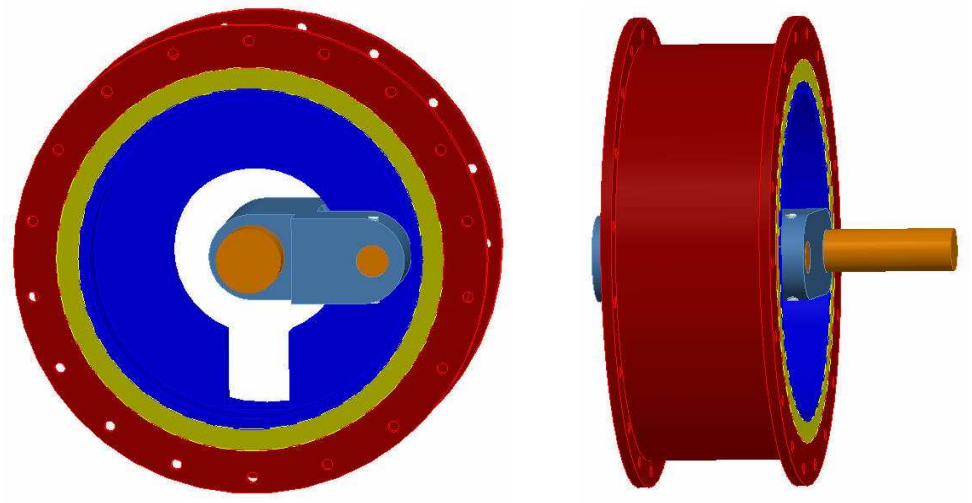

Figure 17: Assembly of Bolt and Set Screw

a. **½" pin/bolt (gold color) that connects the fork to the wheelchair**
b. **Angled view of suspension system. The end of the pin/bolt that connects the fork/wheel to the chair can be seen.**

A block of Urethane rubber is inserted between the bottom of the fork and the flange of the inner hub. Since the fork is fixed in its current position, as the wheel encounters a bump, the Urethane rubber is compressed, and inner hub rotates slightly about the 3/8" diameter pin. See Figure 13 below for a picture of the complete suspension system.

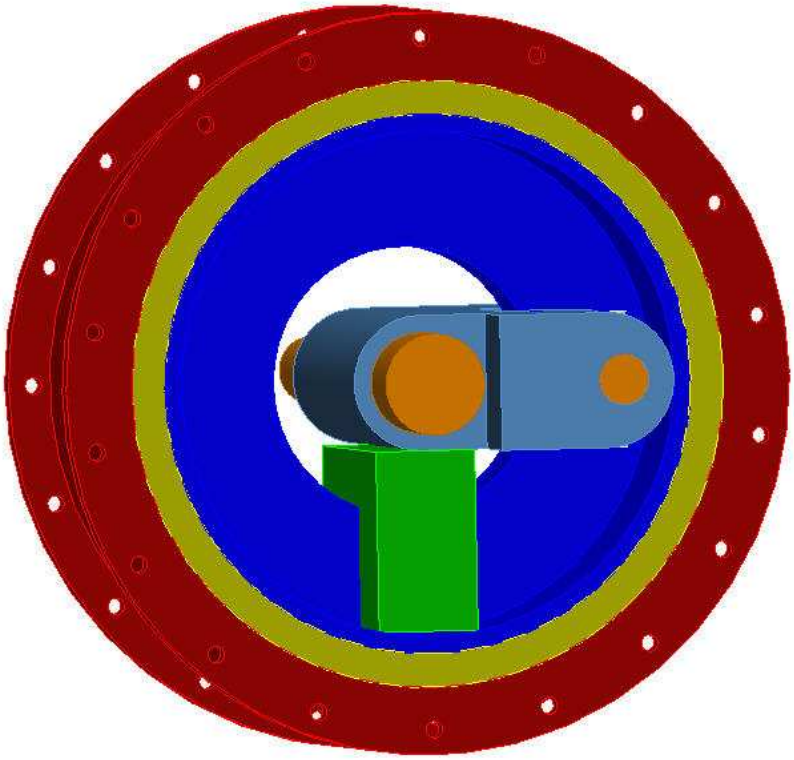

Figure 18: Urethane Rubber (Green), Which Reduces the Shock Loads and Vibrations That Are Transmitted to the User

4.2 Materials Used

The materials chosen for the various components are as follows. The fork, inner hub, and outer hub, are made from 6061 T-6 Aluminum. This is the same material that most light-weight wheelchairs are made from. It has a yield strength of 40,000 psi, and a modulus of elasticity of 10,000 psi. The 3/8" diameter pin is made from 304 stainless steel. It has a yield strength of 31,200 psi, and a modulus of elasticity of 28,000 psi. The

quick-release pin / bolt are standard to all wheelchairs, so no special care was taken in the selection of these parts.

The 4" inner diameter ball-race bearings were purchased from Silverthin Bearing Group . They are made from AISI 52100 bearing steel. Two sets of ball-race bearings, consisting of a radial contact bearing and a four-point contact bearing, are used for each wheel. A radial contact bearing is mainly used for radial loads, but can also withstand some axial and moment loads. A four-point contact bearing is mainly used for moment loading and reverse axial loading, but can also be used for light radial loading [6]. By using a radial contact bearing and a four-point contact bearing on the same wheel, the benefits of both types of bearings can be combined.

The stress ratings for the ball race bearings were obtained from the Silverthin website. Both the radial contact and the four-point contact bearings are rated for a static radial load of 1,293 lbs, and a dynamic radial load of 486 lbs. The four-point bearing is rated for a static moment of 2,748 lbs-inch, and a dynamic moment of 1,035 lbs-inch [7]. The 3/8" inner diameter roller needle bearings were bought from McMaster-Carr and are rated for a dynamic load of 1,300 lbs [8]. As will be shown in section 5.1, the ball race bearing static load rating is greater than the 10 times static load of 1150 lbs that was used for the analysis. However, the dynamic load rating for the ball race bearings is below the 10 times static load of 1150lbs. Further research should be done to determine how the dynamic load rating compares to the static load rating. For this thesis, it is assumed that since a factor of safety of 10 is used, the bearings should not fail. See section 5.1 for discussion about what a 10 times static load was used.

Polyurethane was used for the elastomer. Polyurethane has excellent resistance to oil, abrasion, tearing, and impact. It also has good resistance to weather and chemicals [8]. Since "Frog Legs"™ uses cylinder shaped polyurethane with a 60 shore-A durometer, similar shapes and durometers were tested with the suspension system in order to find out which shape and durometer provided the most comfortable ride. It was decided that a ¾" diameter cylinder of polyurethane, with a durometer of 40 Shore A, was the best combination for the suspension system.

5. Finite Element Analysis (FEA)

As with any design, it is necessary to know if the stresses applied to the system are within the material limits listed in section 4.2. Finite element analysis software was used to perform an elementary analysis of the stresses in this suspension system, in order to show that it will not fail. During the process of creating a FEA model, a number of assumptions and simplifications are made by the program, and by the user. For the suspension, the following process was used. The real world model is simplified and assumptions were made. The materials used are assumed to be homogeneous, isotropic, and free of internal defects; and cosmetic features are suppressed so as to reduce the geometric complexity, allowing for faster solve times [9].

To create a mathematical model that represents the part being analyzed, the FEA program makes various assumptions, such as the linearity of the material, and the nature of the loading conditions. With these assumptions, mathematical models are created that describe the change in the variables of interest within the boundaries of the model. The geometry of the model is then broken up into many elements so that the differential equations created by the mathematical model can be rewritten as a system of simultaneous linear equations to represent the whole model. This network of connected elements is called a mesh [9].

Once these equations are solved, the results obtained represent the variables of interest, such as stress, deformation, etc. However, the accuracy of the results need to be

verified by convergence, "the process of reducing the local error by using smaller and smaller elements or using elements that can approximate more complex point-to-point shapes." One of the differences between FEA programs is the way in which convergence is achieved. The classical approach is to use h-elements, which typically limit the element order to a quadratic formula. To obtain convergence, the mesh has to be refined, or made denser, until the difference between results fall within the desired percentage. The advantage to this approach is that first and second order equations solve relatively quickly. The disadvantage is that the mesh has to be refined for each computer run, and the results have to be compared for convergence.

The other approach is to use p-elements, which can assume higher element edge orders. This allows for better representation of the model. For example, trying to represent an arch with only a 2^{nd} order polynomial is not very accurate if the mesh size is not dense enough. With p-elements, this same arch can be represented by only a few elements, each with a polynomial edge order of nine or higher. While a 9^{th} order polynomial takes longer to solve than a 2^{nd} order polynomial, no mesh refinement is needed. The order of polynomial used to solve the equations starts at one, and keeps increasing until convergence is reached, or until the max edge order available is reached [10].

To monitor this convergence, Pro/ENGINEER Mechanica uses the results obtained for the maximum Von Mises stress and the total strain energy. The FEA program, Pro/ENGINEER Mechanica, does this automatically. Occasionally convergence is still not reached after solving the 9^{th} order polynomial, and the mesh needs to be refined. Pro-Mechanica has the capability to do this mesh refinement itself,

and then another analysis can be run using the refined mesh [9]. The advantages to this method are that mesh refinement is usually not needed, and it is generally easier to use. The disadvantage is that the run times are generally longer. Pro/ENGINEER Mechanica was used for this thesis because it was decided that the ease of use of p-elements was worth the longer solution times.

5.1 Setting Up the FEA Models

To create the FEA models for this thesis, the parts were first created in Pro/ENGINEER, a 3-D computer modeling software. Features not important to the analysis were suppressed, and then the models were sent to Pro/ENGINEER Mechanica. In Mechanica, units and material properties were assigned. Then constraints and loads that helped to simulate real-world conditions were applied. Since Mechanica automatically "welds" surfaces that are in contact with each other, "contact regions" were added to parts like the fork and the bolt. This allowed the two surfaces to separate when a load was applied, like it would in the real world.

It is impractical to analyze the whole model at once, because each run time would take a few days, and trouble shooting problems within the model would be very difficult. Therefore, assumptions were made about what were considered critical areas within the suspension system, and then models were created that focused on these critical areas. The system was broken down into four models: 1) the interaction between the fork and the bolt, 2) the inner hub and the 3/8" diameter pin/needle roller bearing, 3) the inner hub and the 4" inner diameter ball-race bearings, 4) and the outer hub and the spokes.

In the real world, the wheel is subjected to a variety of loads, including static, dynamic, cyclic, fatigue, and torsion/moment loading. To be reasonably sure that failure would not take place, it was decided to analyze the various components at static load, and increase the load until failure took place, or until the load was considered large enough to encompass the loads that a wheelchair wheel would be subjected to. When a force of 10 times the static load was used, the stress on the components was still below the yield stress of the aluminum. To check the acceptability of this value, the following calculations were performed.

A curb height of 6" (152 mm) was used for the calculation. The maximum allowable deflection for the fork/polyurethane when the wheelchair drops 152 mm, is 34 mm. The corresponding static deflection, the deflection caused by a person sitting in the chair, is given by equation 1 below [11].

$$\delta_s = \frac{\delta_m{}^2}{2(h+\delta_m)} = 3.42mm \qquad \text{Eq.1}$$

The static deflection is then used in equation 2 below to determine the dynamic to static load ratio [11].

$$\frac{P}{W} = 1 + \sqrt{1 + \frac{2 \cdot h}{\delta_s}} = 10.48 \qquad \text{Eq.2}$$

Since the shock absorption of the tires and the wheelchair cushion were not considered for the preceding equations, it was decided that a force of 10 times the static load would suffice for this analysis.

Since the most common camber/tilt for wheelchairs wheels is 3 degrees from the vertical, the 10 times static load was applied to the wheel at this angle [12]. To calculate

the static load, a 200 lb person and a 30 lb chair were assumed. Assuming that this weight acts only on the rear wheels, each wheel experiences half of this load, or 115 lbs. With a 3 degree camber, this comes to 114.8 lbs normal to the rim of the wheel, and 6.0 lbs transverse to the rim. For simplicity, the normal portion of the static load will be rounded to 115 lbs. So ten times the static load is 1150 lbs normal to the rim of the wheel, and 60 lbs transverse to the rim of the wheel. See figure 19 below for a free-body diagram of a wheelchair with a three degree camber.

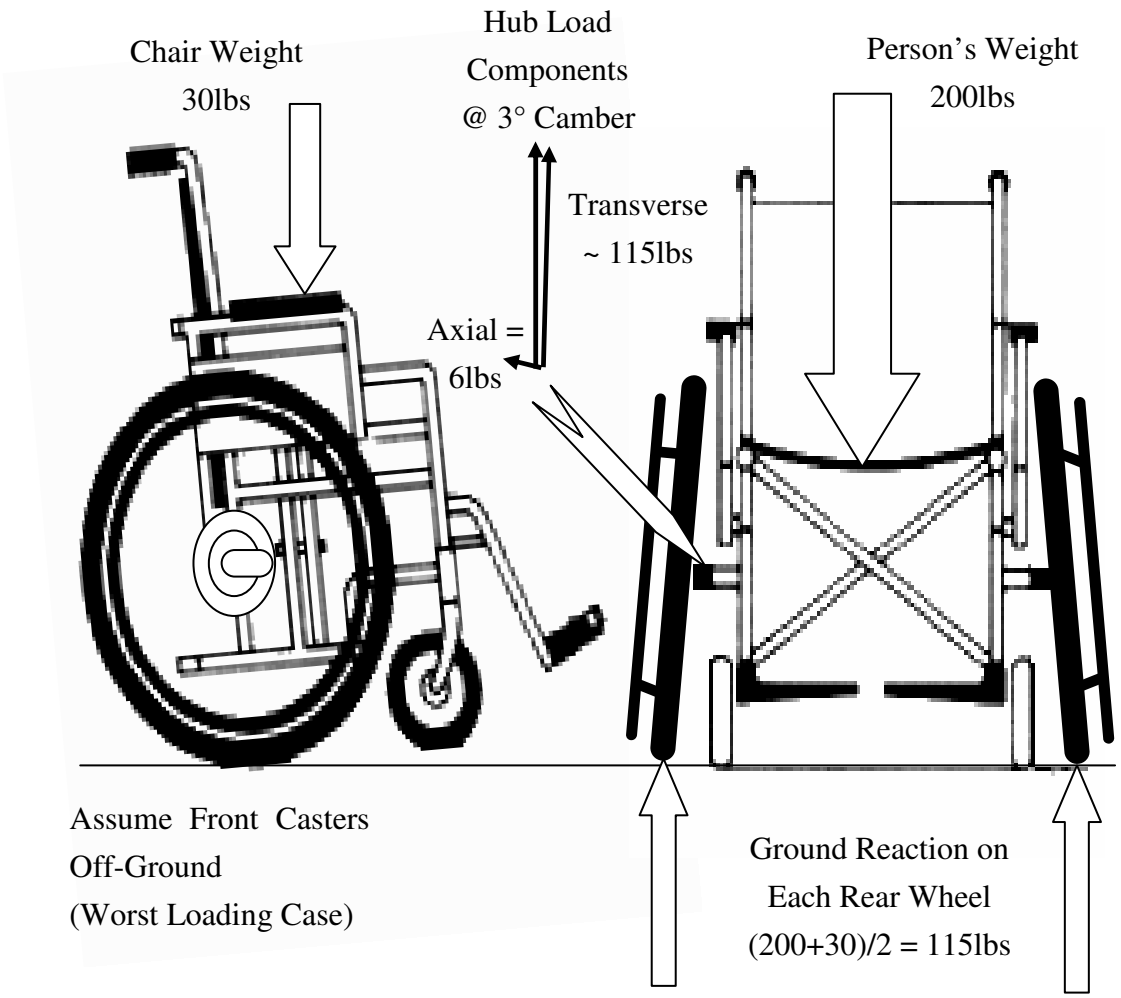

Figure 19: Free-Body Diagram of the Wheelchair

5.2 Simulation of the Fork

The first simulation was of the fork and the bolt. First, the 3/8" diameter holes that the 3/8" diameter pin goes through were constrained in all six degrees of freedom. In Figure 20 below, this is shown by the yellow triangles. Then a contact region was created between the bolt and the ½" diameter hole in the fork. The contact regions are depicted with two parallel red lines with another line intersecting them, and the yellow balance scale icons. To simulate the static load applied to the bolt from the wheelchair, the bolt was cut off at the side of the fork, and a force of 10 times the load, 1150 lbs normal to the rim and 60 lbs transverse to the rim, was applied to its cross-section. This load is depicted by the red arrows on the end of the gold colored bolt.

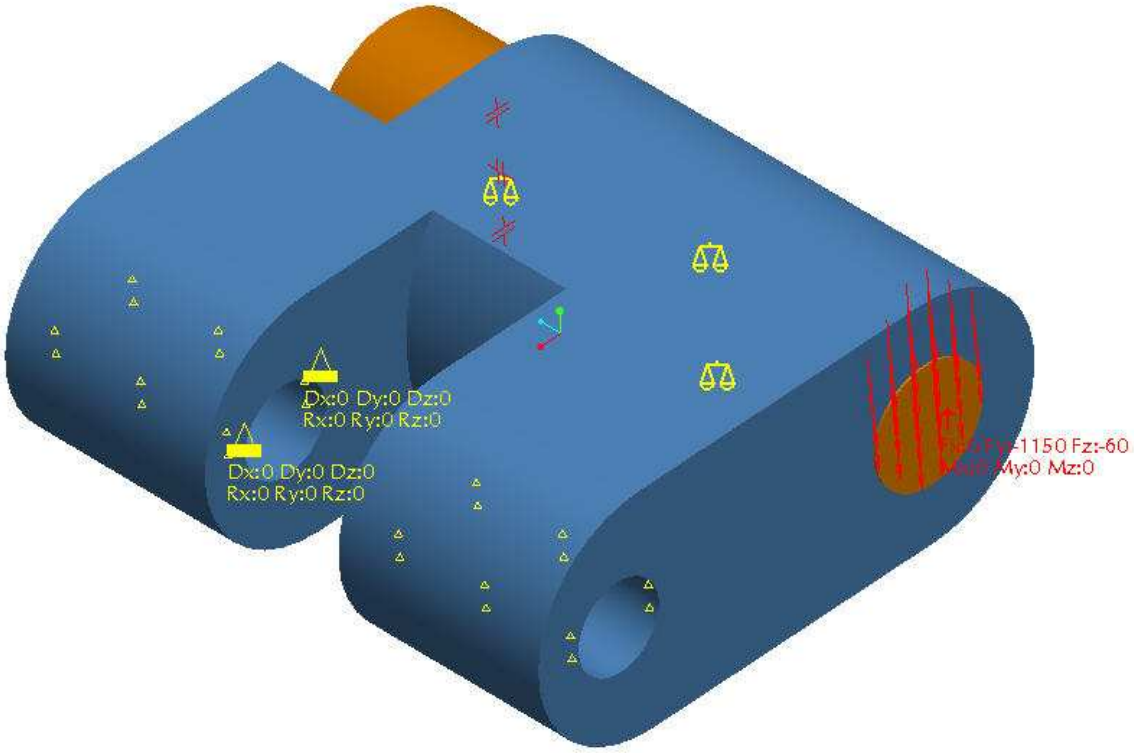

Figure 20: FEA Model of the Fork and Bolt

5.3 Simulation of the Inner Hub and Pin

The second simulation was of the 3/8" diameter pin, the needle roller bearing, and the inner hub. The purpose of this model was to simulate the effect that the needle roller bearing and the pin would have on the inner hub. This analysis took the most time, because it was difficult to Figure out how to best constrain the model so as to simulate real-world conditions. A number of models were created, ranging from very simple to very complex, until a model was obtained that appeared to adequately model the real world conditions. Three of these models will be discussed in the following pages.

Figure 21 shows the first model that was created to simulate the effect the pin would have on the inner hub. In real life, the 9/16" outer diameter needle roller bearing is pressed into the inner hub, and the 3/8" pin is then inserted into the bearing. To simplify the model, a 9/16" diameter pin was used in place of the bearing and pin combination.

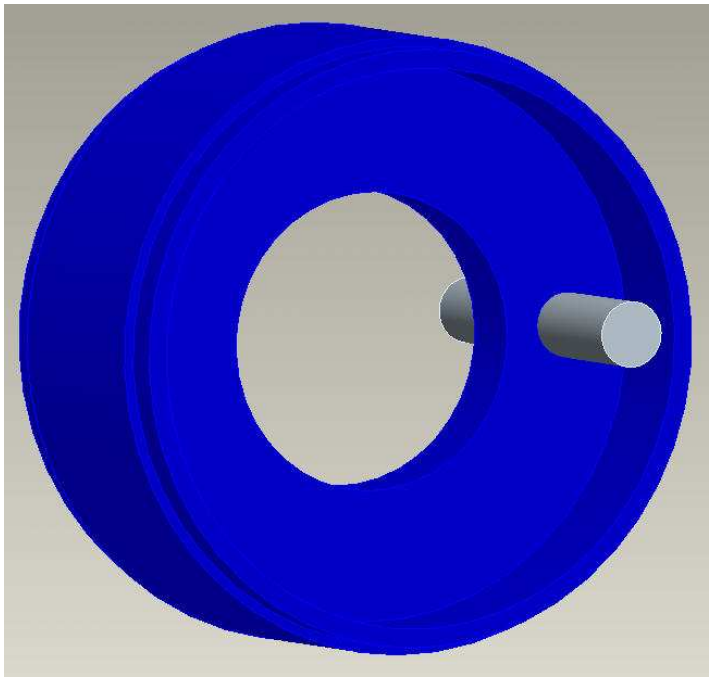

Figure 21: First Model of Interaction Between the Inner Hub and the Pin/Needle Roller Bearing

Next, the ends of the cylinder were cut off at the surface of the inner hub, as shown in Figure 22 below. This simulates the portion of the pin that is not contained by the fork. The constraints applied to the model are also visible in Figure 22. The outer circular surface of the hub was fixed in all six degrees of freedom, and the ends of the pin were fixed in the z-direction, the plane of their surface. These constraints are represented by red triangles.

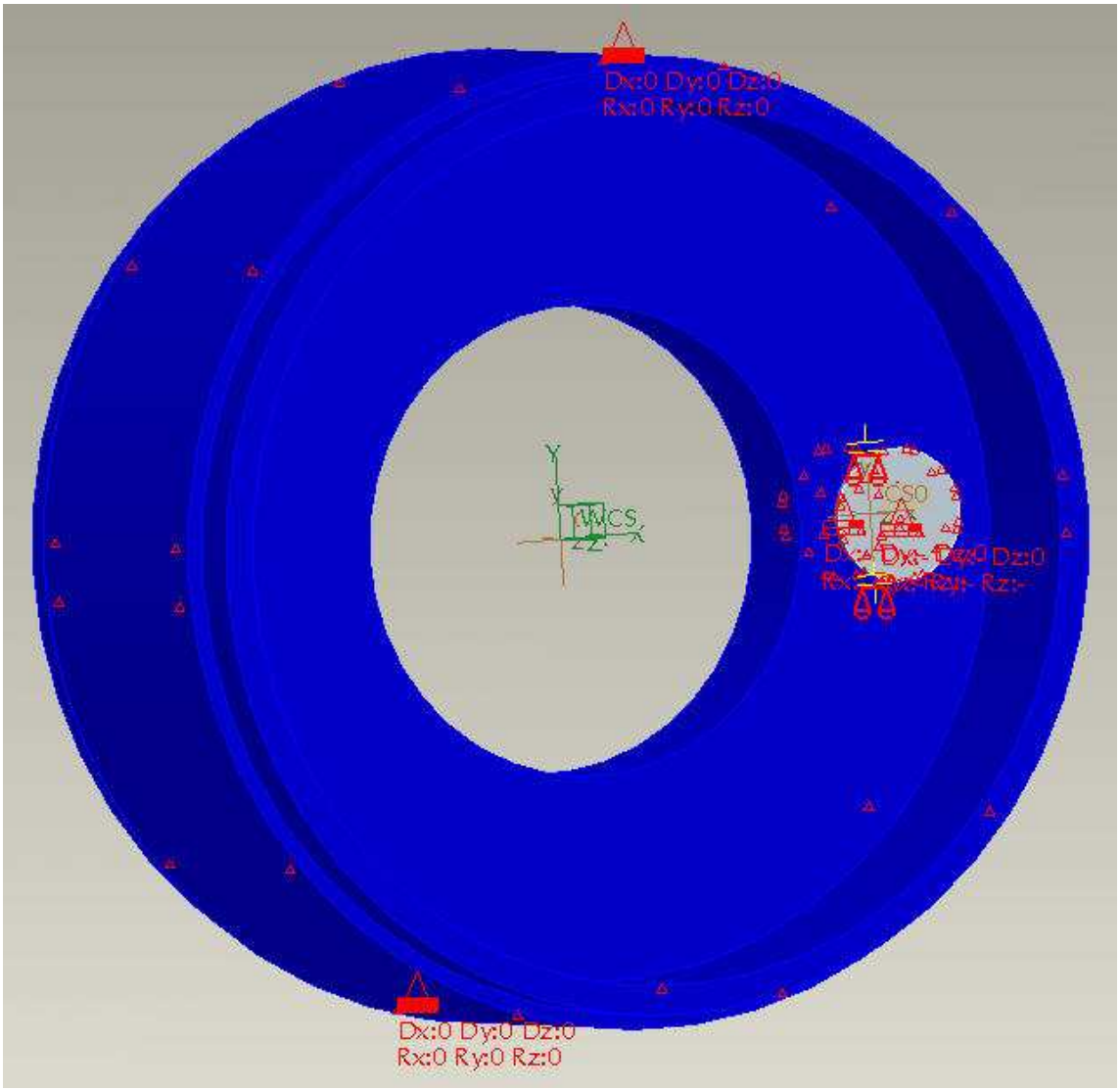

Figure 22: The Constraints Applied to the First Model

In Figure 23, the two red symbols show that there is a contact region between the pin and the inner hub. To apply a torque load to the wheel, 10 times the static transverse load, 60 lbs, was multiplied by the 12" moment arm that it acted over. The resultant torque of 720 in-lbs was then applied to both sides of the cylinder. This load is depicted by the yellow arrows in Figure 23.

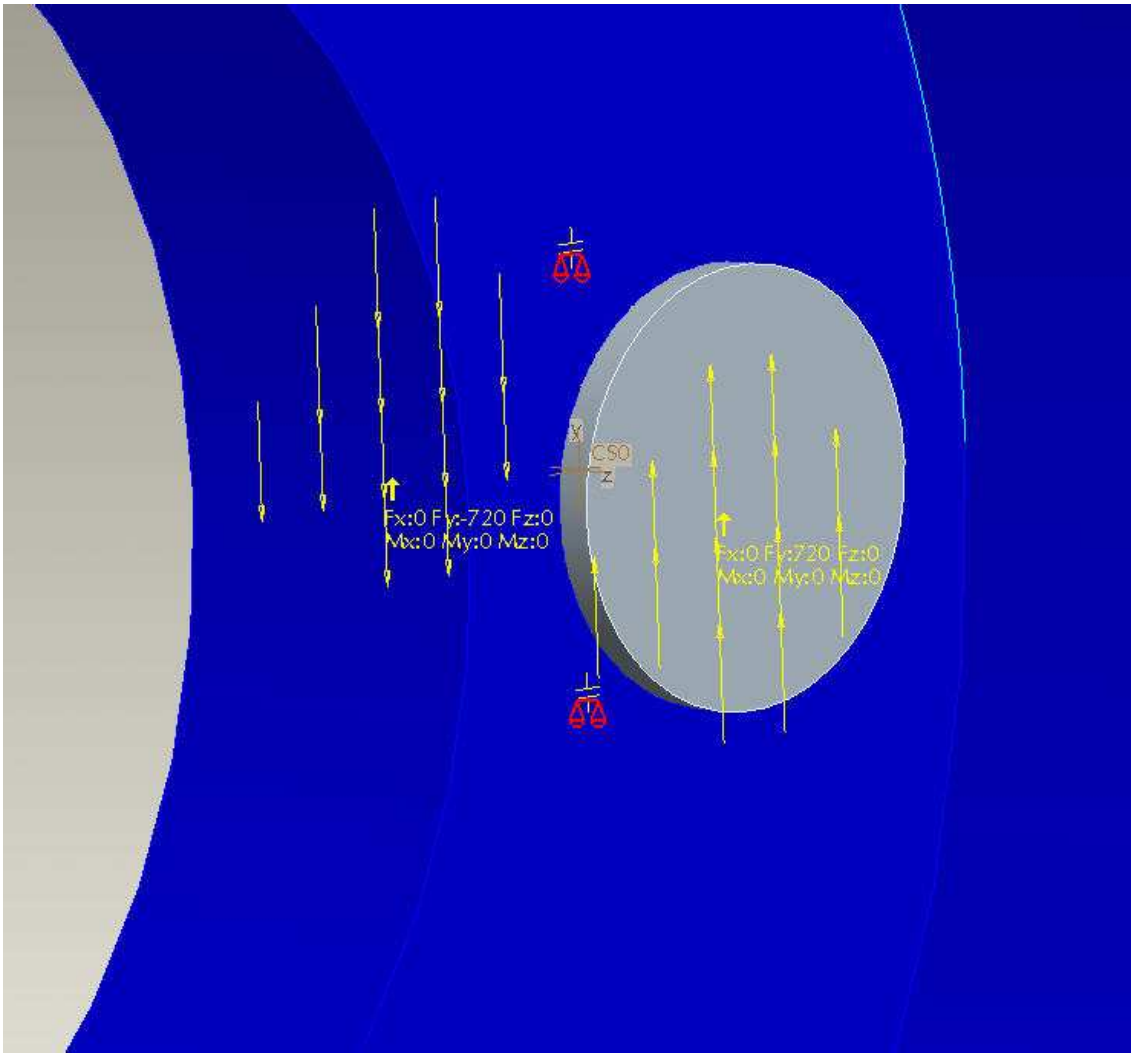

Figure 23: The Contact Areas of the First Model, and the Applied Loads

This model did not depict real world conditions very well because the z-direction constraints on the pin were causing it to deform in a maner not intended.

The second and most complex model that was created is shown below in Figure 24-a, 24-b, 24-c. Square extension planks were added to the inner hub to simulate the spokes and outer diameter of the wheel. The 10 times static load was applied to these extentions.

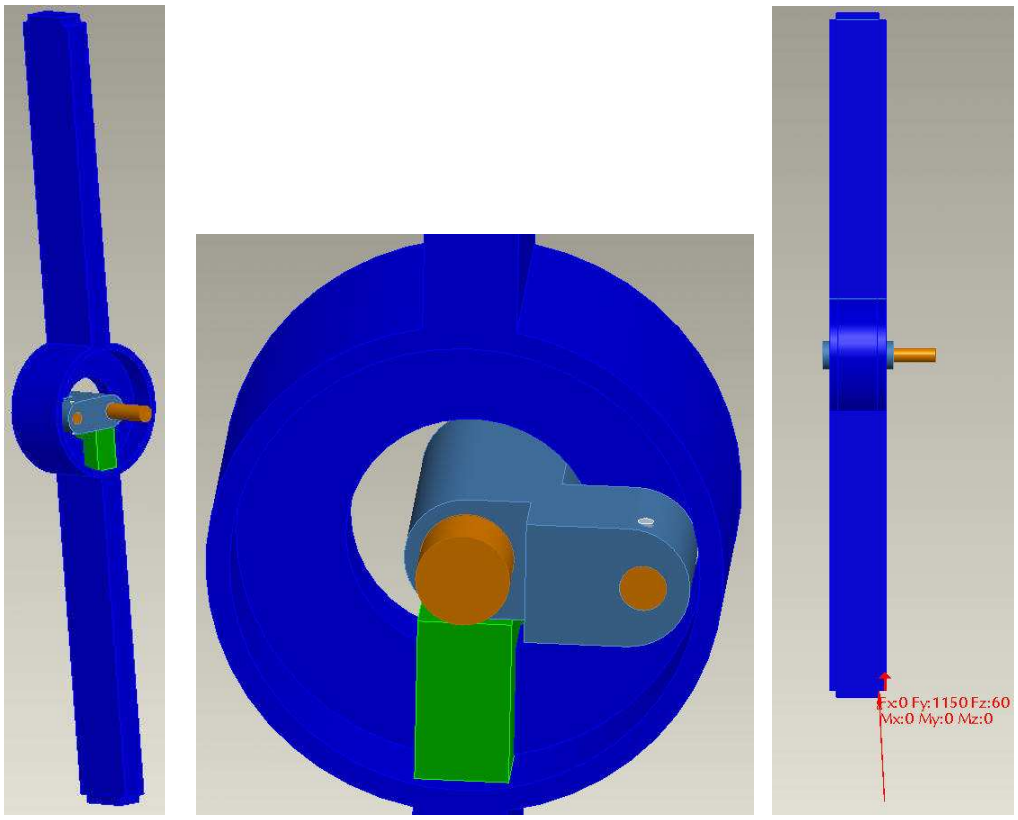

Figure 24: Second FEA Model of the Inner Hub

a. **(left) FEA model of the inner hub, with extensions added to simulate the spokes and outer diameter of the wheel, and the 3/8" pin.**
b. **(center) Close up of the inner hub and 3/8" pin model. The fork, urethane, and bolt were added to try to get a better simulation.**
c. **(right) Shows the upward and sideways load (red arrow at the bottom of the model) that represents the force that the ground exerts on the wheel.**

Then, 10 times the normal portion of the static load (1150 lbs), and 10 times the transverse portion of the static load (60 lbs) were applied to the bottom and the side of the lower extension respectively. The red arrow at the bottom of the model in Figure 24-c represents the effect of the ground on a tilted wheel.

The bolt was fixed in all six degrees of freedom to represent being attached to the wheelchair. This model had numerous contact areas, and it took about a day and a half for each computer run. About 5 models were run, and each time the results file gave warnings about the contact areas and inaccurate pressure results. Also, the model did not behave in the manner that it was intended to, so it was decided to try a more simplified approach.

The third, more simplified model consisted of the inner hub with the extension planks, but the fork, bolt, and urethane were eliminated from the model. This model is very similar to the first model; with the differences being the addition of the extension planks, the square cut-out, the constraints, and where the load was applied. Figure 25 shows the overall model.

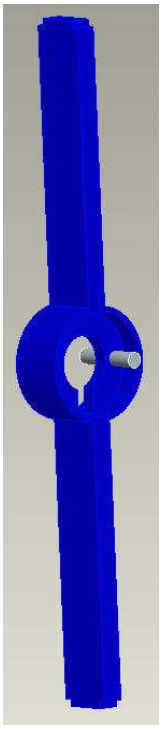

Figure 25: Third (Simplified) Model – Inner Hub and Pin Only

Figure 26 shows the constraints, depicted by yellow triangles, which were applied to the inner hub. To prevent the inner hub from sliding along the pin, the surface of the 9/16" diameter hole in the hub was constrained so that it could not move along its axis. To prevent the inner hub from rotating about the 9/16" diameter hole, the sides of the square cut-out were constrained so that they could not move out of the plane of their surface.

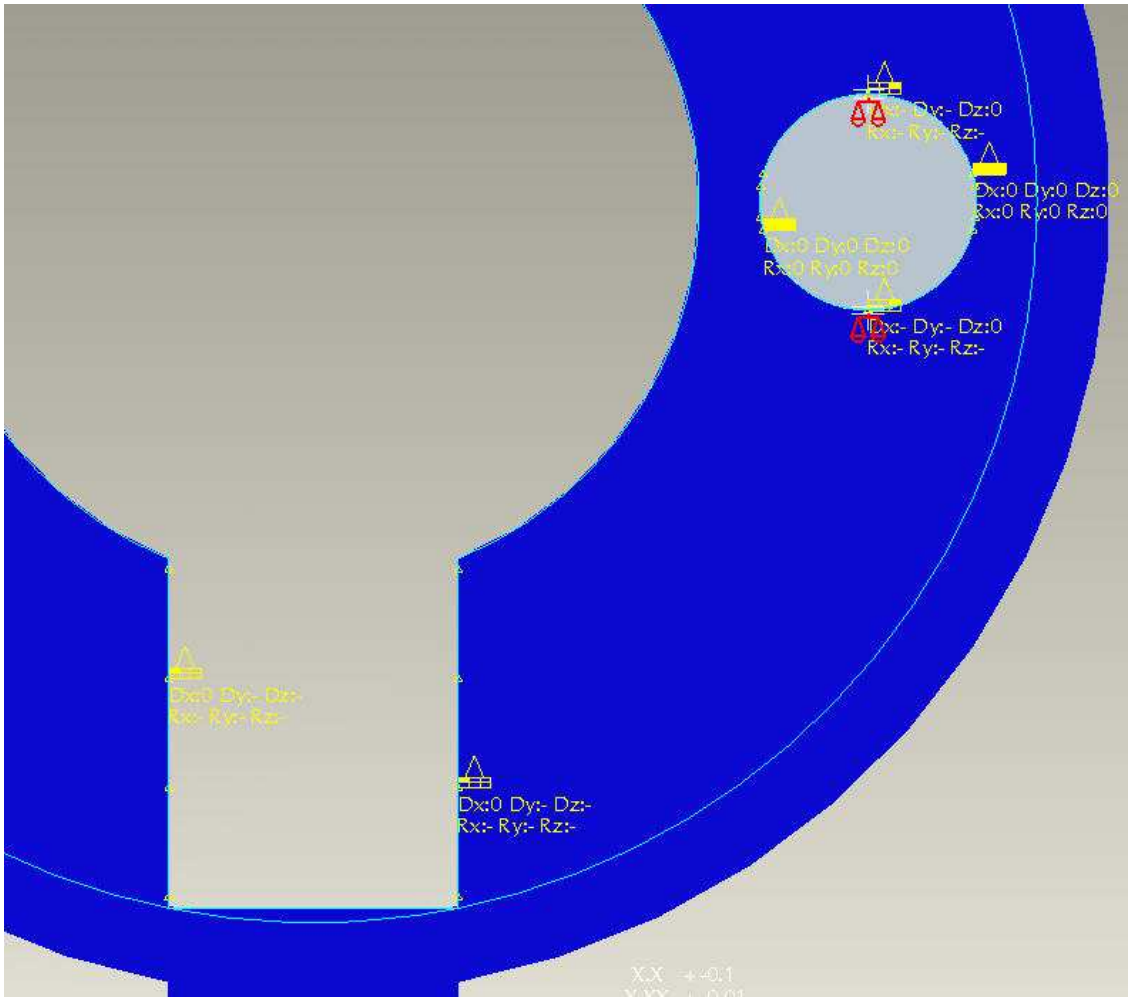

Figure 26: Third Model - Translational and Rotational Constraints

Figure 27 shows that symbols for the contact areas that were created between the inner hub and the pin, and that the pin was constrained in all six degrees of freedom.

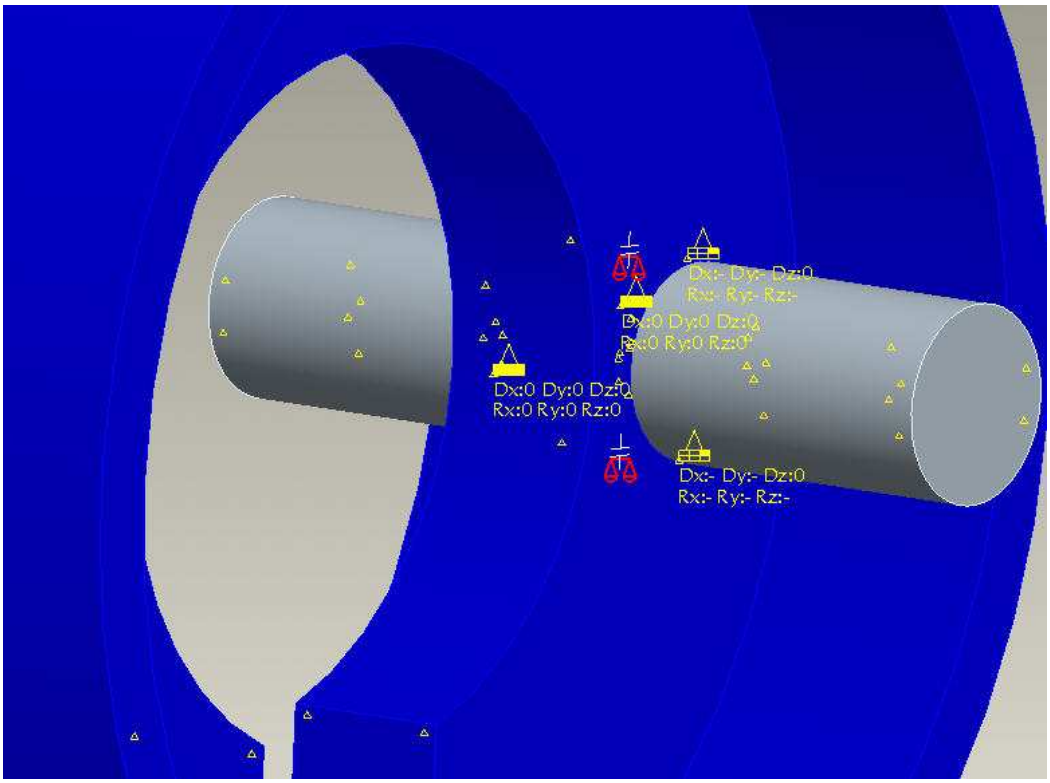

Figure 27: Third Model - Contact Areas Between Inner Hub and Pin

Figure 28 shows a force of 10 times the transverse portion of the load (60 lbs), like the load in 24-c, applied to the bottom of the lower extension. This represents the torque applied to the pin and hub of a tilted wheel. A normal portion of the static load was not used because none of this load should be transmitted to the 9/16" diameter hole. This load should be transferred from the inner hub to the urethane, where it is damped, and then transmitted to the fork, the bolt, and finally to the frame of the chair.

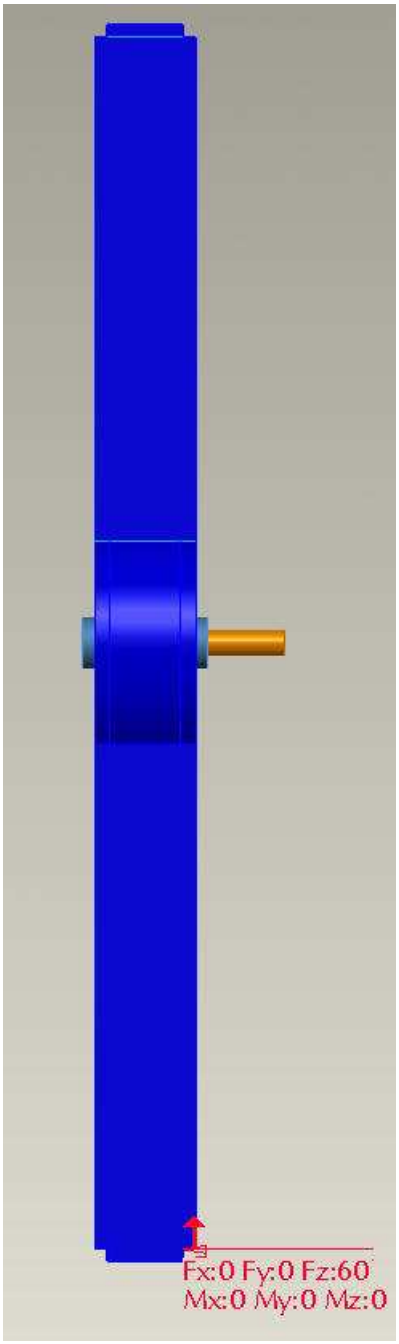

Figure 28: Third Model - Transverse Load Applied to the Lower Extension, Which Represents the Rim of the Wheel

5.4 Simulation of the Inner Hub and the 4" Ball-Race Bearings

The third simulation was of the 4" inner diameter ball-race bearings and the inner hub. A model was created to determine the stress that is created in the inner hub by the load being transmitted from ground to the ball-race bearings, and then to the inner hub. To simplify the model, the inner hub was cut in half. Then a symmetric constraint, which tells the computer that the right side is a mirror of the left side, was applied to the surface of the cut plane. The symmetric constraint is depicted by the halfway filled in red box on the left. See Figure 29 below.

Figure 29: FEA Model of the Inner Hub, Cut in Half

As shown in Figure 29, the constraint added to the bottom surface of the square cut-out constrains the surface in all six degrees of freedom. To simulate the load transmitted from ground to the ball-race bearings, a force of 10 times the normal portion of the static load, 575 lbs on each side of the hub, was applied to the bottom surface of the hub that is in contact with the ball-race bearings. See Figure 30.

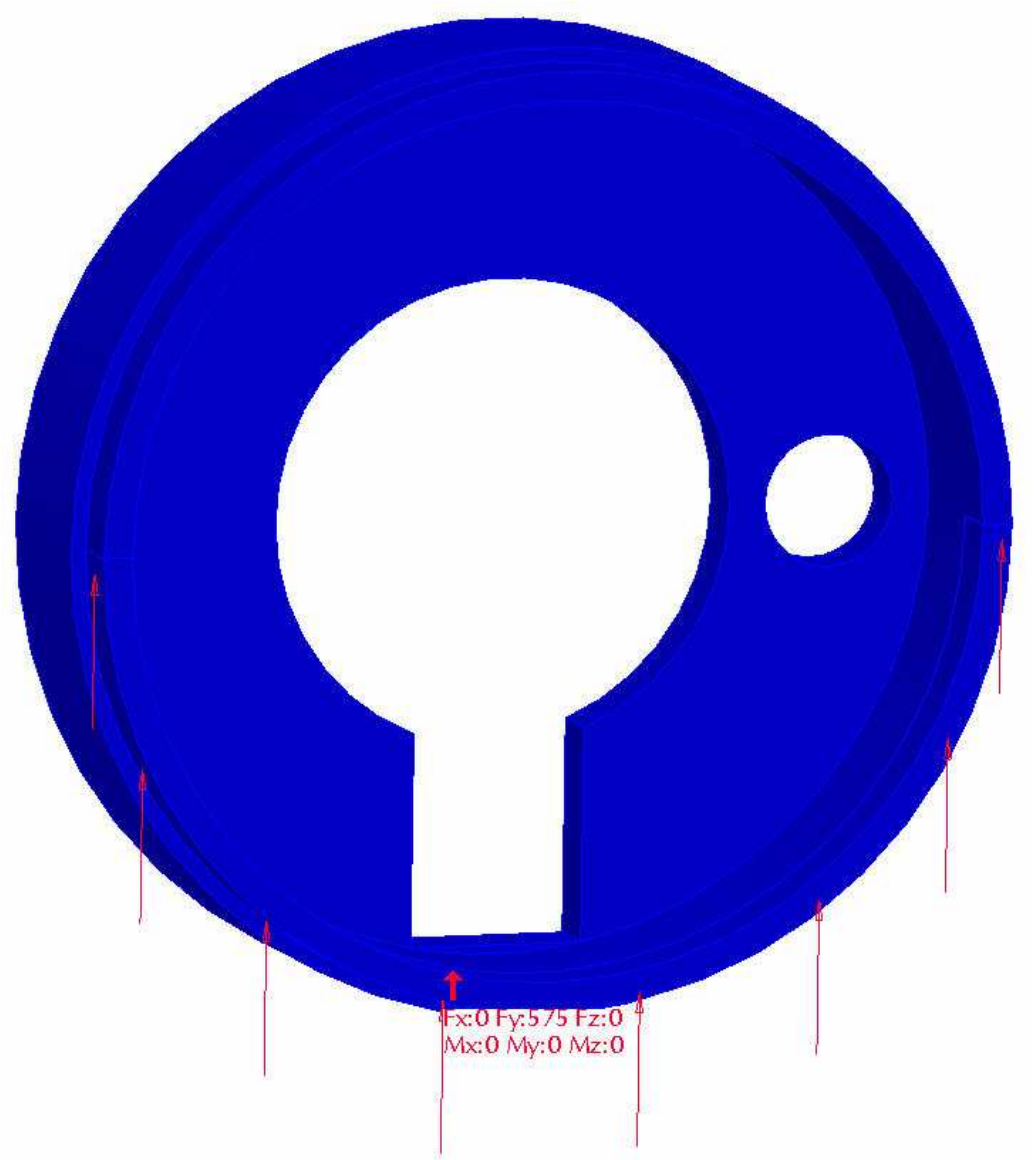

Figure 30: The Load that the Ball-Race Bearings Transmit to the Inner Hub is Depicted by the Red Arrows

5.5 Simulation of the Outer Hub and the Spokes

The fourth and last simulation was of the outer hub. The purpose of this model was to simulate the effect the spokes have on their corresponding holes in the outer hub. The effect of the ball-race bearings on the outer hub was not analyzed because it was assumed that the results would be similar to the results obtained from the inner hub. Since it would be very time consuming and difficult to simulate the loads that are applied by all the spokes to the outer hub, a model was created to analyze the stress on only one of the spoke holes. The bottom spoke hole was constrained in all six degrees of freedom, while the static load was applied to the top spoke hole. See Figure 31 below.

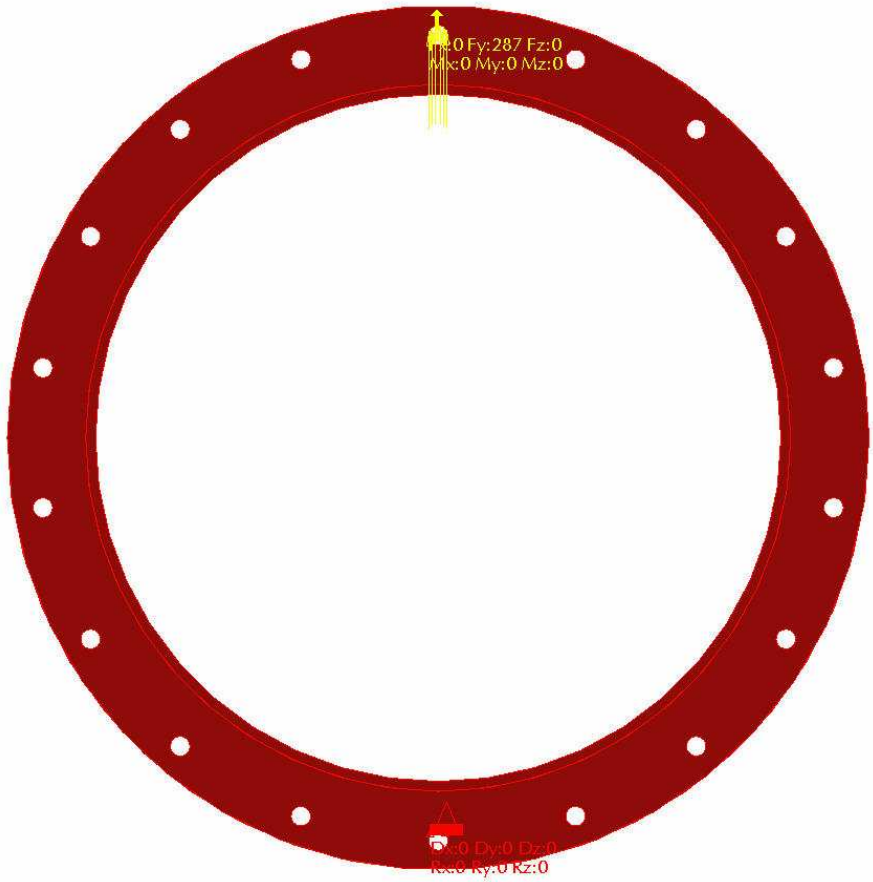

Figure 31: FEA Model of the Outer Hub and Spoke Analysis

The model was then cut in half, in order to shorten the computer run time, and a symmetric constraint was applied. See Figure 32 on the following page. Since only one spoke hole was being loaded, it was decided to only use 5 times the normal portion of the static load, 575 lbs. Since half the static load is applied to each side of the outer hub, 278 lbs was applied to the top spoke hole, as shown in Figure 32. Such an extreme loading condition was chosen in order to show that the strength of the spoke holes should be of no concern.

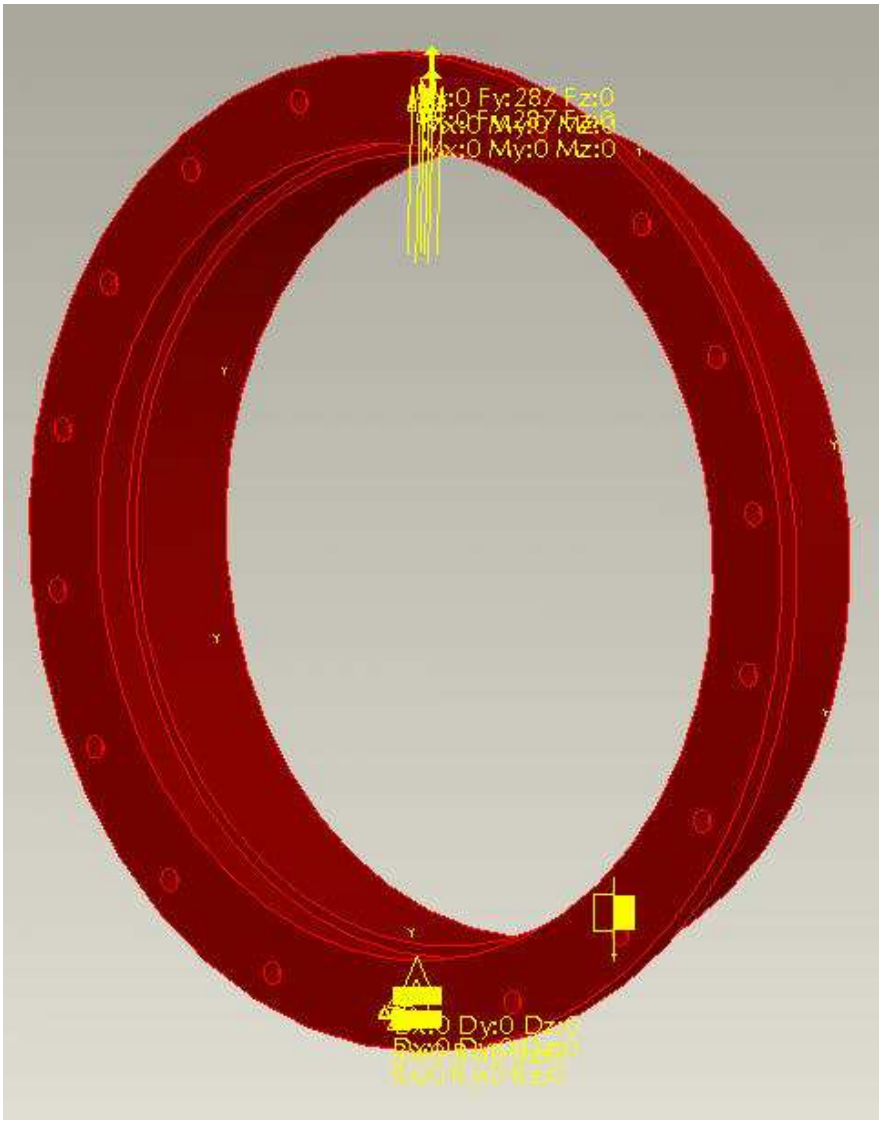

Figure 32: The Model Was Cut in Half and a Symmetric Constraint Was Applied to the Cut Surface

6. FEA Results

FEA programs create a vast amount of data, and the only way to really examine the results is graphically. Pro-Mechanica has numerous ways of displaying this data, including displacement animations, stress distributions, mode shapes, etc [9]. With such a vast amount of data available, the goals of the project need to be reviewed before proceeding with results interpretation. The goal of this analysis was to prove that the suspension system would not fail when subjected to the everyday shock loads that a wheelchair wheel encounters. To prove this, a number of failure modes could have been used. These include the maximum normal stress theory, the maximum shear stress theory, and the distortion energy (Von-Mises-Hencky) theory [10].

When using the maximum normal stress theory, failure happens when the principal stress equals the failure strength of the material, whether in tension or compression. This theory can be used for both ductile and brittle materials, but can only reasonable predict stress behavior if the principal stresses are similar in sign and magnitude. The maximum shear stress theory states that failure will occur when the maximum shear stress is equal to half the yield strength of the material. This theory can only be used for ductile materials because it only predicts failure by yielding. The maximum shear stress theory gives a conservative estimate when used to predict stress. The von-Mises theory states that failure occurs when the effective stress is equal to the yield strength of the material [10].

The von-Mises failure theory is very popular because it can describe very complex stress states, and Adams states that this theory "provides the best match with experimental data" [10]. For this analysis, the Von-Mises stress was used to view the results and determine if failure would take place in the models.

6.1 Fork and Bolt Results

As stated earlier, a load of 1150 lbs and 60 lbs, which are 10 times the normal and transverse portions of the static load respectively, were applied to the model of the fork and bolt. When the model was run, the results output file stated the following:

> ** Warning: Contact area is small in comparison to size
> of adjacent element edges for one or more
> contact regions for all load factors above
> marked with a "*". If you need pressure results
> near the contact regions, use single-pass
> adaptive convergence and select Localized
> Mesh Refinement.

This was done, but the same warnings were stated again, and the results in the output file were exactly the same. The reason for the error was looked into, but an answer could not be found. To solve this dilemma, the results of some of the initial analyses were reanalyzed.

During the initial stages of the analysis, different cambers were used to determine the maximum allowable camber for the suspension system. This maximum allowable camber will be discussed in section 6.2. The largest camber that could be found was 20 degrees, which is used on specialized sport wheelchairs such as tennis chairs [12]. When 10 times static load was applied to a fork and bolt model with 20 degrees of camber, the

values obtained were 1080 lbs normal to the rim of the wheel, and 390 lbs transverse to the rim. When the analysis was run, the contact area warning was displayed for the first two convergence checks, but when a edge order of four was used, which means that a 4th order polynomial was used to model the mesh elements, the warning did not come up. The analysis continued to run until the model converged with an edge order of seven, and no more contact area warnings.

The maximum Von Mises stress obtained for the fork and the bolt when using the 3 degree camber was 33,040 psi, located near the bottom of the ½" diameter hole. In Figure 32 below, the yellow shaded area is where this stress occurs. When the camber of 20 degrees was used, the maximum Von Mises stress was 30,924 psi. Both of these stress results are below the 40,000 psi yield strength for 6061 T-6 Aluminum.

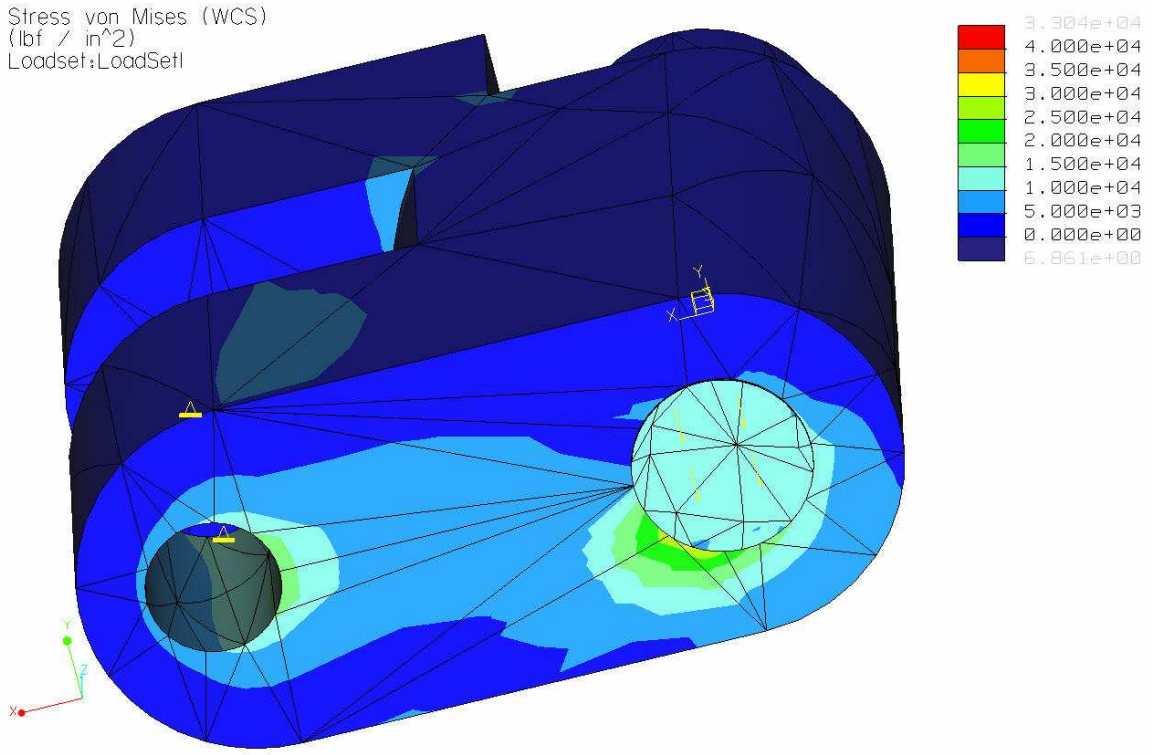

Figure 33: The Max Von-Mises Stress of 33,040 psi, for the 3 Degree Camber Fork and Bolt Analysis

The difference in the stress values was considered to be a result of the change in loading conditions. Because there was not a surprising difference between the two stress values, it was considered safe to be able to disregard the warning about the contact area. As stated earlier in the paper, the bolt/quick-release pin was not analyzed because they are standard to all wheelchairs and have been proven to be reliable. The process by which Pro-Mechanica determines convergence will now be discussed.

The convergence for the 3 degree camber model was set to 10%, which means that the difference between the strain energy for the 6^{th} order polynomial and the 7^{th} order polynomial was within 10%. This was considered sufficient because the analysis was only used to determine how much times the static load the suspension system could withstand. As can be seen from Figure 34-a and 34-b, the von Mises stress can behave rather erratically, while the strain energy increases in an asymptotic manner. Due to this behavior, the strain energy is considered a better measure to use when monitoring convergence [9].

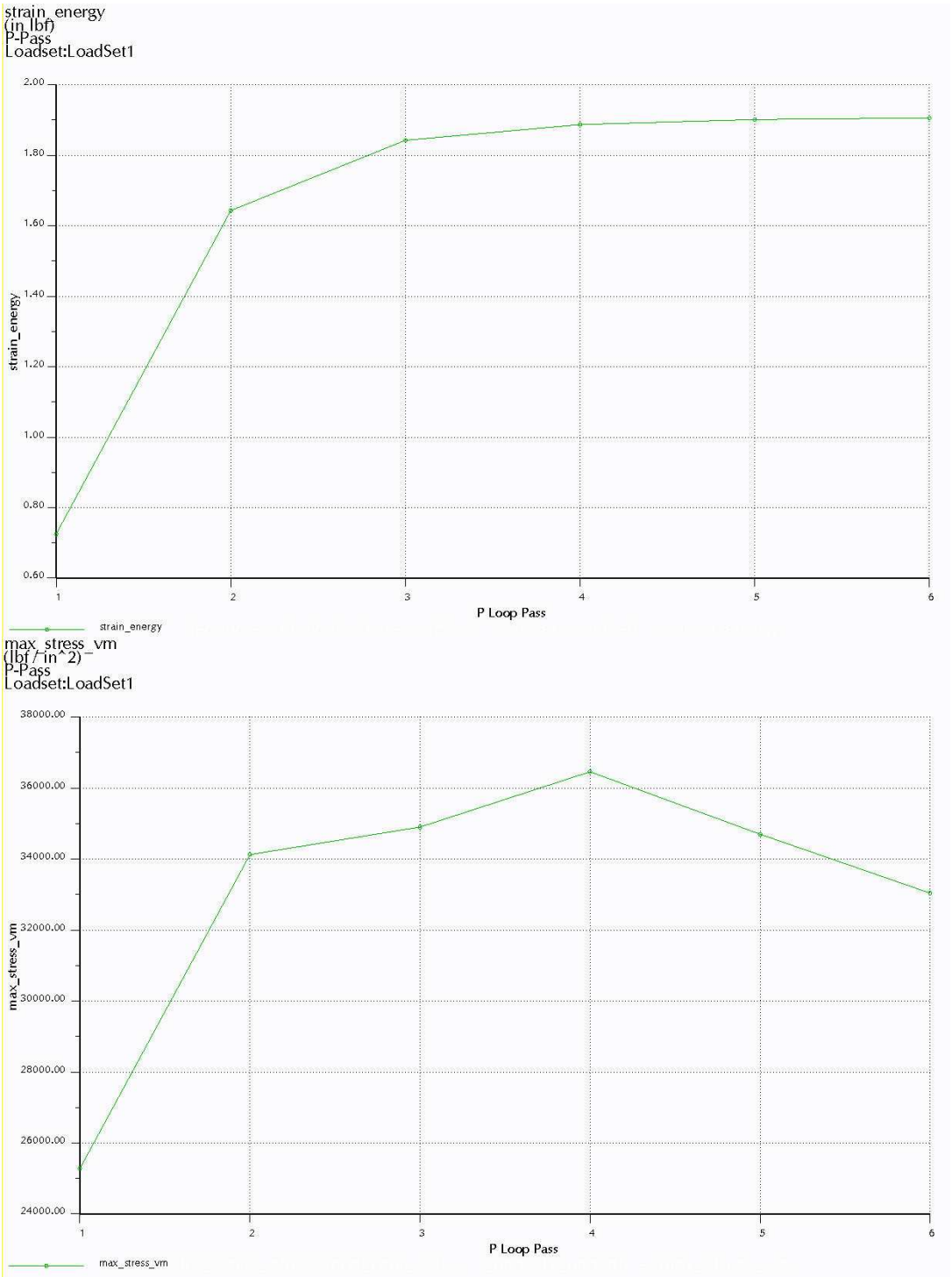

Figure 34: Convergence Graphs

a. **(top) The strain energy convergence graph for the fork and pin analysis.**
b. **(bottom) The max von-Mises stress convergence graph for the fork and pin analysis.**

6.2 Inner Hub and Pin Results

A load of 60 lbs, which is 10 times the transverse portion of the static load, was applied to the side of the lower extension of the inner hub in order to simulate the torque load applied to a tilted wheel. When the model was run, the results output file also gave the following warning:

** Warning: Contact area is small in comparison to size
of adjacent element edges for one or more
contact regions for all load factors above
marked with a "*". If you need pressure results
near the contact regions, use single-pass
adaptive convergence and select Localized
Mesh Refinement.

The model was rerun using single-pass adaptive convergence with localized mesh refinement, but the same warnings were stated again. Also, the stress results in the output file were exactly the same as the stress results in the previous output file. Since using a 20 degree camber caused the warning to go away in the fork and bolt analysis, an analysis using a 20 degree camber was also ran here. However, the warnings still occurred. This is probably due to the fact that while the magnitude of the load was changed, the loading orientation was still the same. For the case with the fork and bolt, when the 20 degree camber load values were used, the load orientation was changed. In the previous analysis of the fork and bolt, it was decided that the warning about the contact area could be disregarded. Therefore, the warning will be disregarded here as well.

Regarding the maximum allowable degree of camber, the von-Mises stress value for the 20 degree camber was 212,618 psi, which exceeds the yield strength of Aluminum. Available angles of camber for wheelchairs include 3, 6, 9, 12, 15, 18, and 20 [12]. A number of analysis were run using the different camber angles in order to find the steepest camber that could be used before the inner hub and pin failed. It was found that the maximum camber that could be used was 3 degrees. When a camber of 6 degrees was used, the transverse portion of the 10 times static load was 120 lbs. The resulting von-Mises stress for this load was 65,421 psi, which exceeds the 40,000 psi yield strength of the aluminum. For further research, the loading of the model should be analyzed further in order to see if the inner hub and pin are subjected to the full transverse portion of the static load, or if the wheels' interaction with the ground lessens some of this load.

Now getting back to the model at hand, the 3 degree camber model converged after an edge order of 8 was used. Again, the convergence for the model was set to 10%. The maximum von-Mises stress obtained for the inner hub was 31,455 psi, located near the bottom of the 3/8" diameter hole. In Figure 35 below, the yellow shaded area is where this stress occurs. Again, since the yielding strength of 6061 T-6 aluminum is 40,000 psi, this FEA analysis has shown that the 3/8" diameter hole in the inner hub should not experience failure.

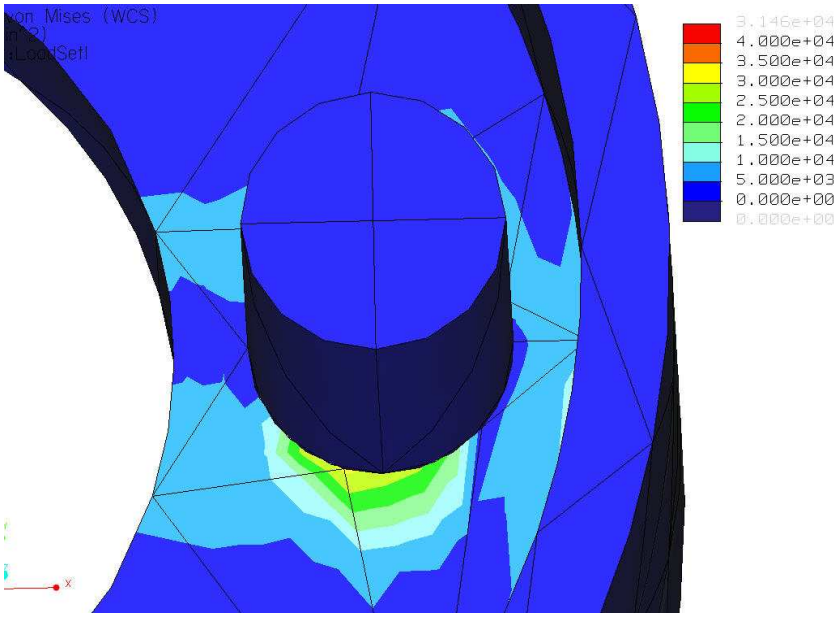

Figure 35: Close-up of the Max Von-Mises Stress of 31,455 psi for the Inner Hub and Pin Analysis

6.3 Inner Hub and Ball Bearing Results

As stated earlier, a load of 575 lbs was applied to both of the surfaces of the inner hub that the ball-race bearings are press fitted onto, to give a total load of 1150 lbs. This is 10 times the normal portion of the static load. The model converged after an edge order of 9 was used, which is the maximum edge order available in Pro-Mechanica. Again, the convergence for the model was set to 10%. This model probably required a 9^{th} order polynomial for convergence because of the sharp edges made by the square cut-out, and because the bottom surface of this cut-out was constrained in all six degrees of freedom.

The maximum von-Mises stress obtained for the inner hub was only 20,380 psi, and is located near the edges of the square cut-out. Figure 36, shows the default legend values, 2,040 psi to 18,340 psi. This range of values is better for showing the details of the stress contour, than the true legend values of 0psi to 40,000 psi shown in Figure 37.

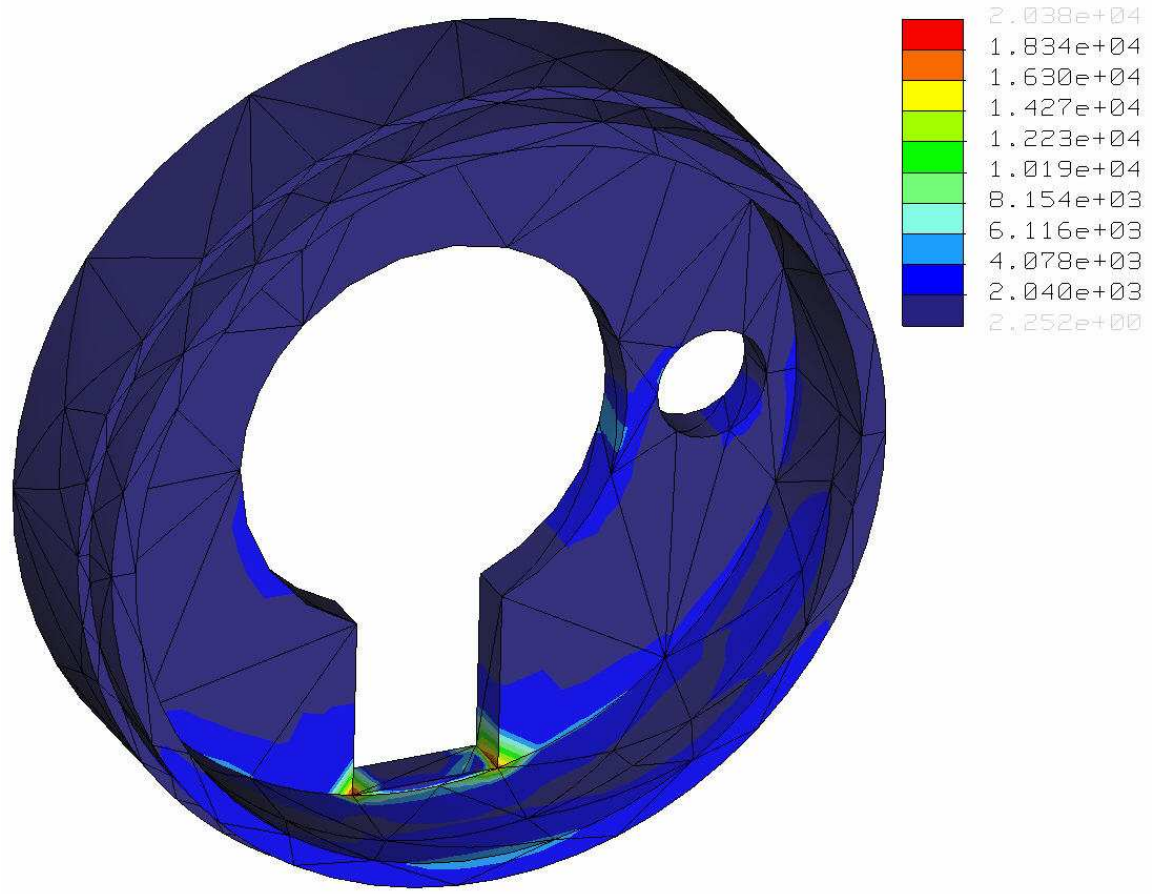

Figure 36: The Max Von-Mises Stress of 20,380 psi, for the Inner Hub and Ball Bearing Analysis Legend Values Are Set Between 2,040 psi and 18,340 psi

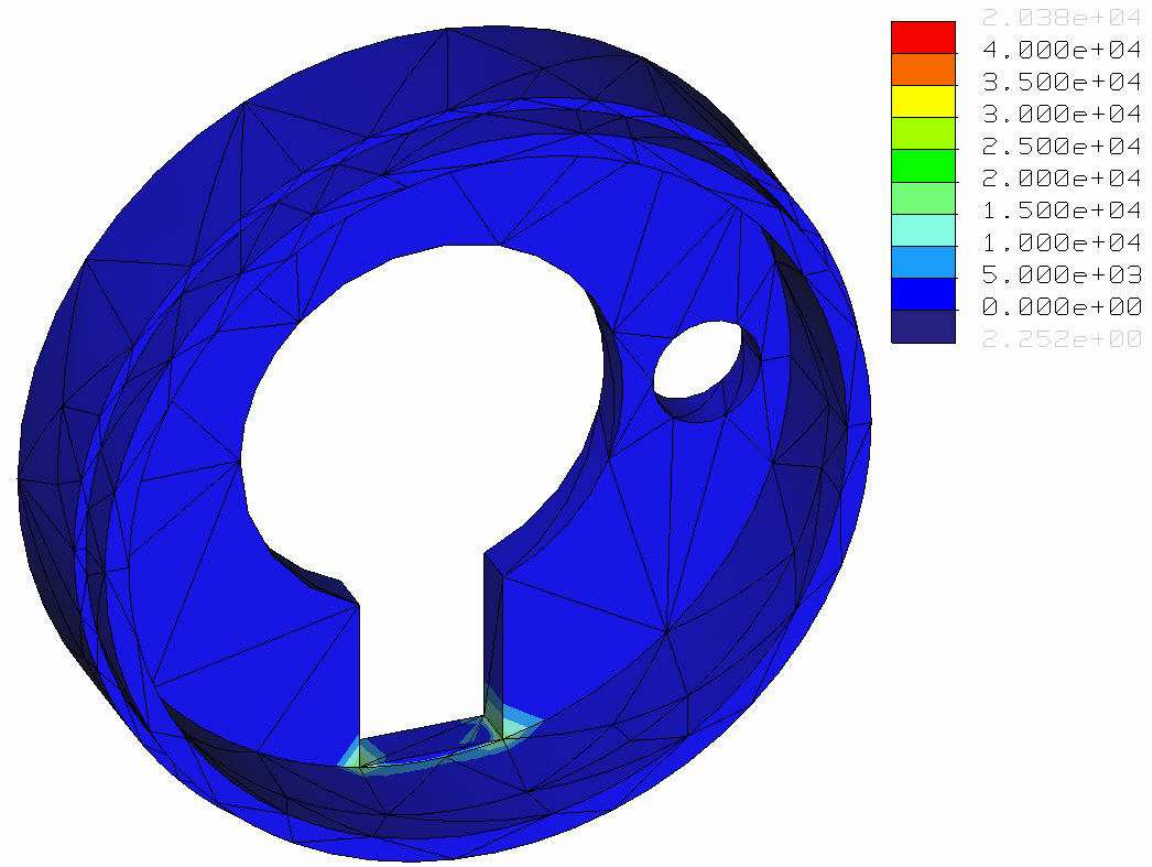

Figure 37: Using a Range of 0 to 40,000 psi for the Legend, the Stress Contour Shows that the Inner Hub Experiences Very Little Stress

This FEA analysis has shown that the stresses in the inner hub do not even come close to the 40,000 psi yield strength of the aluminum, and failure should not occur. These results confirm that the use of symmetry for this model was appropriate. For further analysis, an optimization study should be done in Pro-Mechanica in order to decrease the size/weight of the inner hub. In an optimization study, a desired goal is specified (ie. minimum mass) and Mechanica searches for a design that satisfies the goal based on the constraints applied [9].

6.4 Outer Hub and the Spokes Results

As stated earlier, a load of 287 lbs was applied to the top spoke hole of the outer hub model. When the results of the analysis were examined with the thesis committee, the suggestion was made that a pie-slice model would be more accurate. However, for this elementary analysis, it was determined that the current analysis would suffice. The 287lbs load simulates 5 times the normal portion of the 10 times static load. The model converged after an edge order of 6 was used. Again, the convergence for the model was set to 10%.

The maximum von-Mises stress obtained for the inner hub was 37,231 psi, and is located at the top of the upper spoke hole, as shown in Figure 38 below. This FEA analysis has shown that even with a five times static load applied to one spoke hole, the stresses in the outer hub are still under the 40,000 psi yield strength of the aluminum. Figure 38 is an over all picture stress contours of the outer hub. For further analysis, an optimization study should be done on the outer hub as well as the inner hub in order to decrease its size/weight.

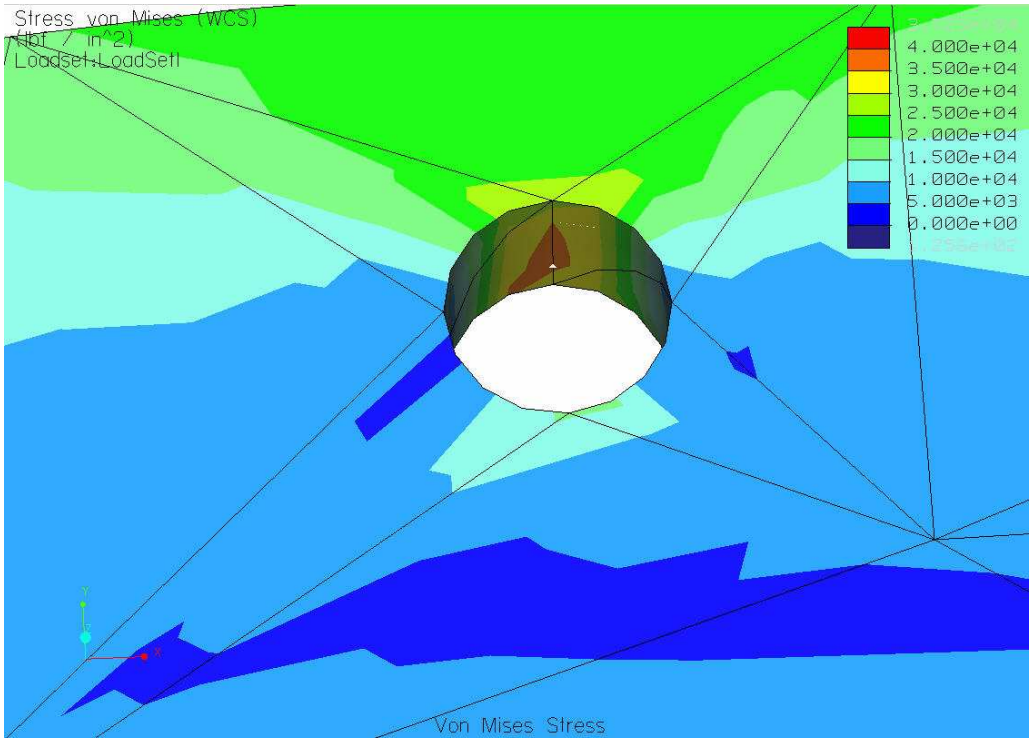

Figure 38: The Max Von-Mises Stress of 37,231 psi, for the Outer Hub Spoke Hole Analysis, is Located at the Top of the Upper Spoke Hole

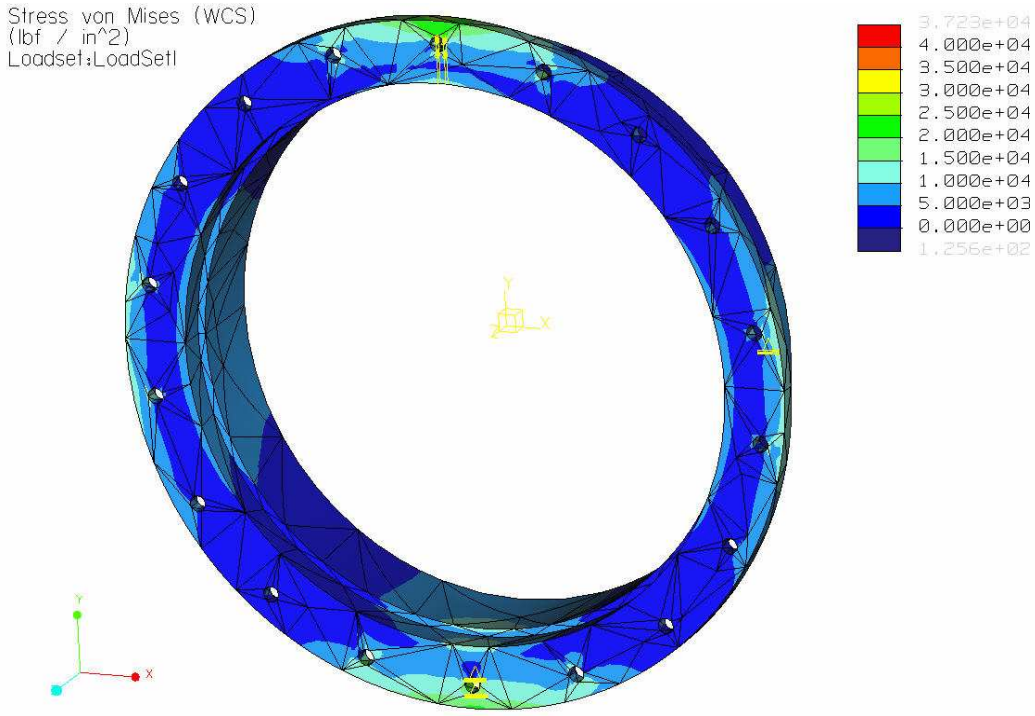

Figure 39: Over-all Von-Mises Stress Contour for the Outer Hub Analysis

7. Prototype

After the FEA results were studied, a prototype was made. Some problems with the design were discovered during the machining and assembly processes, and also while installing the suspension system on a wheelchair. This section will go into further detail about what problems were detected, and what was done to fix them.

7.1 Machining and Assembly Process

During the machining process, it was discovered that the cut-out in the inner hub for the polyurethane was not big enough for the fork to be inserted into the inner hub. To fix this, the slot for the polyurethane rubber was increased from ¾" wide to 1" wide. Then, the 1" tall fork was able to slide through the 1" rubber slot. In section 6.3, the stress in the inner hub was shown to be very low. Therefore, it was assumed that this modification will not significantly affect the stress distribution of the inner hub.

During the assembly of the prototype, a problem with the ball-race bearings was discovered. The recesses in the inner and outer hubs, for the 4" ball-race bearings, have a press fit of 0.0015". This press fit caused the inner diameter of the ball-race bearings to be slightly expanded, and the outer diameter of the ball-race bearings to be slightly compressed. Because of this extra pressure on the balls, the bearings spun more sluggishly. To address this problem, a press fit of 0.001" should be tried for future assemblies. The use of a thin section retaining ring should also be considered.

7.2 Installation on a Wheelchair

When the suspension was installed on a wheelchair, some problems were discovered. This section will discuss these problems, and how they can be fixed.

7.2.1 Wheel Wobble

To start with, the fit between the 3/8" dowel pin and the needle roller bearing in the inner hub is too loose because the diameters of the dowel pin and the bearing are not exactly the same. This causes the wheel to wobble about the fork/pin interface. Four nylon washers, two on either side of the needle roller bearing in the inner hub, were supposed to be inserted between the fork and the bearing/web of the inner hub. However, only 3 washers could be inserted. A couple solutions to this wobble problem will now be discussed.

One solution would be to have a tighter fit between the two sides of the fork and the web of the inner hub. Instead of a 5/8" gap between the two sides of the fork, the gap could be reduced to 11/16", and washers would still be used. Another solution is to have a hardened steel bushing inserted into the inner hub instead of a needle roller bearing. Then, two needle roller bearings would be inserted into each side of the fork. Doing this should eliminate the wobble, and still allow the fork to rotate about the small hole in the inner hub. Set screws would be used to keep the dowel pin from sliding out of the fork. See Figure 40 and 41 below.

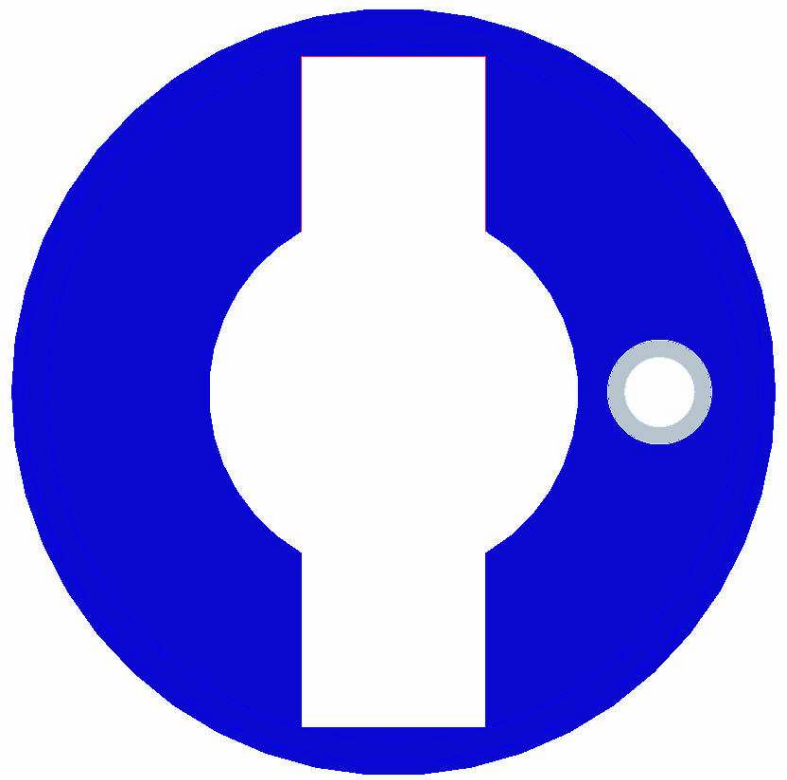

Figure 40: Inner Hub Re-Design - With Hardened Stainless Steel Bushing, and a Second Cut-Out for the Silicone Rubber

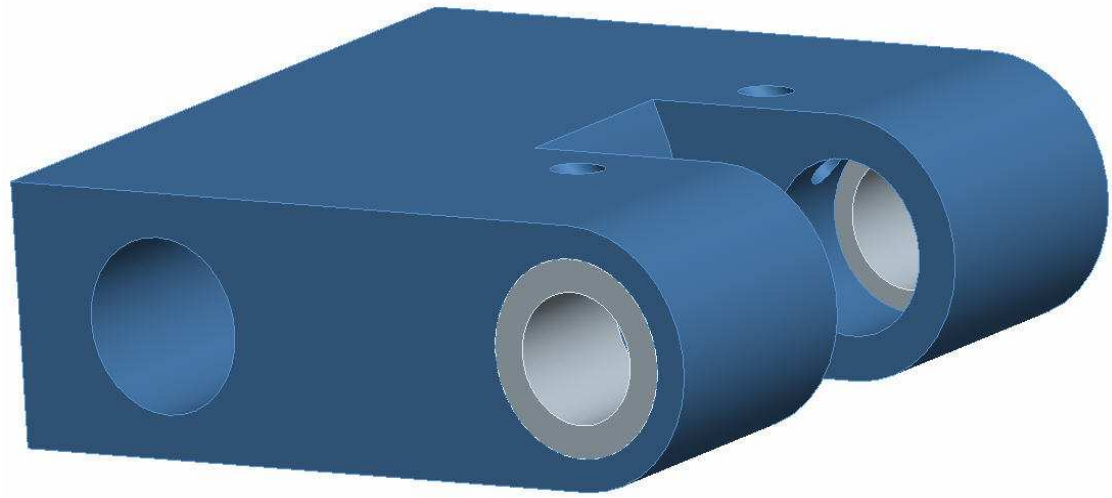

Figure 41: Fork Re-Design - Needle Roller Bearings are Inserted Into Either Side of the Fork

7.2.2 Polyurethane Issues

Another problem that was discovered is that when the polyurethane is inserted into the inner hub, the fork rotates upward with respect to the inner hub, and the bolt is no longer at the center of the wheel. See Figure 42.

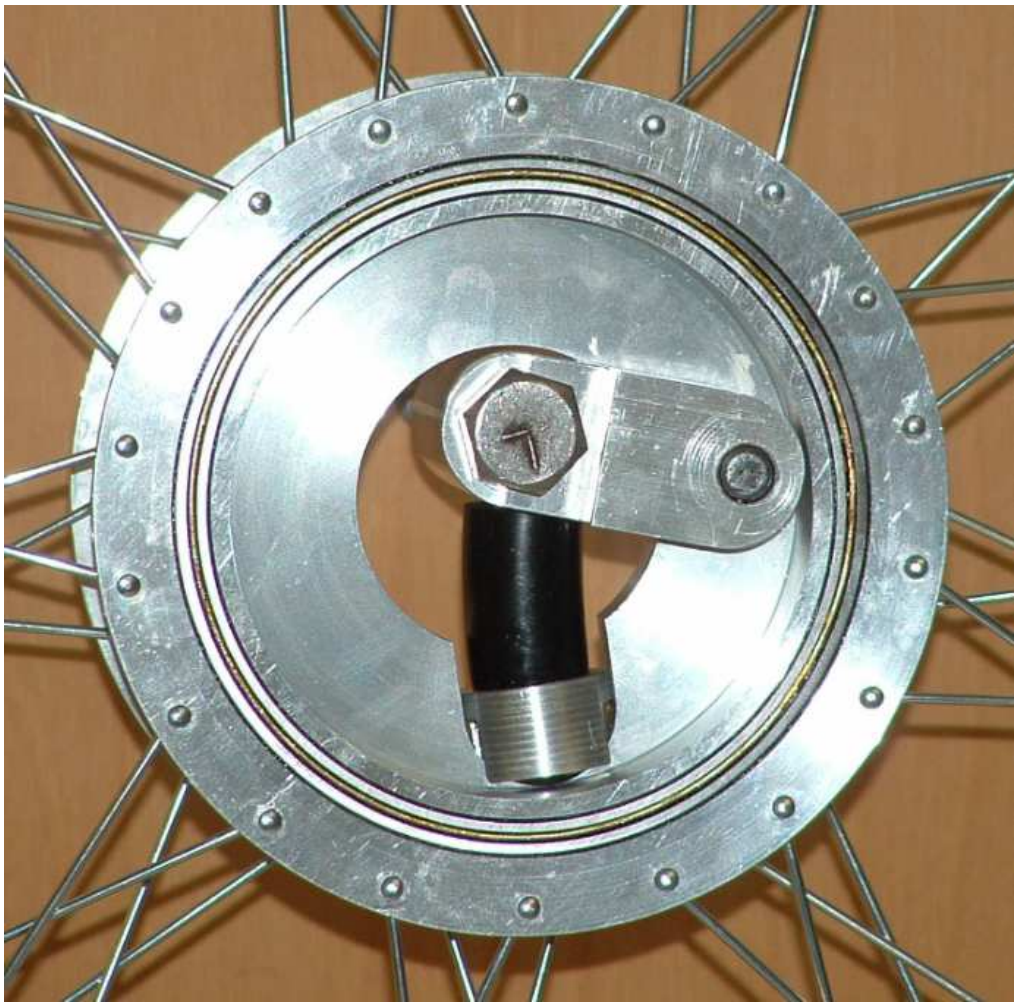

Figure 42: The Polyurethane Causes the Fork to Rotate Upward When there is No One in the Wheelchair

This happens because the polyurethane is oversized so that when the wheelchair user sits in the chair, the fork/bolt will return to center of the wheel. See Figure 43 below.

Figure 43: Suspension System with Someone Sitting in the Wheelchair

However, when the user gets out of the chair, the wheel becomes un-centered again, and the wheelchair brakes are unable to grip the wheel. In order to keep the bolt at the center of the wheel, another cut-out should be made in the inner hub and a piece of silicone rubber should be inserted. Figure 40, from a few pages ago, shows this second cut-out.

A good option for the silicone rubber would be a silicone with a 60 Shore-A durometer. This is stiffer than the 40 Shore-A durometer polyurethane that is used under the fork. The stiffer silicone will be able to keep the bolt centered in the wheel, because it will not be compressed by the force of the polyurethane. The 60 Shore-A Silicone was chosen over a 60 Shore-A Polyurethane because the Silicon is orange, and the

polyurethane is black. This will prevent the wheel from being installed upside down. For a picture of the modified suspension system, see Figure 44 below.

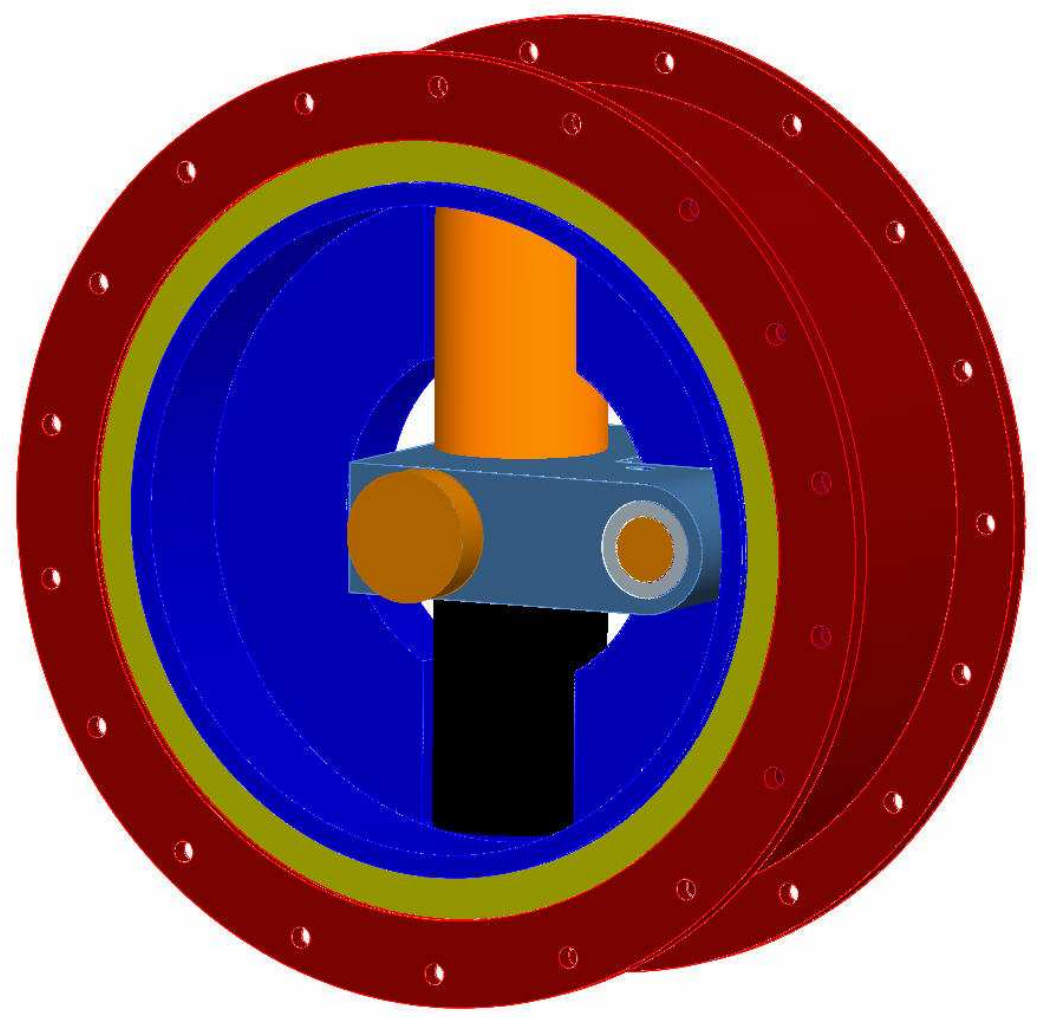

Figure 44: Re-Designed Suspension System

Also of concern is the ability of the polyurethane slip out of place. Figure 42 shows that if the Polyurethane is simply squished between the fork and the inner hub, the only thing preventing it from slipping out is the compression of the cylinder, and the friction between the cylinder, fork, and inner hub. To prevent this from occurring, a collar was made for the Polyurethane. This collar can be seen on the bottom of the

polyurethane in Figure 42. Also, to prevent the Polyurethane from slipping off the back of the fork, the fork should not be rounded at the back. See Figure 44 for a model of a fork that is not rounded at the back.

Even though the inner hub was modified, the FEA results from the original model were considered sufficient. This is because the stainless steel bushing is the same size as the needle roller bearing, and the top cut-out will have the same stress contour as the bottom cut-out, due to symmetry. Since section 6.3 showed that the bottom cut-out was not even close to failure, there is no need to run a new analysis.

Figure 46 is an overall picture of the after-market suspension system on a wheelchair wheel, and Figure 47 is a picture of the suspension system installed on the author's wheelchair.

Figure 45: Overall Picture of After-Market Suspension System

Figure 46: After-Market Suspension System on Author's Wheelchair

8. Conclusions

This thesis has shown a successful design for an after-market suspension system for the rear wheels of wheelchair. The analysis showed that the suspension system should not fail when subjected to 10 times the static load, which was considered large enough to encompass the forces that a wheelchair wheel is typically subjected to.

The modifications that were made to the prototype should be sufficient to eliminate the wobble in the suspension system. There is room for further work in the area of weight reduction, and in the use of the suspension system on steeper wheel cambers. Further study should also be done on the Polyurethane to determine which shape and durometer provides the most shock and vibration reduction. It would also be advisable to perform a double-drum and a curb-drop test on the suspension system to determine how durable it is. It can be seen where failure takes place, and the system can be strengthened.

References

1. Cooper, Rory. Rehabilitation Engineering Applied to Mobility and Manipulation. Philadelphia , PA: Institute of Physics Publishing Bristol and Philadelphia, 1995. Pages 115-116, 255-256.

2. Kwarciak, Cooper, Ammer, Fitzgerald, Boninger, Cooper. "Fatigue Testing of Selected Suspension Manual Wheelchairs Using ANSI/RESNA Standards." Archives of Physical Medicine and Rehabilitation, Volume 86, Issue 1, January 2005, Pages 123-129.

3. Frog Legs. Accessed 1-27-07, http://www.froglegsinc.com/ultrasports.php?black.

4. Ashby, Mike, and Johnson, Kara. Materials and Design, The art and science of Material Selection in Product Design. Woburn, MA: Butterworth-Heinemann, 2002. Pages 179-182.

5. Fitzgerald, Cooper, Boninger, Rentschler. "Comparison of Fatigue Life for 3 Types of Manual wheelchairs." Archives of Physical Medicine and Rehabilitation Volume 82, Issue 10, October 2001, Pages 1484-1488.

6. Silverthin Selection Guide. Accessed 1-27-07, http://www.silverthin.com/1select.htm.

7. Silverthin Precision Thin Section Bearings. Accessed 1-27-07, http://www.silverthin.com/5sa.htm .

8. McMaster-Carr Supply Company. Accessed 1-27-07, http://www.mcmaster.com.

9. Toogood, Roger. Pro-Engineer Wildfire 3.0 Mechanica Tutoril. Edmonton, Alberta: Schroff Development Corporation, 2006. Pages 2-19.

10. Adams, Vince, and Askenazi, Abraham. Building Better Products With Finite Element Analysis. Sante Fe, NM: OnWord Press, 1998. Pages 59-62, 97.

11. Ansel C. Ugural, and Saul K. Fenster. Advanced Strength And Applied Elasticity, 3rd Ed. Prentice Hall, 1995. Upper Saddle River, NJ. Pages 172-175.

12. Wheelchair camber information. Accessed 1-27-07, http://www.spinlife.com/Invacare-Top-End-Terminator-Titanium-Titanium-Wheelchair/spec.cfm?productID=69887.

Appendices

Appendix A: Detailed Drawings of the Fork, Inner Hub, and Outer Hub

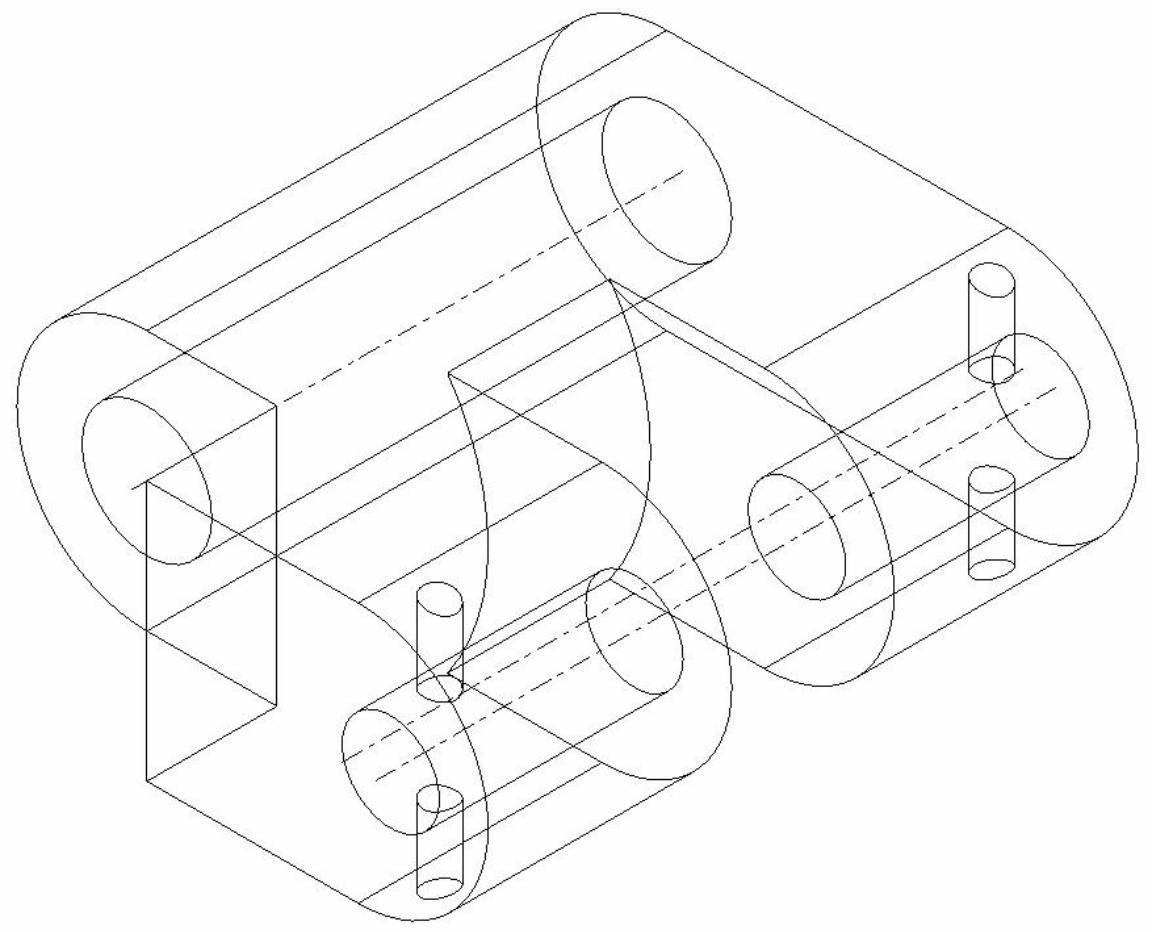

Figure 47: Fork Drawing– Isometric View

Appendix A: (Continued)

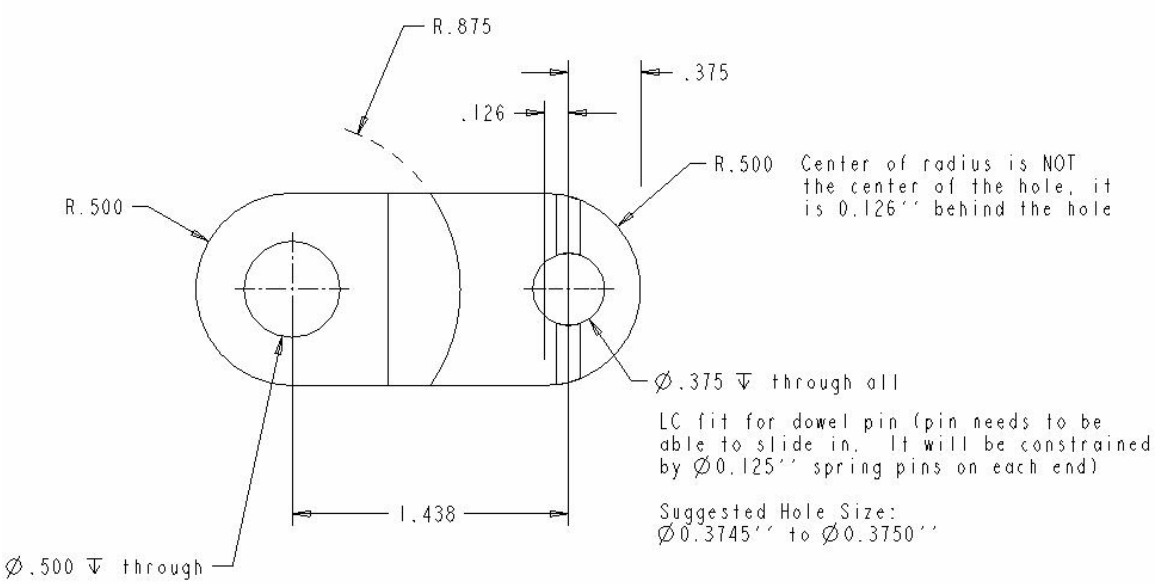

Figure 48: Fork Drawing– Front View

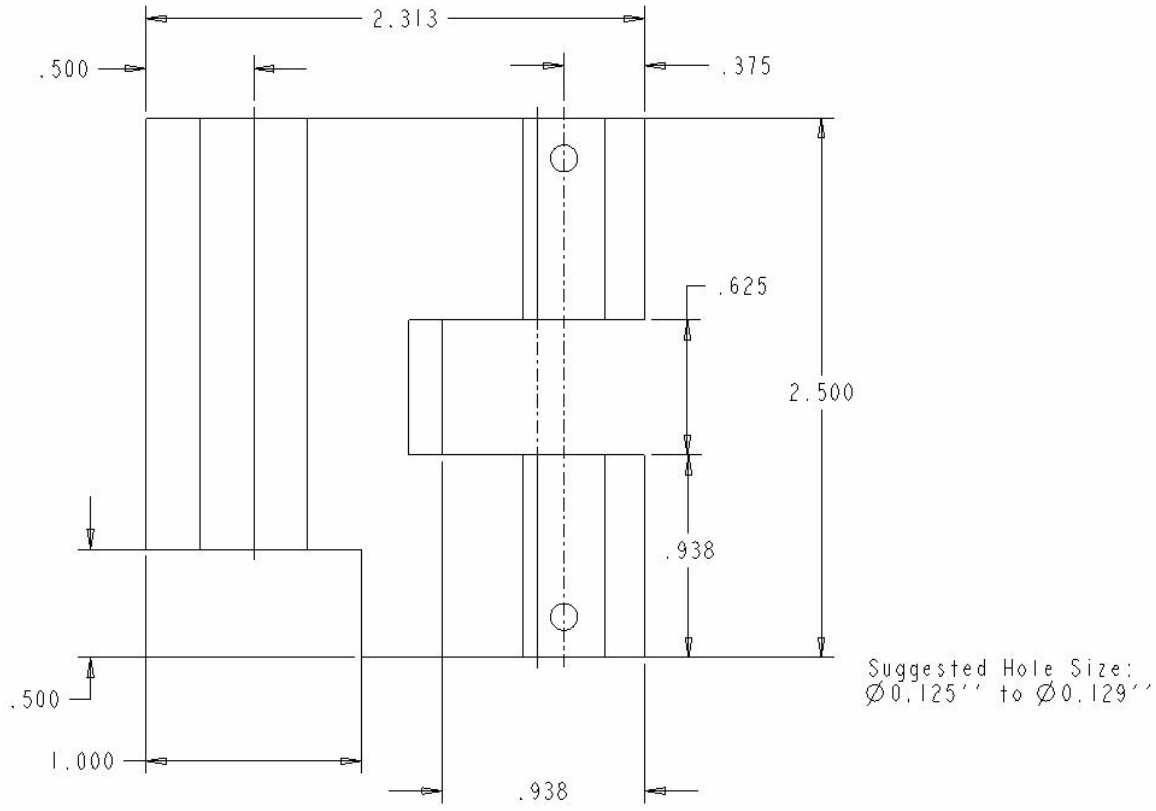

Figure 49: Fork Drawing– Top View

Appendix A: (Continued)

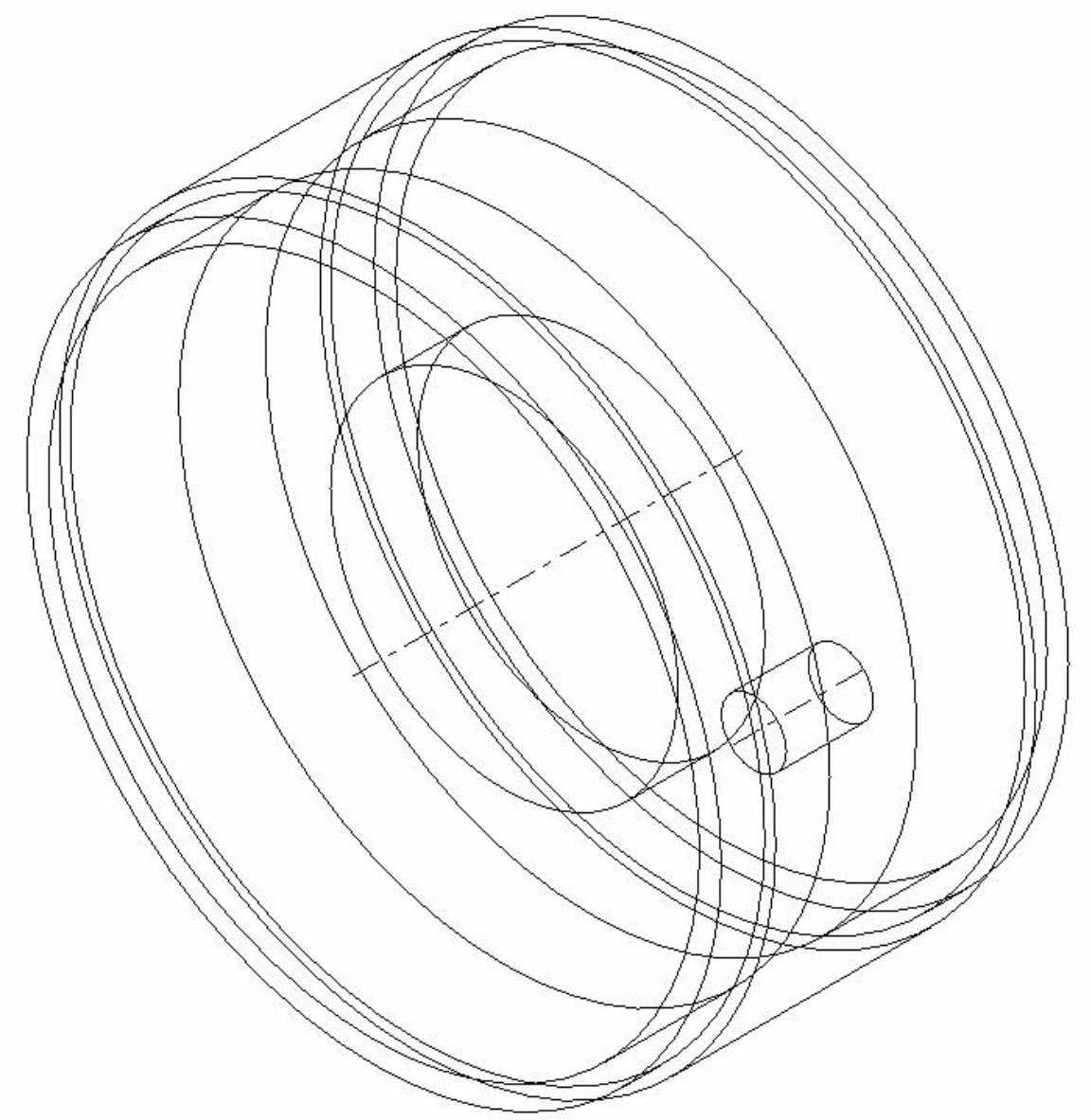

Figure 50: Inner Hub Drawing– Isometric View

Appendix A: (Continued)

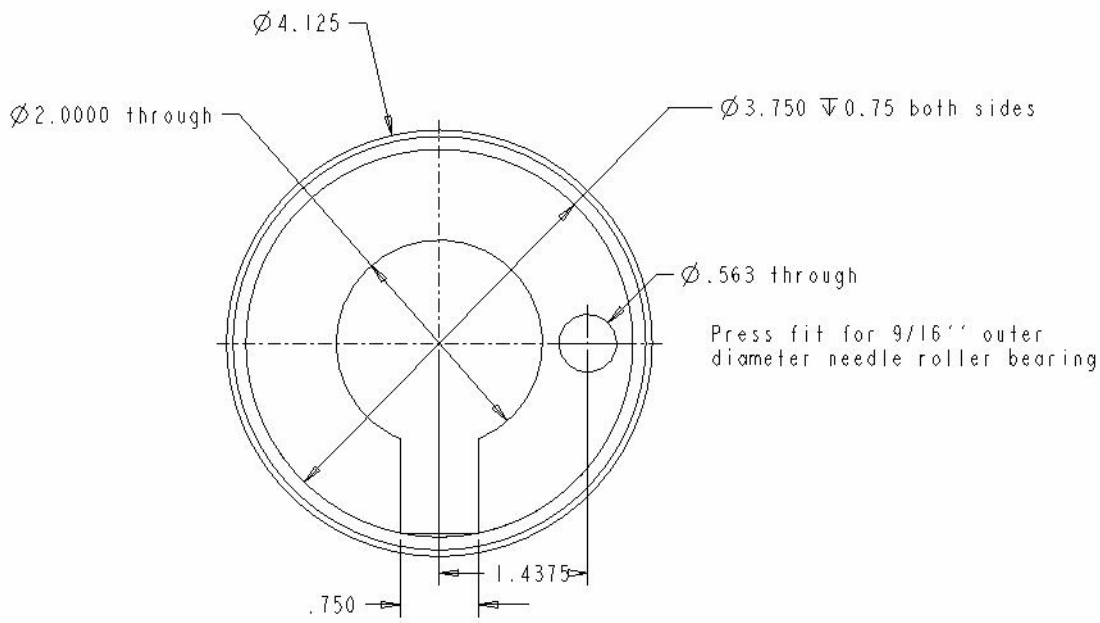

Figure 51: Inner Hub Drawing– Front View

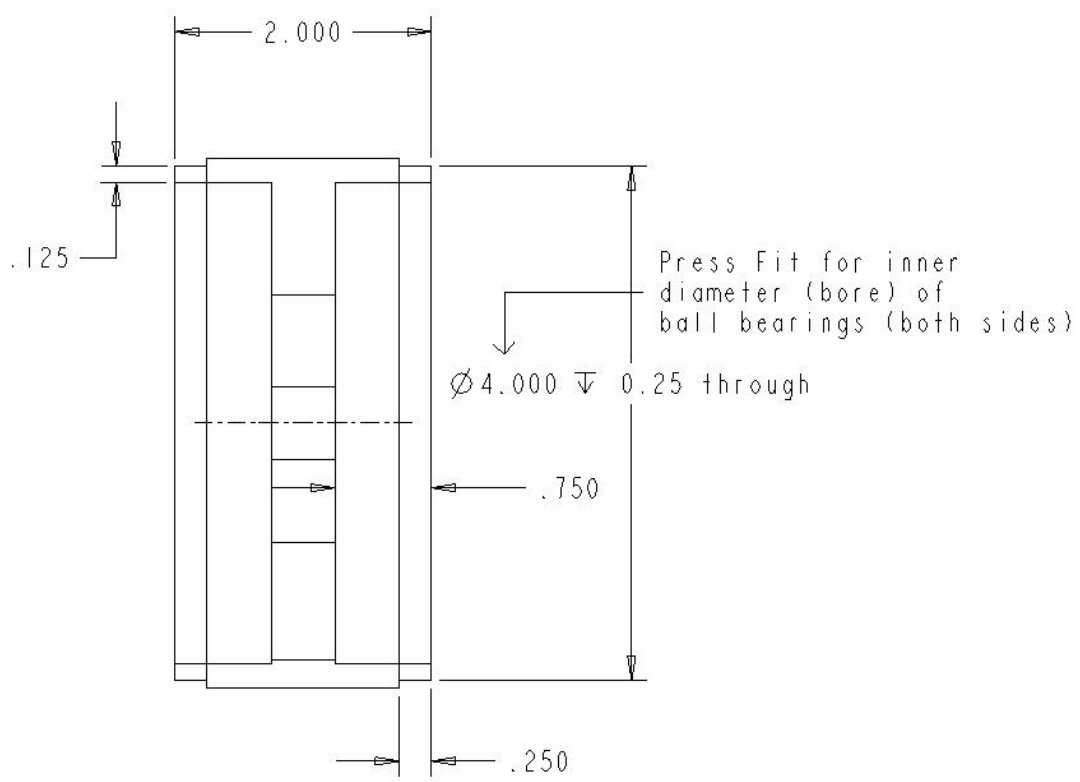

Figure 52: Inner Hub Drawing– Side View

Appendix A: (Continued)

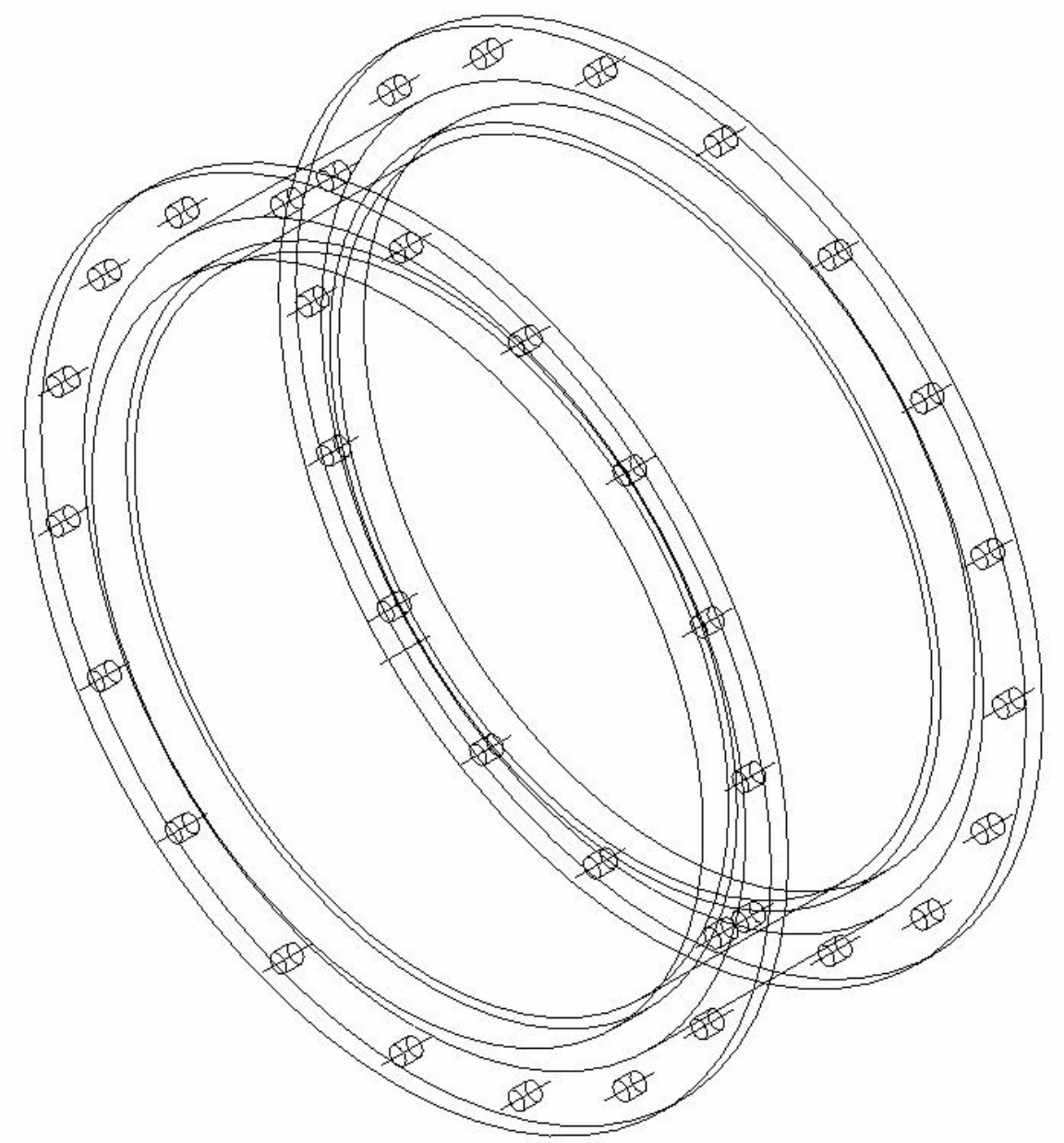

Figure 53: Outer Hub Drawing– Isometric View

Appendix A: (Continued)

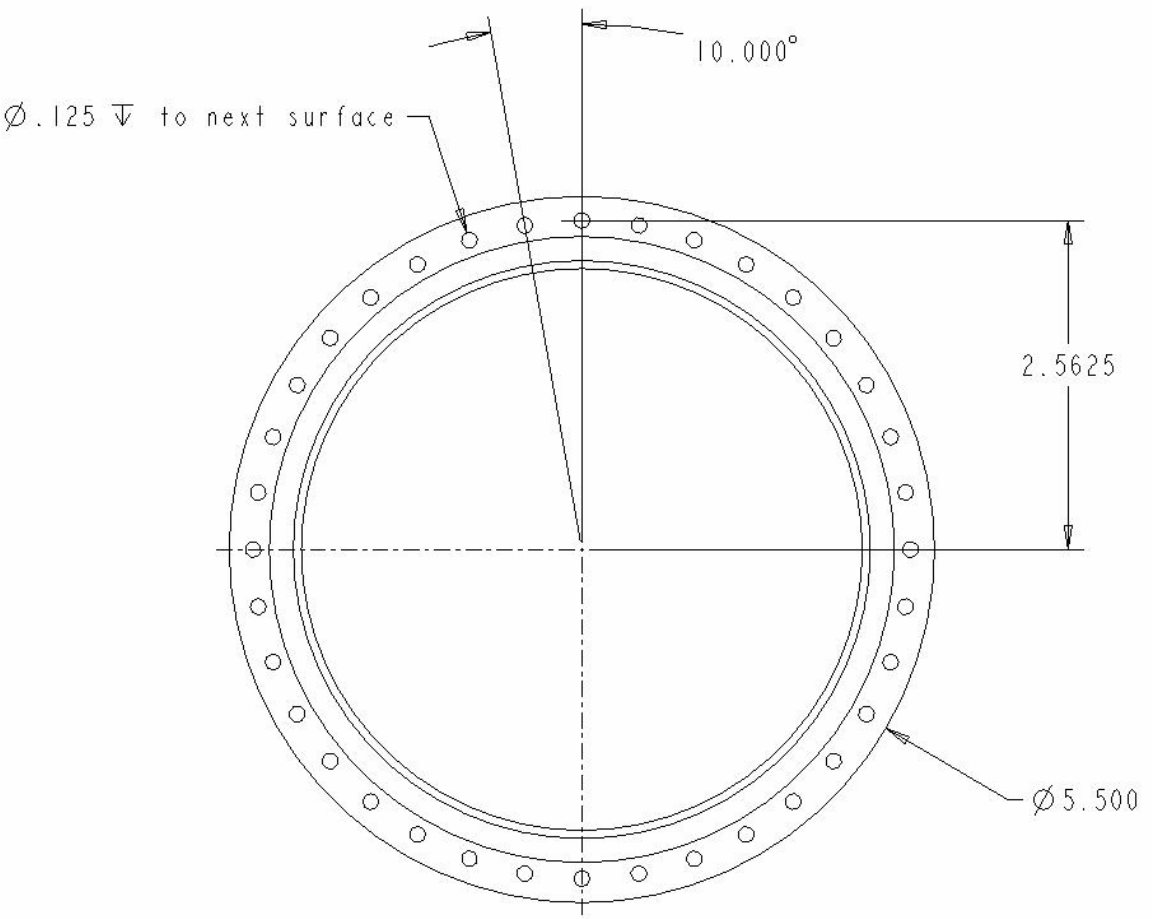

Figure 54: Outer Hub Drawing– Front View

Appendix A: (Continued)

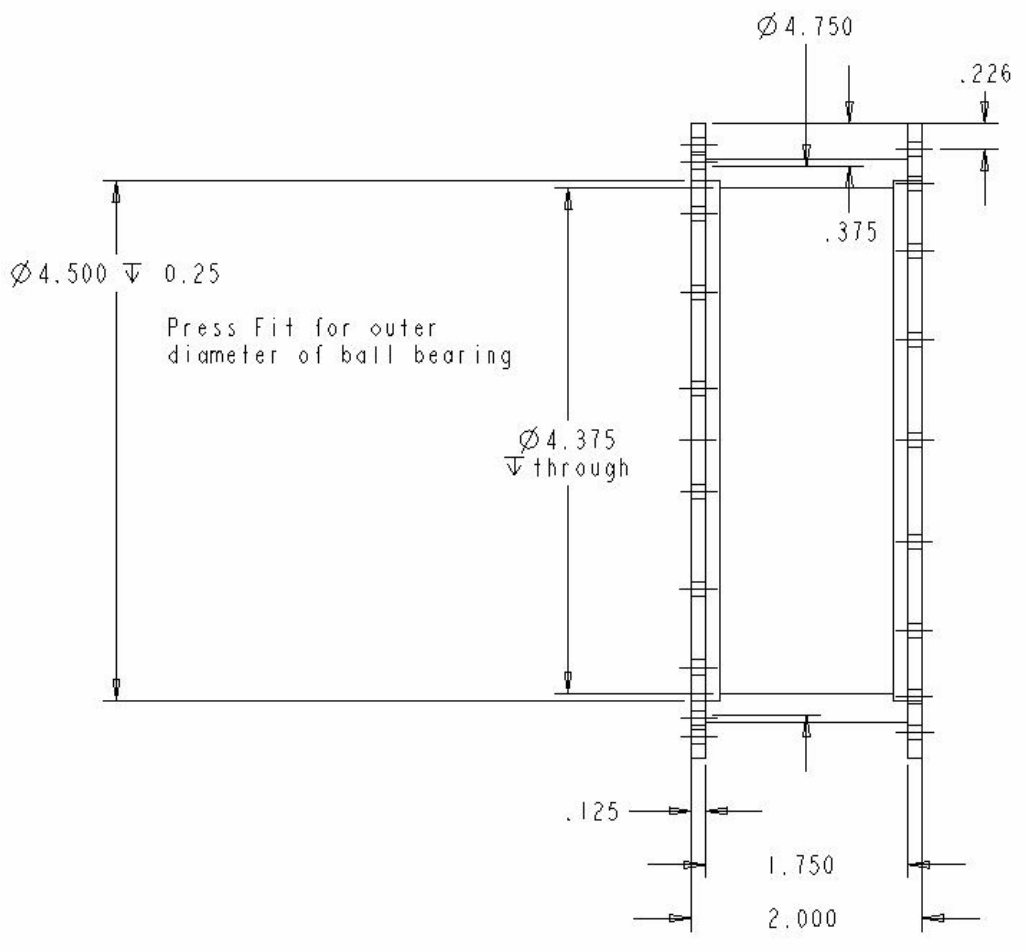

Figure 55: Outer Hub Drawing– Side View

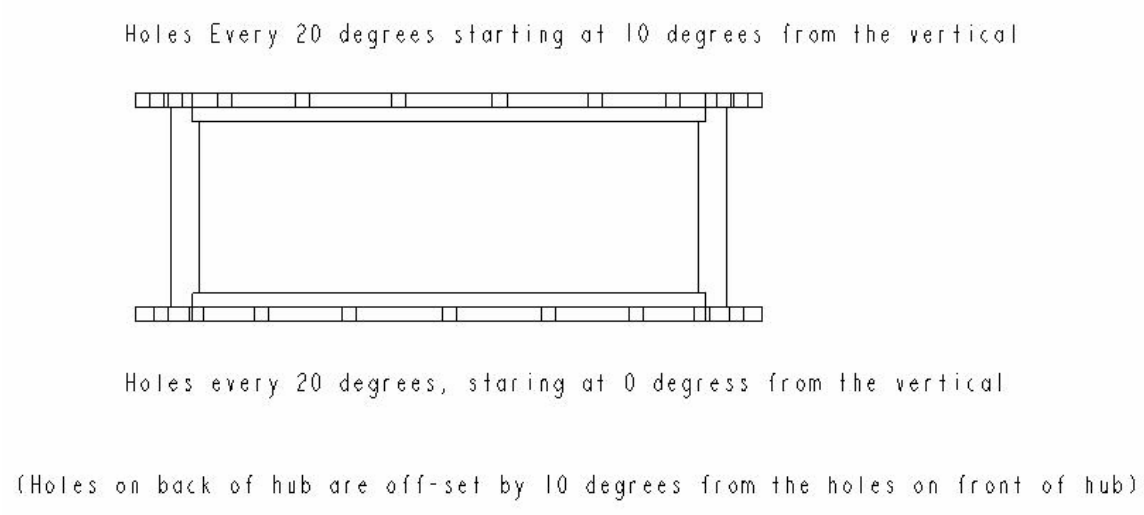

Figure 56: Outer Hub Drawing– Top View

Appendix B: Rubber and Foam Comparison Chart From McMaster-Carr

Resistance to:								
Material	**Oil**	**Abrasion**	**Tearing**	**Impact**	**Weather**	**Chemicals**	**Electricity**	**Flame**
Buna-N	Excellent	Good	Fair	Fair	Poor	Fair	Poor	Poor
Butyl	Poor	Good	Good	Fair	Good	Not Rated	Excellent	Poor
ECH	Excellent	Good	Fair	Fair	Good	Good	Good	Poor
EPDM	Poor	Good	Poor	Fair	Excellent	Good	Fair	Poor
EVA	Good	Good	Good	Excellent	Good	Good	Good	Fair
Gum	Poor	Excellent	Good	Excellent	Fair	Fair	Excellent	Poor
Hypalon	Fair	Good	Fair	Fair	Excellent	Good	Good	Good
Ionomer	Excellent	Excellent	Excellent	Excellent	Excellent	Excellent	Good	Good
Latex	Poor	Excellent	Excellent	Excellent	Fair	Good	Excellent	Poor
Neoprene	Good	Good	Fair	Good	Good	Fair	Fair	Good
Polyethylene	Good	Good	Excellent	Excellent	Good	Good	Fair	Fair
Polyimide	Excellent	Poor	Poor	Poor	Poor	Excellent	Excellent	Excellent
Polyurethane	Excellent	Excellent	Excellent	Excellent	Good	Good	Good	Poor
Santoprene	Fair	Good	Fair	Good	Excellent	Fair	Fair	Poor
SBR	Poor	Good	Good	Excellent	Fair	Poor	Poor	Poor
Silicone	Fair	Poor	Poor	Fair	Excellent	Fair	Good	Fair
Vinyl	Good	Fair	Fair	Good	Good	Fair	Not Rated	Poor
Viton	Excellent	Good	Poor	Poor	Good	Good	Good	Excellent

Figure 57: Comparison of Rubber and Foam Chart

Appendix C: Fork and Bolt Analysis – 20 Degree Camber

This is the "run status" out-put file for the Pro-Mechanica analysis of the Fork and Bolt analysis. A camber of 20 degrees was used, 10 times the static load was applied, and the convergence was set to 10%.

Mechanica Structure Version K-01-41:spg
Summary for Design Study "ten_x_static_load_near_fork_1"
Thu Jan 25, 2007 16:05:34

Run Settings
Memory allocation for block solver: 128.0
Checking the model before creating elements...
These checks take into account the fact that AutoGEM will
automatically create elements in volumes with material
properties, on surfaces with shell properties, and on curves
with beam section properties.

Generate elements automatically.
Checking the model after creating elements...

No errors were found in the model.

Mechanica Structure Model Summary

Principal System of Units: Inch Pound Second (IPS)

Length: in
Force: lbf
Time: sec
Temperature: F

Model Type: Three Dimensional

Appendix C: (Continued)

Points: 265
Edges: 1107
Faces: 1423

Springs: 0
Masses: 0
Beams: 0
Shells: 0
Solids: 582

Elements: 582

Contact Regions: 3

Standard Design Study

Description:
10% convergence
1080 lbs normal
390 lbs transverse

Static Analysis "ten_x_static_load_near_fork_1":
Contact Analysis

Convergence Method: Multiple-Pass Adaptive
Plotting Grid: 4

Convergence Loop Log: (16:05:43)

>> Pass 1 <<
Calculating Element Equations (16:05:43)

Appendix C: (Continued)

Total Number of Equations: 630
Maximum Edge Order: 1
Solving Equations (16:05:44)
Load Increment 0 of 1
Load Factor: 0.00000e+00
Contact Area: 0.00000e+00
Calculating Disp and Stress Results (16:05:45)
Load Increment 1 of 1
Load Factor: 1.00000e+00
*Contact Area: 1.21210e+00

** Warning: Contact area is small in comparison to size
of adjacent element edges for one or more
contact regions for all load factors above
marked with a "*". If you need pressure results
near the contact regions, use single-pass
adaptive convergence and select Localized
Mesh Refinement.
Calculating Disp and Stress Results (16:05:54)

Post-Processing Solution (16:05:55)
Checking Convergence (16:05:55)
Elements Not Converged: 582
Edges Not Converged: 1107
Local Disp/Energy Index: 100.0%
Global RMS Stress Index: 100.0%
Resource Check (16:05:56)
Elapsed Time (sec): 22.18
CPU Time (sec): 20.67
Memory Usage (kb): 192486
Wrk Dir Dsk Usage (kb): 5131

Appendix C: (Continued)

```
>> Pass  2 <<
      Calculating Element Equations          (16:05:56)
        Total Number of Equations:    3579
        Maximum Edge Order:             2
      Solving Equations                      (16:05:56)
      Load Increment 0 of 1
      Load Factor:  0.00000e+00
      Contact Area:  0.00000e+00
      Calculating Disp and Stress Results     (16:05:59)
      Load Increment 1 of 1
      Load Factor:  1.00000e+00
     *Contact Area:  1.63034e+00

** Warning: Contact area is small in comparison to size
        of adjacent element edges for one or more
        contact regions for all load factors above
        marked with a "*". If you need pressure results
        near the contact regions, use single-pass
        adaptive convergence and select Localized
        Mesh Refinement.
      Calculating Disp and Stress Results     (16:06:16)

      Post-Processing Solution               (16:06:18)
      Checking Convergence                    (16:06:18)
        Elements Not Converged:       359
        Edges Not Converged:          824
        Local Disp/Energy Index:    100.0%
        Global RMS Stress Index:     73.9%
      Resource Check                          (16:06:18)
        Elapsed Time     (sec):      44.36
        CPU Time         (sec):     42.59
        Memory Usage      (kb):     192486
        Wrk Dir Dsk Usage (kb):       6155
```

Appendix C: (Continued)

```
>> Pass  3 <<
    Calculating Element Equations          (16:06:18)
      Total Number of Equations:   11109
      Maximum Edge Order:           4
    Solving Equations                      (16:06:18)
    Load Increment 0 of 1
    Load Factor:  0.00000e+00
    Contact Area:  0.00000e+00
    Calculating Disp and Stress Results    (16:06:33)
    Load Increment 1 of 1
    Load Factor:  1.00000e+00
    Contact Area:  1.77322e+00
    Calculating Disp and Stress Results    (16:07:05)

    Post-Processing Solution               (16:07:07)
    Checking Convergence                   (16:07:07)
      Elements Not Converged:      210
      Edges Not Converged:         260
      Local Disp/Energy Index:   100.0%
      Global RMS Stress Index:    32.6%
    Resource Check                         (16:07:07)
      Elapsed Time     (sec):     93.42
      CPU Time         (sec):     91.11
      Memory Usage     (kb):     193634
      Wrk Dir Dsk Usage (kb):     16395

>> Pass  4 <<
    Calculating Element Equations          (16:07:07)
      Total Number of Equations:   22602
      Maximum Edge Order:           4
    Solving Equations                      (16:07:09)
    Load Increment 0 of 1
    Load Factor:  0.00000e+00
```

Appendix C: (Continued)

Contact Area: 0.00000e+00
Calculating Disp and Stress Results (16:07:36)
Load Increment 1 of 1
Load Factor: 1.00000e+00
Contact Area: 1.78534e+00
Calculating Disp and Stress Results (16:09:33)

Post-Processing Solution (16:09:34)
Checking Convergence (16:09:34)
Elements Not Converged: 30
Edges Not Converged: 123
Local Disp/Energy Index: 26.7%
Global RMS Stress Index: 15.5%
Resource Check (16:09:35)
Elapsed Time (sec): 241.36
CPU Time (sec): 236.61
Memory Usage (kb): 197829
Wrk Dir Dsk Usage (kb): 37899

>> Pass 5 <<
Calculating Element Equations (16:09:35)
Total Number of Equations: 36231
Maximum Edge Order: 5
Solving Equations (16:09:41)
Load Increment 0 of 1
Load Factor: 0.00000e+00
Contact Area: 0.00000e+00
Calculating Disp and Stress Results (16:11:08)
Load Increment 1 of 1
Load Factor: 1.00000e+00
Contact Area: 1.79261e+00
Calculating Disp and Stress Results (16:14:05)

Appendix C: (Continued)

Post-Processing Solution (16:14:07)
Checking Convergence (16:14:07)
Elements Not Converged: 1
Edges Not Converged: 0
Local Disp/Energy Index: 10.3%
Global RMS Stress Index: 8.4%
Resource Check (16:14:08)
Elapsed Time (sec): 514.59
CPU Time (sec): 458.59
Memory Usage (kb): 205761
Wrk Dir Dsk Usage (kb): 219147

>> Pass 6 <<
Calculating Element Equations (16:14:08)
Total Number of Equations: 45030
Maximum Edge Order: 6
Solving Equations (16:14:15)
Load Increment 0 of 1
Load Factor: 0.00000e+00
Contact Area: 0.00000e+00
Calculating Disp and Stress Results (16:15:51)
Load Increment 1 of 1
Load Factor: 1.00000e+00
Contact Area: 1.79752e+00
Calculating Disp and Stress Results (16:19:58)

Post-Processing Solution (16:20:25)
Checking Convergence (16:20:25)
Elements Not Converged: 0
Edges Not Converged: 0
Local Disp/Energy Index: 4.3%
Global RMS Stress Index: 4.8%

Appendix C: (Continued)

RMS Stress Error Estimates:

Load Set	Stress Error	% of Max Prin Str
LoadSet1	1.87e+03	9.6% of 1.95e+04

Resource Check (16:20:29)

Elapsed Time (sec): 895.76
CPU Time (sec): 739.63
Memory Usage (kb): 226079
Wrk Dir Dsk Usage (kb): 299019

The analysis converged to within 10% on
edge displacement, element strain energy,
and global RMS stress.

Total Mass of Model: 1.371139e-03

Total Cost of Model: 0.000000e+00

Mass Moments of Inertia about WCS Origin:

Ixx: 8.64826e-04
Ixy: 1.74899e-09 Iyy: 1.50782e-03
Ixz: 5.27724e-06 Iyz: 8.79483e-10 Izz: 8.21515e-04

Principal MMOI and Principal Axes Relative to WCS Origin:

Max Prin	Mid Prin	Min Prin
1.50782e-03	8.65460e-04	8.20881e-04

WCS X: 2.73079e-06 9.92867e-01 -1.19230e-01
WCS Y: 1.00000e+00 -2.86660e-06 -9.67599e-07

Appendix C: (Continued)

WCS Z: 1.30248e-06 1.19230e-01 9.92867e-01

Center of Mass Location Relative to WCS Origin:
(4.48315e-01, -5.37019e-06, -8.40699e-04)

Mass Moments of Inertia about the Center of Mass:

Ixx: 8.64825e-04
Ixy: -1.55207e-09 Iyy: 1.23223e-03
Ixz: 4.76046e-06 Iyz: 8.85674e-10 Izz: 5.45935e-04

Principal MMOI and Principal Axes Relative to COM:

Max Prin	Mid Prin	Min Prin
1.23223e-03	8.64896e-04	5.45864e-04

WCS X: -4.20804e-06 9.99889e-01 -1.49232e-02
WCS Y: 1.00000e+00 4.18875e-06 -1.32397e-06
WCS Z: 1.26132e-06 1.49232e-02 9.99889e-01

Constraint Set: ConstraintSet1

Load Set: LoadSet1

Resultant Load on Model:
in global X direction: -2.047121e-10
in global Y direction: -1.080000e+03
in global Z direction: -3.900000e+02

Appendix C: (Continued)

Measures:

Name	Value	Convergence
contact_area:	1.797523e+00	0.3%
contact_max_pres:	1.944910e+04	11.1%
max_beam_bending:	0.000000e+00	0.0%
max_beam_tensile:	0.000000e+00	0.0%
max_beam_torsion:	0.000000e+00	0.0%
max_beam_total:	0.000000e+00	0.0%
max_disp_mag:	9.808449e-03	1.9%
max_disp_x:	-9.196215e-03	2.0%
max_disp_y:	-9.797444e-03	1.9%
max_disp_z:	-9.702102e-04	0.2%
max_prin_mag:	-1.945152e+04	11.1%
max_rot_mag:	0.000000e+00	0.0%
max_rot_x:	0.000000e+00	0.0%
max_rot_y:	0.000000e+00	0.0%
max_rot_z:	0.000000e+00	0.0%
max_stress_prin:	1.665415e+04	2.1%
max_stress_vm:	3.092423e+04	4.9%
max_stress_xx:	-1.397394e+04	1.1%
max_stress_xy:	1.755868e+04	4.6%
max_stress_xz:	4.280469e+03	0.4%
max_stress_yy:	1.495614e+04	3.7%
max_stress_yz:	7.995832e+03	22.4%
max_stress_zz:	1.558699e+04	0.3%
min_stress_prin:	-1.945152e+04	11.1%
strain_energy:	1.752524e+00	0.2%
cntRgn_001cntArea:	9.684937e-01	0.0%
cntRgn_001maxPres:	4.284050e+03	4.6%
cntRgn_002cntArea:	5.836132e-01	0.8%
cntRgn_002maxPres:	1.944910e+04	11.1%
cntRgn_003cntArea:	2.454163e-01	0.0%

Appendix C: (Continued)

```
   cntRgn_003maxPres:  4.686339e+03      1.3%
    cntRgn_004cntArea:  9.684937e-01      0.0%
    cntRgn_004maxPres:  4.284050e+03      4.6%
    cntRgn_005cntArea:  9.684937e-01      0.0%
    cntRgn_005maxPres:  4.284050e+03      4.6%
    cntRgn_006cntArea:  5.836132e-01      0.8%
    cntRgn_006maxPres:  1.944910e+04     11.1%

Analysis "ten_x_static_load_near_fork_1" Completed  (16:20:30)
------------------------------------------------------------
Memory and Disk Usage:

  Machine Type: Windows NT/x86
  RAM Allocation for Solver (megabytes): 128.0

  Total Elapsed Time (seconds): 898.76
  Total CPU Time     (seconds): 740.02
  Maximum Memory Usage (kilobytes): 226079
  Working Directory Disk Usage (kilobytes): 299019

  Results Directory Size (kilobytes):
  8919 .\ten_x_static_load_near_fork_1

  Maximum Data Base Working File Sizes (kilobytes):
  20480 .\ten_x_static_load_near_fork_1.tmp\gapel1.bas
  198656 .\ten_x_static_load_near_fork_1.tmp\kblk1.bas
  69632 .\ten_x_static_load_near_fork_1.tmp\kel1.bas
  1024 .\ten_x_static_load_near_fork_1.tmp\l1da1.bas
  1024 .\ten_x_static_load_near_fork_1.tmp\l2sq1.bas
  8192 .\ten_x_static_load_near_fork_1.tmp\oel1.bas
------------------------------------------------------------
Run Completed
Thu Jan 25, 2007   16:20:32
```

Appendix D: Fork and Bolt Analysis – 3 Degree Camber

This is the "run status" out-put file for the Pro-Mechanica analysis of the Fork and Bolt analysis. A camber of 3 degrees was used, 10 times the static load was applied, and the convergence was set to 10%.

Mechanica Structure Version K-01-41:spg
Summary for Design Study "ten_times_static_load_near_fork"
Thu Jan 25, 2007 15:43:43

Run Settings
Memory allocation for block solver: 128.0
Checking the model before creating elements...
These checks take into account the fact that AutoGEM will
automatically create elements in volumes with material
properties, on surfaces with shell properties, and on curves
with beam section properties.

Generate elements automatically.
Checking the model after creating elements...

No errors were found in the model.

Mechanica Structure Model Summary

Principal System of Units: Inch Pound Second (IPS)

Length: in
Force: lbf
Time: sec
Temperature: F

Model Type: Three Dimensional

Appendix D: (Continued)

Points: 265
Edges: 1107
Faces: 1423

Springs: 0
Masses: 0
Beams: 0
Shells: 0
Solids: 582

Elements: 582

Contact Regions: 3

Standard Design Study

Description:
10% convergence

Static Analysis "ten_times_static_load_near_fork":
Contact Analysis

Convergence Method: Multiple-Pass Adaptive
Plotting Grid: 4

Convergence Loop Log: (15:43:52)

>> Pass 1 <<
Calculating Element Equations (15:43:53)
Total Number of Equations: 630
Maximum Edge Order: 1

Appendix D: (Continued)

```
 Solving Equations                    (15:43:53)
      Load Increment 0 of 1
      Load Factor:  0.00000e+00
      Contact Area:  0.00000e+00
      Calculating Disp and Stress Results     (15:43:54)
      Load Increment 1 of 1
      Load Factor:  1.00000e+00
     *Contact Area:  1.30032e+00

** Warning: Contact area is small in comparison to size
         of adjacent element edges for one or more
         contact regions for all load factors above
         marked with a "*". If you need pressure results
         near the contact regions, use single-pass
         adaptive convergence and select Localized
         Mesh Refinement.
      Calculating Disp and Stress Results     (15:44:05)

      Post-Processing Solution             (15:44:06)
      Checking Convergence                 (15:44:06)
        Elements Not Converged:       582
        Edges Not Converged:         1107
        Local Disp/Energy Index:    100.0%
        Global RMS Stress Index:    100.0%
      Resource Check                       (15:44:06)
        Elapsed Time     (sec):      24.23
        CPU Time         (sec):     21.52
        Memory Usage      (kb):     193510
        Wrk Dir Dsk Usage (kb):       5131

  >> Pass  2 <<
      Calculating Element Equations          (15:44:06)
        Total Number of Equations:    3579
```

Appendix D: (Continued)

```
    Maximum Edge Order:          2
  Solving Equations              (15:44:06)
  Load Increment 0 of 1
  Load Factor:  0.00000e+00
  Contact Area:  0.00000e+00
  Calculating Disp and Stress Results     (15:44:09)
  Load Increment 1 of 1
  Load Factor:  1.00000e+00
 *Contact Area:  1.56700e+00

** Warning: Contact area is small in comparison to size
    of adjacent element edges for one or more
    contact regions for all load factors above
    marked with a "*". If you need pressure results
    near the contact regions, use single-pass
    adaptive convergence and select Localized
    Mesh Refinement.
  Calculating Disp and Stress Results     (15:44:35)

  Post-Processing Solution        (15:44:37)
  Checking Convergence            (15:44:37)
    Elements Not Converged:       353
    Edges Not Converged:          825
    Local Disp/Energy Index:    100.0%
    Global RMS Stress Index:     74.8%
  Resource Check                  (15:44:37)
    Elapsed Time     (sec):      55.17
    CPU Time         (sec):      51.48
    Memory Usage     (kb):     193510
    Wrk Dir Dsk Usage (kb):      6155

 >> Pass  3 <<
  Calculating Element Equations   (15:44:37)
```

Appendix D: (Continued)

```
      Total Number of Equations:   11070
      Maximum Edge Order:           4
    Solving Equations                (15:44:37)
    Load Increment 0 of 1
    Load Factor:  0.00000e+00
    Contact Area:  0.00000e+00
    Calculating Disp and Stress Results     (15:44:53)
    Load Increment 1 of 1
    Load Factor:  1.00000e+00
   *Contact Area:  1.67904e+00

** Warning: Contact area is small in comparison to size
      of adjacent element edges for one or more
      contact regions for all load factors above
      marked with a "*". If you need pressure results
      near the contact regions, use single-pass
      adaptive convergence and select Localized
      Mesh Refinement.
    Calculating Disp and Stress Results     (15:45:41)

    Post-Processing Solution          (15:45:42)
    Checking Convergence              (15:45:42)
      Elements Not Converged:      209
      Edges Not Converged:         245
      Local Disp/Energy Index:   100.0%
      Global RMS Stress Index:    32.9%
    Resource Check                    (15:45:42)
      Elapsed Time    (sec):    120.55
      CPU Time        (sec):    115.38
      Memory Usage    (kb):     195014
      Wrk Dir Dsk Usage (kb):    16395
```

Appendix D: (Continued)

```
  >> Pass  4 <<
       Calculating Element Equations          (15:45:42)
         Total Number of Equations:   22146
         Maximum Edge Order:            4
       Solving Equations                    (15:45:44)
       Load Increment 0 of 1
       Load Factor:  0.00000e+00
       Contact Area:  0.00000e+00
       Calculating Disp and Stress Results     (15:46:10)
       Load Increment 1 of 1
       Load Factor:  1.00000e+00
      *Contact Area:  1.70496e+00

** Warning: Contact area is small in comparison to size
          of adjacent element edges for one or more
          contact regions for all load factors above
          marked with a "*". If you need pressure results
          near the contact regions, use single-pass
          adaptive convergence and select Localized
          Mesh Refinement.
       Calculating Disp and Stress Results     (15:47:43)

       Post-Processing Solution               (15:47:45)
       Checking Convergence                   (15:47:45)
         Elements Not Converged:        29
         Edges Not Converged:          111
         Local Disp/Energy Index:     24.5%
         Global RMS Stress Index:     15.4%
       Resource Check                         (15:47:45)
         Elapsed Time     (sec):     243.21
         CPU Time         (sec):     235.76
         Memory Usage      (kb):     198413
         Wrk Dir Dsk Usage (kb):      36875
```

Appendix D: (Continued)

```
  >> Pass  5 <<
       Calculating Element Equations          (15:47:45)
         Total Number of Equations:   35934
         Maximum Edge Order:           5
       Solving Equations                      (15:47:49)
       Load Increment 0 of 1
       Load Factor:  0.00000e+00
       Contact Area:  0.00000e+00
       Calculating Disp and Stress Results    (15:48:51)
       Load Increment 1 of 1
       Load Factor:  1.00000e+00
      *Contact Area:  1.71726e+00

** Warning: Contact area is small in comparison to size
          of adjacent element edges for one or more
          contact regions for all load factors above
          marked with a "*". If you need pressure results
          near the contact regions, use single-pass
          adaptive convergence and select Localized
          Mesh Refinement.
       Calculating Disp and Stress Results    (15:51:42)

       Post-Processing Solution               (15:51:50)
       Checking Convergence                   (15:51:50)
         Elements Not Converged:       1
         Edges Not Converged:          0
         Local Disp/Energy Index:    10.2%
         Global RMS Stress Index:     8.7%
       Resource Check                         (15:51:52)
         Elapsed Time    (sec):    490.11
         CPU Time        (sec):    450.92
         Memory Usage     (kb):    222102
         Wrk Dir Dsk Usage (kb):   215051
```

Appendix D: (Continued)

```
  >> Pass  6 <<
       Calculating Element Equations          (15:51:53)
         Total Number of Equations:   44889
         Maximum Edge Order:            6
       Solving Equations                    (15:52:10)
       Load Increment 0 of 1
       Load Factor:  0.00000e+00
       Contact Area:  0.00000e+00
       Calculating Disp and Stress Results     (15:53:46)
       Load Increment 1 of 1
       Load Factor:  1.00000e+00
      *Contact Area:  1.72091e+00

** Warning: Contact area is small in comparison to size
          of adjacent element edges for one or more
          contact regions for all load factors above
          marked with a "*". If you need pressure results
          near the contact regions, use single-pass
          adaptive convergence and select Localized
          Mesh Refinement.
       Calculating Disp and Stress Results     (15:57:57)

       Post-Processing Solution               (15:58:05)
       Checking Convergence                   (15:58:05)
         Elements Not Converged:         0
         Edges Not Converged:            0
         Local Disp/Energy Index:      4.4%
         Global RMS Stress Index:      4.9%
```

Appendix D: (Continued)

RMS Stress Error Estimates:

Load Set	Stress Error	% of Max Prin Str
LoadSet1	1.99e+03	9.5% of 2.09e+04

Resource Check (15:58:09)

Elapsed Time	(sec):	866.86
CPU Time	(sec):	718.91
Memory Usage	(kb):	225934
Wrk Dir Dsk Usage	(kb):	293899

The analysis converged to within 10% on
edge displacement, element strain energy,
and global RMS stress.

Total Mass of Model: 1.371139e-03
Total Cost of Model: 0.000000e+00

Mass Moments of Inertia about WCS Origin:

Ixx: 8.64826e-04
Ixy: 1.74899e-09 Iyy: 1.50782e-03
Ixz: 5.27724e-06 Iyz: 8.79483e-10 Izz: 8.21515e-04

Principal MMOI and Principal Axes Relative to WCS Origin:

Max Prin	Mid Prin	Min Prin
1.50782e-03	8.65460e-04	8.20881e-04

WCS X:	2.73079e-06	9.92867e-01	-1.19230e-01
WCS Y:	1.00000e+00	-2.86660e-06	-9.67599e-07
WCS Z:	1.30248e-06	1.19230e-01	9.92867e-01

Appendix D: (Continued)

Center of Mass Location Relative to WCS Origin:
(4.48315e-01, -5.37019e-06, -8.40699e-04)

Mass Moments of Inertia about the Center of Mass:

Ixx: 8.64825e-04
Ixy: -1.55207e-09 Iyy: 1.23223e-03
Ixz: 4.76046e-06 Iyz: 8.85674e-10 Izz: 5.45935e-04

Principal MMOI and Principal Axes Relative to COM:

Max Prin	Mid Prin	Min Prin
1.23223e-03	8.64896e-04	5.45864e-04

WCS X:	-4.20804e-06	9.99889e-01	-1.49232e-02
WCS Y:	1.00000e+00	4.18875e-06	-1.32397e-06
WCS Z:	1.26132e-06	1.49232e-02	9.99889e-01

Constraint Set: ConstraintSet1

Load Set: LoadSet1

Resultant Load on Model:
in global X direction: -1.577994e-10
in global Y direction: -1.150000e+03
in global Z direction: -6.000000e+01

Measures:

Name	Value	Convergence
contact_area:	1.720907e+00	0.2%
contact_max_pres:	2.090662e+04	10.1%

Appendix D: (Continued)

max_beam_bending: 0.000000e+00 0.0%
max_beam_tensile: 0.000000e+00 0.0%
max_beam_torsion: 0.000000e+00 0.0%
max_beam_total: 0.000000e+00 0.0%
max_disp_mag: 1.306670e-02 1.8%
max_disp_x: 1.237034e-02 1.9%
max_disp_y: -1.305403e-02 1.8%
max_disp_z: -7.257396e-04 0.2%
max_prin_mag: -2.090933e+04 10.1%
max_rot_mag: 0.000000e+00 0.0%
max_rot_x: 0.000000e+00 0.0%
max_rot_y: 0.000000e+00 0.0%
max_rot_z: 0.000000e+00 0.0%
max_stress_prin: 1.777704e+04 2.0%
max_stress_vm: 3.304002e+04 5.0%
max_stress_xx: -1.494734e+04 1.1%
max_stress_xy: 1.876216e+04 4.8%
max_stress_xz: -3.496715e+03 23.7%
max_stress_yy: 1.595143e+04 1.7%
max_stress_yz: 8.546310e+03 26.0%
max_stress_zz: -1.520768e+04 1.8%
min_stress_prin: -2.090933e+04 10.1%
strain_energy: 1.905957e+00 0.2%
cntRgn_001cntArea: 1.036548e+00 0.0%
cntRgn_001maxPres: 4.553970e+03 5.5%
cntRgn_002cntArea: 5.613023e-01 0.6%
cntRgn_002maxPres: 2.090662e+04 10.1%
cntRgn_003cntArea: 1.230561e-01 0.2%
cntRgn_003maxPres: 1.927968e+03 0.1%
cntRgn_004cntArea: 1.036548e+00 0.0%
cntRgn_004maxPres: 4.553970e+03 5.5%
cntRgn_005cntArea: 1.036548e+00 0.0%
cntRgn_005maxPres: 4.553970e+03 5.5%

Appendix D: (Continued)

cntRgn_006cntArea: 5.613023e-01 0.6%
cntRgn_006maxPres: 2.090662e+04 10.1%

Analysis "ten_times_static_load_near_fork" Completed (15:58:09)

Memory and Disk Usage:

Machine Type: Windows NT/x86
RAM Allocation for Solver (megabytes): 128.0

Total Elapsed Time (seconds): 867.41
Total CPU Time (seconds): 719.30
Maximum Memory Usage (kilobytes): 225934
Working Directory Disk Usage (kilobytes): 293899

Results Directory Size (kilobytes):
8908 .\ten_times_static_load_near_fork

Maximum Data Base Working File Sizes (kilobytes):
19456 .\ten_times_static_load_near_fork.tmp\gapel1.bas
194560 .\ten_times_static_load_near_fork.tmp\kblk1.bas
69632 .\ten_times_static_load_near_fork.tmp\kel1.bas
1024 .\ten_times_static_load_near_fork.tmp\l1da1.bas
1024 .\ten_times_static_load_near_fork.tmp\l2sq1.bas
8192 .\ten_times_static_load_near_fork.tmp\oel1.bas

Run Completed
Thu Jan 25, 2007 15:58:09

Appendix E: Inner Hub and Pin Analysis – 3 Degrees Camber

This is the "run status" out-put file for the Pro-Mechanica analysis of the Inner Hub and Pin analysis. A camber of 3 degrees was used, 10 times the static load was applied, and the convergence was set to 10%. This is **with-out** local mesh refinement.

Mechanica Structure Version K-01-41:spg
Summary for Design Study "ih_and_big_fixed_pin_10_x_two_c"
Tue Jan 16, 2007 16:16:21

Run Settings
Memory allocation for block solver: 128.0
Checking the model before creating elements...
These checks take into account the fact that AutoGEM will
automatically create elements in volumes with material
properties, on surfaces with shell properties, and on curves
with beam section properties.

Generate elements automatically.
Checking the model after creating elements...

No errors were found in the model.

Mechanica Structure Model Summary

Principal System of Units: Inch Pound Second (IPS)

Length: in
Force: lbf
Time: sec
Temperature: F

Appendix E: (Continued)

Model Type: Three Dimensional

Points:	225
Edges:	961
Faces:	1253
Springs:	0
Masses:	0
Beams:	0
Shells:	0
Solids:	517
Elements:	517
Contact Regions:	2

Standard Design Study

Description:
I used contact "surfaces" (4 total), instead of contac
t "part" (about 12 total)

Static Analysis "ih_and_big_fixed_pin_10_x_two_c":
Contact Analysis

Convergence Method:	Multiple-Pass Adaptive
Plotting Grid:	4

Appendix E: (Continued)

Convergence Loop Log: (16:16:25)

>> Pass 1 <<
Calculating Element Equations (16:16:25)
Total Number of Equations: 607
Maximum Edge Order: 1
Solving Equations (16:16:25)
Load Increment 0 of 1
Load Factor: 0.00000e+00
Contact Area: 0.00000e+00
Calculating Disp and Stress Results (16:16:26)
Load Increment 1 of 1
Load Factor: 1.00000e+00
Contact Area: 0.00000e+00
Calculating Disp and Stress Results (16:16:27)

Post-Processing Solution (16:16:28)
Checking Convergence (16:16:28)
Elements Not Converged: 517
Edges Not Converged: 961
Local Disp/Energy Index: 100.0%
Global RMS Stress Index: 100.0%
Resource Check (16:16:28)
Elapsed Time (sec): 8.62
CPU Time (sec): 6.11
Memory Usage (kb): 185502
Wrk Dir Dsk Usage (kb): 4098

>> Pass 2 <<
Calculating Element Equations (16:16:28)
Total Number of Equations: 3336
Maximum Edge Order: 2
Solving Equations (16:16:28)

Appendix E: (Continued)

Load Increment 0 of 1
Load Factor: 0.00000e+00
Contact Area: 0.00000e+00
Calculating Disp and Stress Results (16:16:29)
Load Increment 1 of 1
Load Factor: 1.00000e+00
*Contact Area: 1.07992e-02

** Warning: Contact area is small in comparison to size
of adjacent element edges for one or more
contact regions for all load factors above
marked with a "*". If you need pressure results
near the contact regions, use single-pass
adaptive convergence and select Localized
Mesh Refinement.
Calculating Disp and Stress Results (16:16:35)

Post-Processing Solution (16:16:36)
Checking Convergence (16:16:36)
Elements Not Converged: 353
Edges Not Converged: 254
Local Disp/Energy Index: 100.0%
Global RMS Stress Index: 87.9%
Resource Check (16:16:36)
Elapsed Time (sec): 17.26
CPU Time (sec): 14.44
Memory Usage (kb): 186590
Wrk Dir Dsk Usage (kb): 4098

>> Pass 3 <<
Calculating Element Equations (16:16:36)
Total Number of Equations: 9955
Maximum Edge Order: 4

Appendix E: (Continued)

```
        Solving Equations                    (16:16:37)
        Load Increment 0 of 1
        Load Factor:  0.00000e+00
        Contact Area:  0.00000e+00
        Calculating Disp and Stress Results     (16:16:39)
        Load Increment 1 of 1
        Load Factor:  1.00000e+00
       *Contact Area:  1.57080e-02

** Warning: Contact area is small in comparison to size
          of adjacent element edges for one or more
          contact regions for all load factors above
          marked with a "*". If you need pressure results
          near the contact regions, use single-pass
          adaptive convergence and select Localized
          Mesh Refinement.
        Calculating Disp and Stress Results     (16:16:48)

        Post-Processing Solution             (16:16:49)
        Checking Convergence                 (16:16:49)
          Elements Not Converged:       270
          Edges Not Converged:          18
          Local Disp/Energy Index:    100.0%
          Global RMS Stress Index:     47.7%
        Resource Check                       (16:16:49)
          Elapsed Time     (sec):      29.84
          CPU Time         (sec):      26.25
          Memory Usage      (kb):     195934
          Wrk Dir Dsk Usage (kb):      10242


    >> Pass  4 <<
        Calculating Element Equations        (16:16:49)
          Total Number of Equations:   19819
```

Appendix E: (Continued)

Maximum Edge Order: 5
Solving Equations (16:16:51)
Load Increment 0 of 1
Load Factor: 0.00000e+00
Contact Area: 0.00000e+00
Calculating Disp and Stress Results (16:16:56)
Load Increment 1 of 1
Load Factor: 1.00000e+00
*Contact Area: 2.25802e-02

** Warning: Contact area is small in comparison to size
of adjacent element edges for one or more
contact regions for all load factors above
marked with a "*". If you need pressure results
near the contact regions, use single-pass
adaptive convergence and select Localized
Mesh Refinement.
Calculating Disp and Stress Results (16:17:17)

Post-Processing Solution (16:17:18)
Checking Convergence (16:17:18)
Elements Not Converged: 94
Edges Not Converged: 0
Local Disp/Energy Index: 37.2%
Global RMS Stress Index: 25.5%
Resource Check (16:17:19)
Elapsed Time (sec): 59.63
CPU Time (sec): 54.63
Memory Usage (kb): 197534
Wrk Dir Dsk Usage (kb): 23554

Appendix E: (Continued)

```
  >> Pass  5 <<
       Calculating Element Equations          (16:17:19)
         Total Number of Equations:   34342
         Maximum Edge Order:            6
       Solving Equations                    (16:17:24)
       Load Increment 0 of 1
       Load Factor:  0.00000e+00
       Contact Area:  0.00000e+00
       Calculating Disp and Stress Results     (16:17:39)
       Load Increment 1 of 1
       Load Factor:  1.00000e+00
      *Contact Area:  3.33794e-02

** Warning: Contact area is small in comparison to size
          of adjacent element edges for one or more
          contact regions for all load factors above
          marked with a "*". If you need pressure results
          near the contact regions, use single-pass
          adaptive convergence and select Localized
          Mesh Refinement.
       Calculating Disp and Stress Results     (16:18:38)

       Post-Processing Solution               (16:18:40)
       Checking Convergence                   (16:18:40)
         Elements Not Converged:        17
         Edges Not Converged:            0
         Local Disp/Energy Index:     17.5%
         Global RMS Stress Index:     16.0%
       Resource Check                         (16:18:41)
         Elapsed Time     (sec):     141.36
         CPU Time         (sec):     133.28
         Memory Usage      (kb):     202301
         Wrk Dir Dsk Usage (kb):      54274
```

Appendix E: (Continued)

```
  >> Pass  6 <<
       Calculating Element Equations          (16:18:41)
         Total Number of Equations:   53481
         Maximum Edge Order:            7
       Solving Equations                    (16:18:53)
       Load Increment 0 of 1
       Load Factor:  0.00000e+00
       Contact Area:  0.00000e+00
       Calculating Disp and Stress Results     (16:19:38)
       Load Increment 1 of 1
       Load Factor:  1.00000e+00
      *Contact Area:  3.43612e-02

** Warning: Contact area is small in comparison to size
          of adjacent element edges for one or more
          contact regions for all load factors above
          marked with a "*". If you need pressure results
          near the contact regions, use single-pass
          adaptive convergence and select Localized
          Mesh Refinement.
       Calculating Disp and Stress Results     (16:21:43)

       Post-Processing Solution               (16:21:46)
       Checking Convergence                   (16:21:46)
         Elements Not Converged:         1
         Edges Not Converged:            0
         Local Disp/Energy Index:     10.0%
         Global RMS Stress Index:     11.3%
       Resource Check                         (16:21:47)
         Elapsed Time     (sec):     328.22
         CPU Time         (sec):     263.38
         Memory Usage      (kb):     226922
         Wrk Dir Dsk Usage (kb):     296962
```

Appendix E: (Continued)

```
  >> Pass  7 <<
       Calculating Element Equations          (16:21:47)
         Total Number of Equations:   74534
         Maximum Edge Order:            8
       Solving Equations                    (16:22:18)
       Load Increment 0 of 1
       Load Factor:  0.00000e+00
       Contact Area:  0.00000e+00
       Calculating Disp and Stress Results     (16:24:07)
       Load Increment 1 of 1
       Load Factor:  1.00000e+00
      *Contact Area:  4.61421e-02

** Warning: Contact area is small in comparison to size
          of adjacent element edges for one or more
          contact regions for all load factors above
          marked with a "*". If you need pressure results
          near the contact regions, use single-pass
          adaptive convergence and select Localized
          Mesh Refinement.
       Calculating Disp and Stress Results     (16:32:17)

       Post-Processing Solution              (16:33:15)
       Checking Convergence                  (16:33:15)
         Elements Not Converged:        0
         Edges Not Converged:           0
         Local Disp/Energy Index:      7.0%
         Global RMS Stress Index:      8.6%
```

Appendix E: (Continued)

RMS Stress Error Estimates:

Load Set	Stress Error	% of Max Prin Str
LoadSet1	3.75e+02	0.8% of 4.61e+04

Resource Check (16:33:27)
Elapsed Time (sec): 1027.84
CPU Time (sec): 594.52
Memory Usage (kb): 238822
Wrk Dir Dsk Usage (kb): 498690

The analysis converged to within 10% on
edge displacement, element strain energy,
and global RMS stress.

Total Mass of Model: 1.023137e-02
Total Cost of Model: 0.000000e+00

Mass Moments of Inertia about WCS Origin:

Ixx: 4.63460e-01
Ixy: -2.21914e-08 Iyy: 7.85365e-03
Ixz: 2.07545e-09 Iyz: -4.77616e-09 Izz: 4.64919e-01

Principal MMOI and Principal Axes Relative to WCS Origin:

Max Prin	Mid Prin	Min Prin
4.64919e-01	4.63460e-01	7.85365e-03

WCS X:	1.42221e-06	1.00000e+00	4.87076e-08
WCS Y:	-1.04497e-08	-4.87075e-08	1.00000e+00
WCS Z:	1.00000e+00	-1.42221e-06	1.04496e-08

Appendix E: (Continued)

Center of Mass Location Relative to WCS Origin:
(5.94321e-02, 1.12547e-02, 2.40077e-07)

Mass Moments of Inertia about the Center of Mass:

Ixx: 4.63458e-01
Ixy: 6.82150e-06 Iyy: 7.81751e-03
Ixz: 2.22144e-09 Iyz: -4.74851e-09 Izz: 4.64882e-01

Principal MMOI and Principal Axes Relative to COM:

Max Prin	Mid Prin	Min Prin
4.64882e-01	4.63458e-01	7.81751e-03

WCS X:	1.56085e-06	1.00000e+00	-1.49712e-05
WCS Y:	-1.03659e-08	1.49712e-05	1.00000e+00
WCS Z:	1.00000e+00	-1.56085e-06	1.03892e-08

Constraint Set: ConstraintSet1

Load Set: LoadSet1

Resultant Load on Model:
in global X direction: -9.346590e-11
in global Y direction: -4.433882e-10
in global Z direction: 6.000000e+01

Measures:

Name	Value	Convergence
contact_area:	4.614214e-02	25.5%
contact_max_pres:	4.244370e+04	7.6%
max_beam_bending:	0.000000e+00	0.0%

Appendix E: (Continued)

max_beam_tensile: 0.000000e+00 0.0%
max_beam_torsion: 0.000000e+00 0.0%
max_beam_total: 0.000000e+00 0.0%
max_disp_mag: 7.590963e-02 0.7%
max_disp_x: -2.286037e-03 0.6%
max_disp_y: -6.997755e-03 0.6%
max_disp_z: 7.571832e-02 0.7%
max_prin_mag: -4.610517e+04 2.6%
max_rot_mag: 0.000000e+00 0.0%
max_rot_x: 0.000000e+00 0.0%
max_rot_y: 0.000000e+00 0.0%
max_rot_z: 0.000000e+00 0.0%
max_stress_prin: 2.584570e+04 14.0%
max_stress_vm: 3.145544e+04 1.6%
max_stress_xx: -2.418541e+04 2.4%
max_stress_xy: 1.009556e+04 11.7%
max_stress_xz: 7.840168e+03 2.1%
max_stress_yy: -4.244165e+04 9.2%
max_stress_yz: -9.826774e+03 21.6%
max_stress_zz: -1.849277e+04 8.1%
min_stress_prin: -4.610517e+04 2.6%
strain_energy: 2.117846e+00 0.7%
cntRgn_009cntArea: 2.945243e-02 30.0%
cntRgn_009maxPres: 3.565886e+04 1.6%
cntRgn_010cntArea: 1.668971e-02 17.6%
cntRgn_010maxPres: 4.244370e+04 7.6%

Analysis "ih_and_big_fixed_pin_10_x_two_c" Completed (16:33:28)

Appendix E: (Continued)

Memory and Disk Usage:

Machine Type: Windows NT/x86
RAM Allocation for Solver (megabytes): 128.0

Total Elapsed Time (seconds): 1028.37
Total CPU Time (seconds): 594.88
Maximum Memory Usage (kilobytes): 238822
Working Directory Disk Usage (kilobytes): 498690

Results Directory Size (kilobytes):
10482 .\ih_and_big_fixed_pin_10_x_two_c

Maximum Data Base Working File Sizes (kilobytes):
1024 .\ih_and_big_fixed_pin_10_x_two_c.tmp\gapel1.bas
305152 .\ih_and_big_fixed_pin_10_x_two_c.tmp\kblk1.bas
169984 .\ih_and_big_fixed_pin_10_x_two_c.tmp\kel1.bas
2048 .\ih_and_big_fixed_pin_10_x_two_c.tmp\l1da1.bas
1024 .\ih_and_big_fixed_pin_10_x_two_c.tmp\l2sq1.bas
19456 .\ih_and_big_fixed_pin_10_x_two_c.tmp\oel1.bas

Run Completed
Tue Jan 16, 2007 16:33:28

Appendix F: Inner Hub and Pin Analysis – 3 Degree Camber – With Local Mesh Refinement

This is the "run status" out-put file for the Pro-Mechanica analysis of the Inner Hub and Pin analysis. A camber of 3 degrees was used, 10 times the static load was applied, and the convergence was set to 10%. This is **with** local mesh refinement (did not help)

Mechanica Structure Version K-01-41:spg
Summary for Design Study "ih_bfp_ten_x"
Tue Jan 16, 2007 16:46:06

Run Settings
Memory allocation for block solver: 128.0
Checking the model before creating elements...
These checks take into account the fact that AutoGEM will
automatically create elements in volumes with material
properties, on surfaces with shell properties, and on curves
with beam section properties.

Generate elements automatically.
Checking the model after creating elements...

No errors were found in the model.

Mechanica Structure Model Summary

Principal System of Units: Inch Pound Second (IPS)

Length: in
Force: lbf
Time: sec
Temperature: F
0

Appendix F: (Continued)

Model Type: Three Dimensional

Points: 225
Edges: 961
Faces: 1253

Springs: 0
Masses: 0
Beams: 0
Shells: 0
Solids: 517

Elements: 517

Contact Regions: 2

Standard Design Study

Description:
ran with elements from local mech refinment of ih_bfp_
ten_x_two_contact_local_mesh_refin

Static Analysis "ih_bfp_ten_x":
Contact Analysis

Convergence Method: Multiple-Pass Adaptive
Plotting Grid: 4

Convergence Loop Log: (16:46:08)

Appendix F: (Continued)

```
>> Pass  1 <<
     Calculating Element Equations          (16:46:08)
       Total Number of Equations:     607
       Maximum Edge Order:              1

     Solving Equations                      (16:46:09)
     Load Increment 0 of 1
     Load Factor:  0.00000e+00
     Contact Area:  0.00000e+00
     Calculating Disp and Stress Results     (16:46:09)
     Load Increment 1 of 1
     Load Factor:  1.00000e+00
     Contact Area:  0.00000e+00
     Calculating Disp and Stress Results     (16:46:10)

     Post-Processing Solution               (16:46:11)
     Checking Convergence                    (16:46:11)
       Elements Not Converged:       517
       Edges Not Converged:          961
       Local Disp/Energy Index:    100.0%
       Global RMS Stress Index:    100.0%
     Resource Check                          (16:46:11)
       Elapsed Time     (sec):       5.88
       CPU Time         (sec):       4.33
       Memory Usage      (kb):     185566
       Wrk Dir Dsk Usage (kb):       4098

>> Pass  2 <<
     Calculating Element Equations          (16:46:11)
       Total Number of Equations:    3336
       Maximum Edge Order:              2
     Solving Equations                      (16:46:11)
```

Appendix F: (Continued)

Load Increment 0 of 1
Load Factor: 0.00000e+00
Contact Area: 0.00000e+00
Calculating Disp and Stress Results (16:46:12)
Load Increment 1 of 1
Load Factor: 1.00000e+00

*Contact Area: 1.07992e-02

** Warning: Contact area is small in comparison to size
of adjacent element edges for one or more
contact regions for all load factors above
marked with a "*". If you need pressure results
near the contact regions, use single-pass
adaptive convergence and select Localized
Mesh Refinement.
Calculating Disp and Stress Results (16:46:18)

Post-Processing Solution (16:46:19)
Checking Convergence (16:46:19)
Elements Not Converged: 353
Edges Not Converged: 254
Local Disp/Energy Index: 100.0%
Global RMS Stress Index: 87.9%
Resource Check (16:46:19)
Elapsed Time (sec): 14.30
CPU Time (sec): 12.61
Memory Usage (kb): 186654
Wrk Dir Dsk Usage (kb): 4098

Appendix F: (Continued)

```
  >> Pass  3 <<
       Calculating Element Equations          (16:46:20)
         Total Number of Equations:    9955
         Maximum Edge Order:            4
       Solving Equations                    (16:46:20)
       Load Increment 0 of 1
       Load Factor:  0.00000e+00
       Contact Area:  0.00000e+00
       Calculating Disp and Stress Results     (16:46:23)
       Load Increment 1 of 1
       Load Factor:  1.00000e+00
      *Contact Area:  1.57080e-02

** Warning: Contact area is small in comparison to size
          of adjacent element edges for one or more
          contact regions for all load factors above
          marked with a "*". If you need pressure results
          near the contact regions, use single-pass
          adaptive convergence and select Localized
          Mesh Refinement.
       Calculating Disp and Stress Results     (16:46:31)

       Post-Processing Solution               (16:46:32)
       Checking Convergence                   (16:46:32)
         Elements Not Converged:       270
         Edges Not Converged:           18
         Local Disp/Energy Index:    100.0%
         Global RMS Stress Index:     47.7%
       Resource Check                         (16:46:32)
         Elapsed Time     (sec):      27.14
         CPU Time         (sec):      24.61
         Memory Usage      (kb):     196338
         Wrk Dir Dsk Usage (kb):      10242
```

Appendix F: (Continued)

```
>> Pass  4 <<
     Calculating Element Equations          (16:46:32)
       Total Number of Equations:   19819
       Maximum Edge Order:           5
     Solving Equations                      (16:46:34)
     Load Increment 0 of 1
     Load Factor:  0.00000e+00
     Contact Area:  0.00000e+00
     Calculating Disp and Stress Results    (16:46:39)

     Load Increment 1 of 1
     Load Factor:  1.00000e+00
    *Contact Area:  2.25802e-02

** Warning: Contact area is small in comparison to size
       of adjacent element edges for one or more
       contact regions for all load factors above
       marked with a "*". If you need pressure results
       near the contact regions, use single-pass
       adaptive convergence and select Localized
       Mesh Refinement.
     Calculating Disp and Stress Results    (16:46:59)

     Post-Processing Solution               (16:47:01)
     Checking Convergence                   (16:47:01)
       Elements Not Converged:       94
       Edges Not Converged:          0
       Local Disp/Energy Index:     37.2%
       Global RMS Stress Index:     25.5%
     Resource Check                         (16:47:01)
```

Appendix F: (Continued)

```
        Elapsed Time     (sec):      55.87
        CPU Time         (sec):      52.94
        Memory Usage     (kb):     197598
        Wrk Dir Dsk Usage (kb):      23554

  >> Pass  5 <<
      Calculating Element Equations          (16:47:01)
        Total Number of Equations:   34342
        Maximum Edge Order:              6
      Solving Equations                      (16:47:06)
      Load Increment 0 of 1
      Load Factor:  0.00000e+00
      Contact Area:  0.00000e+00

      Calculating Disp and Stress Results     (16:47:20)
      Load Increment 1 of 1
      Load Factor:  1.00000e+00
     *Contact Area:  3.33794e-02

** Warning: Contact area is small in comparison to size
        of adjacent element edges for one or more
        contact regions for all load factors above
        marked with a "*". If you need pressure results
        near the contact regions, use single-pass
        adaptive convergence and select Localized
        Mesh Refinement.
      Calculating Disp and Stress Results     (16:48:20)

      Post-Processing Solution               (16:48:22)
      Checking Convergence                   (16:48:22)
        Elements Not Converged:         17
        Edges Not Converged:             0
```

Appendix F: (Continued)

```
        Local Disp/Energy Index:     17.5%
        Global RMS Stress Index:     16.0%
      Resource Check                 (16:48:22)
        Elapsed Time     (sec):     137.05
        CPU Time         (sec):     131.58
        Memory Usage     (kb):      203389
        Wrk Dir Dsk Usage (kb):     54274

  >> Pass  6 <<
      Calculating Element Equations          (16:48:22)
        Total Number of Equations:   53481
        Maximum Edge Order:           7
      Solving Equations                      (16:48:35)
      Load Increment 0 of 1
      Load Factor:  0.00000e+00

      Contact Area:  0.00000e+00
      Calculating Disp and Stress Results    (16:49:20)
      Load Increment 1 of 1
      Load Factor:  1.00000e+00
     *Contact Area:  3.43612e-02

** Warning: Contact area is small in comparison to size
        of adjacent element edges for one or more
        contact regions for all load factors above
        marked with a "*". If you need pressure results
        near the contact regions, use single-pass
        adaptive convergence and select Localized
        Mesh Refinement.
      Calculating Disp and Stress Results    (16:50:50)

      Post-Processing Solution               (16:50:53)
```

Appendix F: (Continued)

```
        Checking Convergence                (16:50:53)
          Elements Not Converged:       1
          Edges Not Converged:          0
          Local Disp/Energy Index:    10.0%
          Global RMS Stress Index:    11.3%
        Resource Check                      (16:50:54)
          Elapsed Time    (sec):    289.26
          CPU Time        (sec):    261.24
          Memory Usage    (kb):     228842
          Wrk Dir Dsk Usage (kb):   296962

  >> Pass  7 <<
        Calculating Element Equations       (16:50:55)
          Total Number of Equations:  74534
          Maximum Edge Order:           8
        Solving Equations                   (16:51:23)
        Load Increment 0 of 1

        Load Factor:  0.00000e+00
        Contact Area:  0.00000e+00
        Calculating Disp and Stress Results    (16:52:49)
        Load Increment 1 of 1
        Load Factor:  1.00000e+00
       *Contact Area:  4.61421e-02

** Warning: Contact area is small in comparison to size
          of adjacent element edges for one or more
          contact regions for all load factors above
          marked with a "*". If you need pressure results
          near the contact regions, use single-pass
          adaptive convergence and select Localized
          Mesh Refinement.
```

Appendix F: (Continued)

Calculating Disp and Stress Results (16:59:30)

Post-Processing Solution (16:59:51)
Checking Convergence (16:59:51)
Elements Not Converged: 0
Edges Not Converged: 0
Local Disp/Energy Index: 7.0%
Global RMS Stress Index: 8.6%

RMS Stress Error Estimates:

Load Set	Stress Error	% of Max Prin Str
LoadSet1	3.75e+02	0.8% of 4.61e+04

Resource Check (17:00:00)
Elapsed Time (sec): 834.93
CPU Time (sec): 586.49
Memory Usage (kb): 239078
Wrk Dir Dsk Usage (kb): 498690

The analysis converged to within 10% on
edge displacement, element strain energy,
and global RMS stress.

Total Mass of Model: 1.023137e-02

Total Cost of Model: 0.000000e+00

Appendix F: (Continued)

Mass Moments of Inertia about WCS Origin:

Ixx: 4.63460e-01
Ixy: -2.21914e-08 Iyy: 7.85365e-03
Ixz: 2.07545e-09 Iyz: -4.77616e-09 Izz: 4.64919e-01

Principal MMOI and Principal Axes Relative to WCS Origin:

Max Prin	Mid Prin	Min Prin
4.64919e-01	4.63460e-01	7.85365e-03

WCS X:	1.42221e-06	1.00000e+00	4.87076e-08
WCS Y:	-1.04497e-08	-4.87075e-08	1.00000e+00
WCS Z:	1.00000e+00	-1.42221e-06	1.04496e-08

Center of Mass Location Relative to WCS Origin:
(5.94321e-02, 1.12547e-02, 2.40077e-07)

Mass Moments of Inertia about the Center of Mass:

Ixx: 4.63458e-01
Ixy: 6.82150e-06 Iyy: 7.81751e-03
Ixz: 2.22144e-09 Iyz: -4.74851e-09 Izz: 4.64882e-01

Principal MMOI and Principal Axes Relative to COM:

Max Prin	Mid Prin	Min Prin
4.64882e-01	4.63458e-01	7.81751e-03

WCS X:	1.56085e-06	1.00000e+00	-1.49712e-05
WCS Y:	-1.03659e-08	1.49712e-05	1.00000e+00
WCS Z:	1.00000e+00	-1.56085e-06	1.03892e-08

Appendix F: (Continued)

Constraint Set: ConstraintSet1

Load Set: LoadSet1

Resultant Load on Model:
in global X direction: -9.346590e-11
in global Y direction: -4.433882e-10
in global Z direction: 6.000000e+01

Measures:

Name	Value	Convergence
contact_area:	4.614214e-02	25.5%
contact_max_pres:	4.244370e+04	7.6%
max_beam_bending:	0.000000e+00	0.0%
max_beam_tensile:	0.000000e+00	0.0%
max_beam_torsion:	0.000000e+00	0.0%
max_beam_total:	0.000000e+00	0.0%
max_disp_mag:	7.590963e-02	0.7%
max_disp_x:	-2.286037e-03	0.6%
max_disp_y:	-6.997755e-03	0.6%
max_disp_z:	7.571832e-02	0.7%
max_prin_mag:	-4.610517e+04	2.6%
max_rot_mag:	0.000000e+00	0.0%
max_rot_x:	0.000000e+00	0.0%
max_rot_y:	0.000000e+00	0.0%
max_rot_z:	0.000000e+00	0.0%
max_stress_prin:	2.584570e+04	14.0%
max_stress_vm:	3.145544e+04	1.6%
max_stress_xx:	-2.418541e+04	2.4%
max_stress_xy:	1.009556e+04	11.7%

Appendix F: (Continued)

```
    max_stress_xz:      7.840168e+03      2.1%
    max_stress_yy:     -4.244165e+04      9.2%
    max_stress_yz:     -9.826774e+03     21.6%
    max_stress_zz:     -1.849277e+04      8.1%
    min_stress_prin:   -4.610517e+04      2.6%
    strain_energy:      2.117846e+00      0.7%
    cntRgn_009cntArea:  2.945243e-02     30.0%
    cntRgn_009maxPres:  3.565886e+04      1.6%
    cntRgn_010cntArea:  1.668971e-02     17.6%
    cntRgn_010maxPres:  4.244370e+04      7.6%

Analysis "ih_bfp_ten_x" Completed  (17:00:00)

------------------------------------------------------------
Memory and Disk Usage:

  Machine Type: Windows NT/x86
  RAM Allocation for Solver (megabytes): 128.0

  Total Elapsed Time (seconds): 835.28
  Total CPU Time     (seconds): 586.77
  Maximum Memory Usage (kilobytes): 239078
  Working Directory Disk Usage (kilobytes): 498690

  Results Directory Size (kilobytes):
  10475 .\ih_bfp_ten_x

  Maximum Data Base Working File Sizes (kilobytes):
  1024 .\ih_bfp_ten_x.tmp\gapel1.bas
  305152 .\ih_bfp_ten_x.tmp\kblk1.bas
  169984 .\ih_bfp_ten_x.tmp\kel1.bas
  2048 .\ih_bfp_ten_x.tmp\l1da1.bas
```

Appendix F: (Continued)

```
   1024 .\ih_bfp_ten_x.tmp\l2sq1.bas
   19456 .\ih_bfp_ten_x.tmp\oel1.bas

------------------------------------------------------------
Run Completed
Tue Jan 16, 2007    17:00:01
```

Appendix G: Inner Hub and Pin Analysis – 20 Degrees Camber

This is the "run status" out-put file for the Pro-Mechanica analysis of the Inner Hub and Pin analysis. A camber of 20 degrees was used, 10 times the static load was applied, and the convergence was set to 10%.

Mechanica Structure Version K-01-41:spg
Summary for Design Study "tewnty_deg_camber_ten_x_static"
Thu Jan 25, 2007 17:35:15

Run Settings
Memory allocation for block solver: 128.0
Checking the model before creating elements...
These checks take into account the fact that AutoGEM will
automatically create elements in volumes with material
properties, on surfaces with shell properties, and on curves
with beam section properties.

Generate elements automatically.
Checking the model after creating elements...

No errors were found in the model.

Mechanica Structure Model Summary

Principal System of Units: Inch Pound Second (IPS)

Length: in
Force: lbf
Time: sec
Temperature: F

Model Type: Three Dimensional

Appendix G: (Continued)

Points: 227
Edges: 971
Faces: 1266

Springs: 0
Masses: 0
Beams: 0
Shells: 0
Solids: 522

Elements: 522

Contact Regions: 2

Standard Design Study

Description:
hub with planks, 390 lb transverse load, fixed pin, 2 con
tact areas, x- constraints on square slot, z-constrain
t on hole

Static Analysis "tewnty_deg_camber_ten_x_static":
Contact Analysis

Convergence Method: Multiple-Pass Adaptive
Plotting Grid: 4

Convergence Loop Log: (17:35:19)

Appendix G: (Continued)

```
 >> Pass  1 <<
      Calculating Element Equations          (17:35:19)
        Total Number of Equations:     612
        Maximum Edge Order:              1
      Solving Equations                     (17:35:19)
      Load Increment 0 of 1
      Load Factor:  0.00000e+00
      Contact Area:  0.00000e+00
      Calculating Disp and Stress Results     (17:35:20)
      Load Increment 1 of 1
      Load Factor:  1.00000e+00
     *Contact Area:  1.79502e-02

** Warning: Contact area is small in comparison to size
        of adjacent element edges for one or more
        contact regions for all load factors above
        marked with a "*". If you need pressure results
        near the contact regions, use single-pass
        adaptive convergence and select Localized
        Mesh Refinement.
      Calculating Disp and Stress Results     (17:35:22)

      Post-Processing Solution              (17:35:23)
      Checking Convergence                  (17:35:23)
        Elements Not Converged:       522
        Edges Not Converged:          971
        Local Disp/Energy Index:    100.0%
        Global RMS Stress Index:    100.0%
      Resource Check                        (17:35:23)
        Elapsed Time     (sec):       9.61
        CPU Time         (sec):       7.92
        Memory Usage      (kb):     185502
        Wrk Dir Dsk Usage (kb):       4098
```

Appendix G: (Continued)

```
  >> Pass  2 <<
       Calculating Element Equations          (17:35:24)
         Total Number of Equations:    3369
         Maximum Edge Order:             2
       Solving Equations                    (17:35:24)
       Load Increment 0 of 1
       Load Factor:  0.00000e+00
       Contact Area:  0.00000e+00
       Calculating Disp and Stress Results     (17:35:25)
       Load Increment 1 of 1
       Load Factor:  1.00000e+00
      *Contact Area:  4.57656e-02

** Warning: Contact area is small in comparison to size
          of adjacent element edges for one or more
          contact regions for all load factors above
          marked with a "*". If you need pressure results
          near the contact regions, use single-pass
          adaptive convergence and select Localized
          Mesh Refinement.
       Calculating Disp and Stress Results     (17:35:30)

       Post-Processing Solution               (17:35:31)
       Checking Convergence                   (17:35:31)
         Elements Not Converged:       371
         Edges Not Converged:          220
         Local Disp/Energy Index:    100.0%
         Global RMS Stress Index:     90.6%
       Resource Check                         (17:35:31)
         Elapsed Time     (sec):      17.10
         CPU Time         (sec):      15.28
         Memory Usage      (kb):     186590
         Wrk Dir Dsk Usage (kb):       4098
```

Appendix G: (Continued)

```
  >> Pass  3 <<
       Calculating Element Equations          (17:35:31)
         Total Number of Equations:    9872
         Maximum Edge Order:             4
       Solving Equations                      (17:35:32)
       Load Increment 0 of 1
       Load Factor:  0.00000e+00
       Contact Area:  0.00000e+00
       Calculating Disp and Stress Results     (17:35:34)
       Load Increment 1 of 1
       Load Factor:  1.00000e+00
      *Contact Area:  9.78108e-02

** Warning: Contact area is small in comparison to size
          of adjacent element edges for one or more
          contact regions for all load factors above
          marked with a "*". If you need pressure results
          near the contact regions, use single-pass
          adaptive convergence and select Localized
          Mesh Refinement.
       Calculating Disp and Stress Results     (17:35:47)

       Post-Processing Solution               (17:35:48)
       Checking Convergence                    (17:35:48)
         Elements Not Converged:       259
         Edges Not Converged:           27
         Local Disp/Energy Index:    100.0%
         Global RMS Stress Index:     49.6%
       Resource Check                         (17:35:48)
         Elapsed Time     (sec):      33.93
         CPU Time         (sec):     31.58
         Memory Usage      (kb):     195698
         Wrk Dir Dsk Usage (kb):      10242
```

Appendix G: (Continued)

```
  >> Pass  4 <<
       Calculating Element Equations          (17:35:48)
         Total Number of Equations:   19765
         Maximum Edge Order:            4
       Solving Equations                    (17:35:49)
       Load Increment 0 of 1
       Load Factor:  0.00000e+00
       Contact Area:  0.00000e+00
       Calculating Disp and Stress Results     (17:35:56)
       Load Increment 1 of 1
       Load Factor:  1.00000e+00
      *Contact Area:  1.47220e-01

** Warning: Contact area is small in comparison to size
          of adjacent element edges for one or more
          contact regions for all load factors above
          marked with a "*". If you need pressure results
          near the contact regions, use single-pass
          adaptive convergence and select Localized
          Mesh Refinement.
       Calculating Disp and Stress Results     (17:36:27)

       Post-Processing Solution               (17:36:30)
       Checking Convergence                   (17:36:30)
         Elements Not Converged:       116
         Edges Not Converged:            0
         Local Disp/Energy Index:     40.1%
         Global RMS Stress Index:     28.0%
       Resource Check                         (17:36:30)
         Elapsed Time     (sec):      76.14
         CPU Time         (sec):      71.61
         Memory Usage      (kb):     197534
         Wrk Dir Dsk Usage (kb):      23554
```

Appendix G: (Continued)

```
  >> Pass  5 <<
       Calculating Element Equations          (17:36:30)
         Total Number of Equations:   34664
         Maximum Edge Order:           5
       Solving Equations                      (17:36:35)
       Load Increment 0 of 1
       Load Factor:  0.00000e+00
       Contact Area:  0.00000e+00
       Calculating Disp and Stress Results    (17:36:52)
       Load Increment 1 of 1
       Load Factor:  1.00000e+00
      *Contact Area:  1.77811e-01

** Warning: Contact area is small in comparison to size
          of adjacent element edges for one or more
          contact regions for all load factors above
          marked with a "*". If you need pressure results
          near the contact regions, use single-pass
          adaptive convergence and select Localized
          Mesh Refinement.
       Calculating Disp and Stress Results    (17:37:50)

       Post-Processing Solution               (17:37:52)
       Checking Convergence                   (17:37:52)
         Elements Not Converged:       24
         Edges Not Converged:           0
         Local Disp/Energy Index:     25.3%
         Global RMS Stress Index:     17.4%
       Resource Check                         (17:37:52)
         Elapsed Time     (sec):     158.51
         CPU Time         (sec):     150.88
         Memory Usage      (kb):     202371
         Wrk Dir Dsk Usage (kb):      55298
```

Appendix G: (Continued)

```
  >> Pass  6 <<
       Calculating Element Equations          (17:37:52)
         Total Number of Equations:   54364
         Maximum Edge Order:            6
       Solving Equations                    (17:38:05)
       Load Increment 0 of 1
       Load Factor:  0.00000e+00
       Contact Area:  0.00000e+00
       Calculating Disp and Stress Results     (17:39:07)
       Load Increment 1 of 1
       Load Factor:  1.00000e+00
      *Contact Area:  1.91521e-01

** Warning: Contact area is small in comparison to size
          of adjacent element edges for one or more
          contact regions for all load factors above
          marked with a "*". If you need pressure results
          near the contact regions, use single-pass
          adaptive convergence and select Localized
          Mesh Refinement.
       Calculating Disp and Stress Results     (17:42:51)

       Post-Processing Solution               (17:42:54)
       Checking Convergence                   (17:42:54)
         Elements Not Converged:         1
         Edges Not Converged:            0
         Local Disp/Energy Index:     11.7%
         Global RMS Stress Index:     11.5%
       Resource Check                         (17:42:55)
         Elapsed Time     (sec):     461.30
         CPU Time         (sec):     344.20
         Memory Usage      (kb):     226872
         Wrk Dir Dsk Usage (kb):     299010
```

Appendix G: (Continued)

```
  >> Pass  7 <<
       Calculating Element Equations          (17:42:55)
         Total Number of Equations:   76902
         Maximum Edge Order:            7
       Solving Equations                    (17:43:25)
       Load Increment 0 of 1
       Load Factor:  0.00000e+00
       Contact Area:  0.00000e+00
       Calculating Disp and Stress Results     (17:45:22)
       Load Increment 1 of 1
       Load Factor:  1.00000e+00
      *Contact Area:  1.96470e-01

** Warning: Contact area is small in comparison to size
          of adjacent element edges for one or more
          contact regions for all load factors above
          marked with a "*". If you need pressure results
          near the contact regions, use single-pass
          adaptive convergence and select Localized
          Mesh Refinement.
       Calculating Disp and Stress Results     (17:52:59)

       Post-Processing Solution              (17:53:26)
       Checking Convergence                  (17:53:26)
         Elements Not Converged:        0
         Edges Not Converged:           0
         Local Disp/Energy Index:      7.5%
         Global RMS Stress Index:      8.5%
```

Appendix G: (Continued)

RMS Stress Error Estimates:

Load Set	Stress Error	% of Max Prin Str
LoadSet1	2.71e+03	0.9% of 2.89e+05

Resource Check (17:53:36)

Elapsed Time	(sec):	1102.00
CPU Time	(sec):	667.33
Memory Usage	(kb):	236762
Wrk Dir Dsk Usage	(kb):	518146

The analysis converged to within 10% on
edge displacement, element strain energy,
and global RMS stress.

Total Mass of Model: 1.023144e-02

Total Cost of Model: 0.000000e+00

Mass Moments of Inertia about WCS Origin:

Ixx: 4.63460e-01
Ixy: -3.08734e-08 Iyy: 7.85380e-03
Ixz: -1.48154e-09 Iyz: -2.04349e-09 Izz: 4.64919e-01

Principal MMOI and Principal Axes Relative to WCS Origin:

Max Prin	Mid Prin	Min Prin
4.64919e-01	4.63460e-01	7.85380e-03

WCS X:	-1.01513e-06	1.00000e+00	6.77633e-08
WCS Y:	-4.47083e-09	-6.77633e-08	1.00000e+00
WCS Z:	1.00000e+00	1.01513e-06	4.47090e-09

Appendix G: (Continued)

Center of Mass Location Relative to WCS Origin:
(5.94376e-02, 1.12540e-02, 7.60935e-07)

Mass Moments of Inertia about the Center of Mass:
Ixx: 4.63458e-01
Ixy: 6.81303e-06 Iyy: 7.81765e-03
Ixz: -1.01879e-09 Iyz: -1.95588e-09 Izz: 4.64882e-01

Principal MMOI and Principal Axes Relative to COM:

Max Prin	Mid Prin	Min Prin
4.64882e-01	4.63458e-01	7.81765e-03

WCS X:	-7.15809e-07	1.00000e+00	-1.49526e-05
WCS Y:	-4.28989e-09	1.49526e-05	1.00000e+00
WCS Z:	1.00000e+00	7.15809e-07	4.27919e-09

Constraint Set: ConstraintSet1

Load Set: LoadSet1

Resultant Load on Model:
in global X direction: 3.176963e-09
in global Y direction: 1.278931e-09
in global Z direction: 3.900000e+02

Measures:

Name	Value	Convergence
contact_area:	1.964696e-01	2.5%
contact_max_pres:	2.652123e+05	5.4%
max_beam_bending:	0.000000e+00	0.0%
max_beam_tensile:	0.000000e+00	0.0%

Appendix G: (Continued)

```
max_beam_torsion:   0.000000e+00      0.0%
max_beam_total:     0.000000e+00      0.0%
max_disp_mag:       4.428371e-01      0.7%
max_disp_x:        -1.710132e-02      0.6%
max_disp_y:        -4.132111e-02      0.7%
max_disp_z:         4.414927e-01      0.7%
max_prin_mag:      -2.889458e+05      6.3%
max_rot_mag:        0.000000e+00      0.0%
max_rot_x:          0.000000e+00      0.0%
max_rot_y:          0.000000e+00      0.0%
max_rot_z:          0.000000e+00      0.0%
max_stress_prin:    1.566489e+05     16.3%
max_stress_vm:      2.126187e+05      6.5%
max_stress_xx:     -1.237603e+05      8.8%
max_stress_xy:     -7.144047e+04      5.5%
max_stress_xz:      6.076288e+04      9.4%
max_stress_yy:     -2.652244e+05      5.5%
max_stress_yz:     -6.601131e+04     10.8%
max_stress_zz:     -1.080627e+05      8.2%
min_stress_prin:   -2.889458e+05      6.3%
strain_energy:      8.490668e+01      0.7%
cntRgn_007cntArea:  1.168257e-01      2.3%
cntRgn_007maxPres:  1.928679e+05      6.2%
cntRgn_008cntArea:  7.964386e-02      2.9%
cntRgn_008maxPres:  2.652123e+05      5.4%

Analysis "tewnty_deg_camber_ten_x_static" Completed  (17:53:36)
------------------------------------------------------------
Memory and Disk Usage:
  Machine Type: Windows NT/x86
  RAM Allocation for Solver (megabytes): 128.0

  Total Elapsed Time (seconds): 1102.37
```

Appendix G: (Continued)

```
  Total CPU Time     (seconds): 667.69
  Maximum Memory Usage (kilobytes): 236762
  Working Directory Disk Usage (kilobytes): 518146

  Results Directory Size (kilobytes):
  11238 .\tewnty_deg_camber_ten_x_static

  Maximum Data Base Working File Sizes (kilobytes):
  1024 .\tewnty_deg_camber_ten_x_static.tmp\gapel1.bas
  315392 .\tewnty_deg_camber_ten_x_static.tmp\kblk1.bas
  178176 .\tewnty_deg_camber_ten_x_static.tmp\kel1.bas
  2048 .\tewnty_deg_camber_ten_x_static.tmp\l1da1.bas
  1024 .\tewnty_deg_camber_ten_x_static.tmp\l2sq1.bas
  20480 .\tewnty_deg_camber_ten_x_static.tmp\oel1.bas
------------------------------------------------------------
Run Completed
Thu Jan 25, 2007   17:53:36
```

Appendix H: Inner Hub and Pin Analysis – 6 Degrees Camber

This is the "run status" out-put file for the Pro-Mechanica analysis of the Inner Hub and Pin analysis. A camber of 6 degrees was used, 10 times the static load was applied, and the convergence was set to 10%.

Mechanica Structure Version K-01-41:spg
Summary for Design Study "six_deg_camber_ten_x_static"
Mon Jan 29, 2007 10:01:26

Run Settings
Memory allocation for block solver: 128.0
Checking the model before creating elements...
These checks take into account the fact that AutoGEM will
automatically create elements in volumes with material
properties, on surfaces with shell properties, and on curves
with beam section properties.

Generate elements automatically.
Checking the model after creating elements...

No errors were found in the model.

Mechanica Structure Model Summary

Principal System of Units: Inch Pound Second (IPS)

Length: in
Force: lbf
Time: sec
Temperature: F

Model Type: Three Dimensional

Appendix H: (Continued)

Points: 227
Edges: 971
Faces: 1266

Springs: 0
Masses: 0
Beams: 0
Shells: 0
Solids: 522

Elements: 522

Contact Regions: 2

Standard Design Study

Description:
hub with planks, 120 lb transverse load, fixed pin, 2 con
tact areas, x- constraints on square slot, z-constrain
t on hole

Static Analysis "six_deg_camber_ten_x_static":
Contact Analysis

Convergence Method: Multiple-Pass Adaptive
Plotting Grid: 4

Convergence Loop Log: (10:01:28)

Appendix H: (Continued)

```
  >> Pass  1 <<
       Calculating Element Equations          (10:01:28)
         Total Number of Equations:     612
         Maximum Edge Order:             1
       Solving Equations                    (10:01:29)
       Load Increment 0 of 1
       Load Factor:  0.00000e+00
       Contact Area:  0.00000e+00
       Calculating Disp and Stress Results     (10:01:29)
       Load Increment 1 of 1
       Load Factor:  1.00000e+00
      *Contact Area:  1.79502e-02

** Warning: Contact area is small in comparison to size
          of adjacent element edges for one or more
          contact regions for all load factors above
          marked with a "*". If you need pressure results
          near the contact regions, use single-pass
          adaptive convergence and select Localized
          Mesh Refinement.
       Calculating Disp and Stress Results     (10:01:32)

       Post-Processing Solution              (10:01:33)
       Checking Convergence                  (10:01:33)
         Elements Not Converged:       522
         Edges Not Converged:          971
         Local Disp/Energy Index:    100.0%
         Global RMS Stress Index:    100.0%
       Resource Check                        (10:01:33)
         Elapsed Time     (sec):      10.09
         CPU Time         (sec):      5.91
         Memory Usage      (kb):     185566
         Wrk Dir Dsk Usage (kb):       4098
```

Appendix H: (Continued)

```
 >> Pass  2 <<
      Calculating Element Equations          (10:01:33)
        Total Number of Equations:    3369
        Maximum Edge Order:              2
      Solving Equations                      (10:01:33)
      Load Increment 0 of 1
      Load Factor:  0.00000e+00
      Contact Area:  0.00000e+00
      Calculating Disp and Stress Results     (10:01:34)
      Load Increment 1 of 1
      Load Factor:  1.00000e+00
     *Contact Area:  4.57656e-02

** Warning: Contact area is small in comparison to size
        of adjacent element edges for one or more
        contact regions for all load factors above
        marked with a "*". If you need pressure results
        near the contact regions, use single-pass
        adaptive convergence and select Localized
        Mesh Refinement.
      Calculating Disp and Stress Results     (10:01:39)

      Post-Processing Solution               (10:01:40)
      Checking Convergence                    (10:01:40)
        Elements Not Converged:       371
        Edges Not Converged:          220
        Local Disp/Energy Index:    100.0%
        Global RMS Stress Index:     90.6%
      Resource Check                          (10:01:40)
        Elapsed Time     (sec):      17.25
        CPU Time         (sec):     12.84
        Memory Usage      (kb):     187070
        Wrk Dir Dsk Usage (kb):       4098
```

Appendix H: (Continued)

```
 >> Pass  3 <<
      Calculating Element Equations          (10:01:40)
        Total Number of Equations:    9872
        Maximum Edge Order:             4
      Solving Equations                      (10:01:40)
      Load Increment 0 of 1
      Load Factor:  0.00000e+00
      Contact Area:  0.00000e+00
      Calculating Disp and Stress Results     (10:01:43)
      Load Increment 1 of 1
      Load Factor:  1.00000e+00
     *Contact Area:  9.78108e-02

** Warning: Contact area is small in comparison to size
        of adjacent element edges for one or more
        contact regions for all load factors above
        marked with a "*". If you need pressure results
        near the contact regions, use single-pass
        adaptive convergence and select Localized
        Mesh Refinement.
      Calculating Disp and Stress Results     (10:01:55)

      Post-Processing Solution               (10:01:56)
      Checking Convergence                    (10:01:56)
        Elements Not Converged:       259
        Edges Not Converged:           27
        Local Disp/Energy Index:    100.0%
        Global RMS Stress Index:     49.6%
      Resource Check                          (10:01:56)
        Elapsed Time     (sec):      33.68
        CPU Time         (sec):     28.35
        Memory Usage      (kb):     188766
        Wrk Dir Dsk Usage (kb):      10242
```

Appendix H: (Continued)

```
  >> Pass  4 <<
       Calculating Element Equations          (10:01:56)
         Total Number of Equations:   19765
         Maximum Edge Order:            4
       Solving Equations                    (10:01:57)
       Load Increment 0 of 1
       Load Factor:  0.00000e+00
       Contact Area:  0.00000e+00
       Calculating Disp and Stress Results     (10:02:04)
       Load Increment 1 of 1
       Load Factor:  1.00000e+00
      *Contact Area:  1.47220e-01

** Warning: Contact area is small in comparison to size
          of adjacent element edges for one or more
          contact regions for all load factors above
          marked with a "*". If you need pressure results
          near the contact regions, use single-pass
          adaptive convergence and select Localized
          Mesh Refinement.
       Calculating Disp and Stress Results     (10:02:36)

       Post-Processing Solution               (10:02:37)
       Checking Convergence                   (10:02:37)
         Elements Not Converged:       116
         Edges Not Converged:            0
         Local Disp/Energy Index:     40.1%
         Global RMS Stress Index:     28.0%
       Resource Check                         (10:02:38)
         Elapsed Time     (sec):      75.07
         CPU Time         (sec):      66.47
         Memory Usage      (kb):     197694
         Wrk Dir Dsk Usage (kb):      23554
```

Appendix H: (Continued)

```
  >> Pass  5 <<
       Calculating Element Equations          (10:02:38)
         Total Number of Equations:   34664
         Maximum Edge Order:           5
       Solving Equations                      (10:02:52)
       Load Increment 0 of 1
       Load Factor:  0.00000e+00
       Contact Area:  0.00000e+00
       Calculating Disp and Stress Results    (10:03:10)
       Load Increment 1 of 1
       Load Factor:  1.00000e+00
      *Contact Area:  1.77811e-01

** Warning: Contact area is small in comparison to size
          of adjacent element edges for one or more
          contact regions for all load factors above
          marked with a "*". If you need pressure results
          near the contact regions, use single-pass
          adaptive convergence and select Localized
          Mesh Refinement.
       Calculating Disp and Stress Results    (10:04:08)

       Post-Processing Solution               (10:04:09)
       Checking Convergence                   (10:04:09)
         Elements Not Converged:       24
         Edges Not Converged:           0
         Local Disp/Energy Index:     25.3%
         Global RMS Stress Index:     17.4%
       Resource Check                         (10:04:10)
         Elapsed Time     (sec):     167.28
         CPU Time         (sec):     144.70
         Memory Usage      (kb):     202754
         Wrk Dir Dsk Usage (kb):      55298
```

Appendix H: (Continued)

```
  >> Pass  6 <<
       Calculating Element Equations          (10:04:10)
         Total Number of Equations:   54364
         Maximum Edge Order:            6
       Solving Equations                    (10:04:24)
       Load Increment 0 of 1
       Load Factor:  0.00000e+00
       Contact Area:  0.00000e+00
       Calculating Disp and Stress Results     (10:05:12)
       Load Increment 1 of 1
       Load Factor:  1.00000e+00
      *Contact Area:  1.91521e-01

** Warning: Contact area is small in comparison to size
          of adjacent element edges for one or more
          contact regions for all load factors above
          marked with a "*". If you need pressure results
          near the contact regions, use single-pass
          adaptive convergence and select Localized
          Mesh Refinement.
       Calculating Disp and Stress Results     (10:07:57)

       Post-Processing Solution               (10:07:59)
       Checking Convergence                   (10:07:59)
         Elements Not Converged:         1
         Edges Not Converged:            0
         Local Disp/Energy Index:     11.7%
         Global RMS Stress Index:     11.5%
       Resource Check                       (10:08:00)
         Elapsed Time     (sec):     397.82
         CPU Time         (sec):     323.83
         Memory Usage      (kb):     227832
         Wrk Dir Dsk Usage (kb):     299010
```

Appendix H: (Continued)

```
  >> Pass  7 <<
       Calculating Element Equations          (10:08:01)
         Total Number of Equations:   76902
         Maximum Edge Order:            7
       Solving Equations                    (10:08:45)
       Load Increment 0 of 1
       Load Factor:  0.00000e+00
       Contact Area:  0.00000e+00
       Calculating Disp and Stress Results     (10:10:26)
       Load Increment 1 of 1
       Load Factor:  1.00000e+00
      *Contact Area:  1.96470e-01

** Warning: Contact area is small in comparison to size
          of adjacent element edges for one or more
          contact regions for all load factors above
          marked with a "*". If you need pressure results
          near the contact regions, use single-pass
          adaptive convergence and select Localized
          Mesh Refinement.
       Calculating Disp and Stress Results     (10:15:37)

       Post-Processing Solution              (10:16:00)
       Checking Convergence                  (10:16:00)
         Elements Not Converged:        0
         Edges Not Converged:           0
         Local Disp/Energy Index:      7.5%
         Global RMS Stress Index:      8.5%
```

Appendix H: (Continued)

RMS Stress Error Estimates:

Load Set	Stress Error	% of Max Prin Str
LoadSet1	8.33e+02	0.9% of 8.89e+04

Resource Check (10:16:09)
Elapsed Time (sec): 886.63
CPU Time (sec): 626.45
Memory Usage (kb): 239510
Wrk Dir Dsk Usage (kb): 518146

The analysis converged to within 10% on
edge displacement, element strain energy,
and global RMS stress.

Total Mass of Model: 1.023144e-02

Total Cost of Model: 0.000000e+00

Mass Moments of Inertia about WCS Origin:

Ixx: 4.63460e-01
Ixy: -3.08734e-08 Iyy: 7.85380e-03
Ixz: -1.48154e-09 Iyz: -2.04349e-09 Izz: 4.64919e-01

Principal MMOI and Principal Axes Relative to WCS Origin:

Max Prin	Mid Prin	Min Prin
4.64919e-01	4.63460e-01	7.85380e-03

WCS X:	-1.01513e-06	1.00000e+00	6.77633e-08
WCS Y:	-4.47083e-09	-6.77633e-08	1.00000e+00
WCS Z:	1.00000e+00	1.01513e-06	4.47090e-09

Appendix H: (Continued)

Center of Mass Location Relative to WCS Origin:
(5.94376e-02, 1.12540e-02, 7.60935e-07)

Mass Moments of Inertia about the Center of Mass:
Ixx: 4.63458e-01
Ixy: 6.81303e-06 Iyy: 7.81765e-03
Ixz: -1.01879e-09 Iyz: -1.95588e-09 Izz: 4.64882e-01

Principal MMOI and Principal Axes Relative to COM:

Max Prin	Mid Prin	Min Prin
4.64882e-01	4.63458e-01	7.81765e-03

WCS X:	-7.15809e-07	1.00000e+00	-1.49526e-05
WCS Y:	-4.28989e-09	1.49526e-05	1.00000e+00
WCS Z:	1.00000e+00	7.15809e-07	4.27919e-09

Constraint Set: ConstraintSet1

Load Set: LoadSet1

Resultant Load on Model:
in global X direction: 1.059246e-09
in global Y direction: -9.444218e-12
in global Z direction: 1.200000e+02

Measures:

Name	Value	Convergence
contact_area:	1.964696e-01	2.5%
contact_max_pres:	8.160378e+04	5.4%
max_beam_bending:	0.000000e+00	0.0%
max_beam_tensile:	0.000000e+00	0.0%

Appendix H: (Continued)

max_beam_torsion:	0.000000e+00	0.0%
max_beam_total:	0.000000e+00	0.0%
max_disp_mag:	1.362576e-01	0.7%
max_disp_x:	-5.261943e-03	0.6%
max_disp_y:	-1.271419e-02	0.7%
max_disp_z:	1.358439e-01	0.7%
max_prin_mag:	-8.890640e+04	6.3%
max_rot_mag:	0.000000e+00	0.0%
max_rot_x:	0.000000e+00	0.0%
max_rot_y:	0.000000e+00	0.0%
max_rot_z:	0.000000e+00	0.0%
max_stress_prin:	4.819966e+04	16.3%
max_stress_vm:	6.542112e+04	6.5%
max_stress_xx:	-3.808010e+04	8.8%
max_stress_xy:	-2.198168e+04	5.5%
max_stress_xz:	1.869627e+04	9.4%
max_stress_yy:	-8.160752e+04	5.5%
max_stress_yz:	-2.031117e+04	10.8%
max_stress_zz:	-3.325007e+04	8.2%
min_stress_prin:	-8.890640e+04	6.3%
strain_energy:	8.038502e+00	0.7%
cntRgn_007cntArea:	1.168257e-01	2.3%
cntRgn_007maxPres:	5.934398e+04	6.2%
cntRgn_008cntArea:	7.964386e-02	2.9%
cntRgn_008maxPres:	8.160378e+04	5.4%

Analysis "six_deg_camber_ten_x_static" Completed (10:16:09)

Memory and Disk Usage:

Machine Type: Windows NT/x86

RAM Allocation for Solver (megabytes): 128.0

Appendix H: (Continued)

Total Elapsed Time (seconds): 886.99
Total CPU Time (seconds): 626.78
Maximum Memory Usage (kilobytes): 239510
Working Directory Disk Usage (kilobytes): 518146

Results Directory Size (kilobytes):
10690 .\six_deg_camber_ten_x_static

Maximum Data Base Working File Sizes (kilobytes):
1024 .\six_deg_camber_ten_x_static.tmp\gapel1.bas
315392 .\six_deg_camber_ten_x_static.tmp\kblk1.bas
178176 .\six_deg_camber_ten_x_static.tmp\kel1.bas
2048 .\six_deg_camber_ten_x_static.tmp\l1da1.bas
1024 .\six_deg_camber_ten_x_static.tmp\l2sq1.bas
20480 .\six_deg_camber_ten_x_static.tmp\oel1.bas

Run Completed
Mon Jan 29, 2007 10:16:10

Appendix I: Inner Hub and Ball Bearing Analysis

This is the "run status" out-put file for the Pro-Mechanica analysis of the Inner Hub and Ball Bearing Vertical Symmetry analysis. A camber of 3 degrees was used, 10 times the static load was applied, and the convergence was set to 10%.

Mechanica Structure Version K-01-41:spg
Summary for Design Study "IH_and_BB_vert_sym"
Fri Mar 23, 2007 16:38:53

Run Settings
Memory allocation for block solver: 128.0
Checking the model before creating elements...
These checks take into account the fact that AutoGEM will automatically create elements in volumes with material properties, on surfaces with shell properties, and on curves with beam section properties.

Generate elements automatically.
Checking the model after creating elements...

No errors were found in the model.

Mechanica Structure Model Summary

Principal System of Units: Inch Pound Second (IPS)

Length: in
Force: lbf
Time: sec
Temperature: F

Appendix I: (Continued)

Model Type: Three Dimensional

Points: 187
Edges: 845
Faces: 1125

Springs: 0
Masses: 0
Beams: 0
Shells: 0
Solids: 468

Elements: 468

Standard Design Study

Description:
10 times static load
bottom of rubber slot fixed
vertical symmetry

Static Analysis "IH_and_BB_vert_sym":

Convergence Method: Multiple-Pass Adaptive
Plotting Grid: 4

Convergence Loop Log: (16:38:57)

>> Pass 1 <<
Calculating Element Equations (16:38:57)
Total Number of Equations: 521

Appendix I: (Continued)

Maximum Edge Order: 1
Solving Equations (16:38:57)
Post-Processing Solution (16:38:57)
Calculating Disp and Stress Results (16:38:57)
Checking Convergence (16:38:58)
Elements Not Converged: 468
Edges Not Converged: 845
Local Disp/Energy Index: 100.0%
Global RMS Stress Index: 100.0%
Resource Check (16:38:58)
Elapsed Time (sec): 6.51
CPU Time (sec): 5.47
Memory Usage (kb): 181350
Wrk Dir Dsk Usage (kb): 2048

>> Pass 2 <<
Calculating Element Equations (16:38:59)
Total Number of Equations: 2979
Maximum Edge Order: 2
Solving Equations (16:38:59)
Post-Processing Solution (16:38:59)
Calculating Disp and Stress Results (16:38:59)
Checking Convergence (16:39:00)
Elements Not Converged: 325
Edges Not Converged: 829
Local Disp/Energy Index: 100.0%
Global RMS Stress Index: 80.4%
Resource Check (16:39:00)
Elapsed Time (sec): 8.40
CPU Time (sec): 6.97
Memory Usage (kb): 182430
Wrk Dir Dsk Usage (kb): 2048

Appendix I: (Continued)

```
>> Pass  3 <<
    Calculating Element Equations          (16:39:00)
      Total Number of Equations:   10403
      Maximum Edge Order:           4
    Solving Equations                      (16:39:01)
    Post-Processing Solution               (16:39:02)
    Calculating Disp and Stress Results    (16:39:02)
    Checking Convergence                   (16:39:03)
      Elements Not Converged:      189
      Edges Not Converged:         713
      Local Disp/Energy Index:    84.1%
      Global RMS Stress Index:    40.0%
    Resource Check                         (16:39:03)
      Elapsed Time    (sec):     11.35
      CPU Time        (sec):     9.63
      Memory Usage    (kb):    182430
      Wrk Dir Dsk Usage (kb):    10240

>> Pass  4 <<
    Calculating Element Equations          (16:39:03)
      Total Number of Equations:   19211
      Maximum Edge Order:           5
    Solving Equations                      (16:39:05)
    Post-Processing Solution               (16:39:07)
    Calculating Disp and Stress Results    (16:39:08)
    Checking Convergence                   (16:39:09)
      Elements Not Converged:      41
      Edges Not Converged:         1
      Local Disp/Energy Index:    46.4%
      Global RMS Stress Index:    36.2%
    Resource Check                         (16:39:09)
      Elapsed Time    (sec):     17.43
      CPU Time        (sec):     14.72
```

Appendix I: (Continued)

Memory Usage (kb): 184240
Wrk Dir Dsk Usage (kb): 22528

>> Pass 5 <<
Calculating Element Equations (16:39:09)
Total Number of Equations: 30696
Maximum Edge Order: 5
Solving Equations (16:39:14)
Post-Processing Solution (16:39:18)
Calculating Disp and Stress Results (16:39:20)
Checking Convergence (16:39:21)
Elements Not Converged: 11
Edges Not Converged: 0
Local Disp/Energy Index: 27.5%
Global RMS Stress Index: 23.5%
Resource Check (16:39:21)
Elapsed Time (sec): 29.44
CPU Time (sec): 25.22
Memory Usage (kb): 192478
Wrk Dir Dsk Usage (kb): 46080

>> Pass 6 <<
Calculating Element Equations (16:39:21)
Total Number of Equations: 42823
Maximum Edge Order: 6
Solving Equations (16:39:30)
Post-Processing Solution (16:39:41)
Calculating Disp and Stress Results (16:39:44)
Checking Convergence (16:39:46)
Elements Not Converged: 6
Edges Not Converged: 0
Local Disp/Energy Index: 21.2%
Global RMS Stress Index: 21.0%

Appendix I: (Continued)

Resource Check (16:39:47)
Elapsed Time (sec): 55.01
CPU Time (sec): 45.98
Memory Usage (kb): 197127
Wrk Dir Dsk Usage (kb): 205824

>> Pass 7 <<
Calculating Element Equations (16:39:47)
Total Number of Equations: 53068
Maximum Edge Order: 7
Solving Equations (16:40:02)
Post-Processing Solution (16:40:22)
Calculating Disp and Stress Results (16:40:27)
Checking Convergence (16:40:29)
Elements Not Converged: 3
Edges Not Converged: 0
Local Disp/Energy Index: 17.1%
Global RMS Stress Index: 17.1%
Resource Check (16:40:31)
Elapsed Time (sec): 99.15
CPU Time (sec): 81.80
Memory Usage (kb): 201066
Wrk Dir Dsk Usage (kb): 301056

>> Pass 8 <<
Calculating Element Equations (16:40:31)
Total Number of Equations: 61904
Maximum Edge Order: 8
Solving Equations (16:41:09)
Post-Processing Solution (16:41:54)
Calculating Disp and Stress Results (16:42:08)
Checking Convergence (16:42:29)
Elements Not Converged: 1

Appendix I: (Continued)

```
      Edges Not Converged:          0
      Local Disp/Energy Index:    13.0%
      Global RMS Stress Index:    14.3%
    Resource Check                (16:42:30)
      Elapsed Time    (sec):    218.33
      CPU Time        (sec):    136.50
      Memory Usage    (kb):     219446
      Wrk Dir Dsk Usage (kb):   412672

 >> Pass  9 <<
    Calculating Element Equations        (16:42:30)
      Total Number of Equations:  69053
      Maximum Edge Order:          9
    Solving Equations                    (16:43:00)
    Post-Processing Solution             (16:43:58)
    Calculating Disp and Stress Results  (16:44:10)
    Checking Convergence                 (16:44:33)
      Elements Not Converged:       1
      Edges Not Converged:          0
      Local Disp/Energy Index:    10.4%
      Global RMS Stress Index:    12.3%

    RMS Stress Error Estimates:

    Load Set        Stress Error  % of Max Prin Str
    --------------  ------------  -----------------
    LoadSet1         1.83e+02      0.8% of  2.30e+04

** Warning: Convergence was not obtained because the maximum
      polynomial order of 9 was reached.

    Resource Check                (16:44:44)
      Elapsed Time    (sec):    352.38
```

Appendix I: (Continued)

CPU Time (sec): 218.69
Memory Usage (kb): 225768
Wrk Dir Dsk Usage (kb): 509952

The analysis did not converge to within 10% on
edge displacement, element strain energy,
and global RMS stress.

Total Mass of Model: 9.819899e-04

Total Cost of Model: 0.000000e+00

Mass Moments of Inertia about WCS Origin:

Ixx: 1.68629e-03
Ixy: 2.03344e-10 Iyy: 1.73531e-03
Ixz: 2.83163e-06 Iyz: -7.19532e-06 Izz: 3.08892e-03

Principal MMOI and Principal Axes Relative to WCS Origin:

Max Prin	Mid Prin	Min Prin
3.08897e-03	1.73527e-03	1.68629e-03

WCS X:	2.01870e-03	3.11410e-04	9.99998e-01
WCS Y:	-5.31539e-03	9.99986e-01	-3.00676e-04
WCS Z:	9.99984e-01	5.31477e-03	-2.02033e-03

Center of Mass Location Relative to WCS Origin:
(-2.30649e-02, 5.86321e-02, 3.10996e-01)

Appendix I: (Continued)

Mass Moments of Inertia about the Center of Mass:

Ixx: 1.58794e-03
Ixy: -1.32778e-06 Iyy: 1.63981e-03
Ixz: -4.21226e-06 Iyz: 1.07106e-05 Izz: 3.08503e-03

Principal MMOI and Principal Axes Relative to COM:

Max Prin	Mid Prin	Min Prin
3.08512e-03	1.63977e-03	1.58790e-03

WCS X:	-2.81996e-03	-2.50040e-02	9.99683e-01
WCS Y:	7.41299e-03	9.99659e-01	2.50243e-02
WCS Z:	9.99969e-01	-7.48121e-03	2.63364e-03

Constraint Set: ConstraintSet1

Load Set: LoadSet1

Resultant Load on Model:
in global X direction: -1.646741e-11
in global Y direction: 5.750003e+02
in global Z direction: -6.880718e-12

Measures:

Name	Value	Convergence
max_beam_bending:	0.000000e+00	0.0%
max_beam_tensile:	0.000000e+00	0.0%
max_beam_torsion:	0.000000e+00	0.0%
max_beam_total:	0.000000e+00	0.0%
max_disp_mag:	1.437177e-03	0.7%

Appendix I: (Continued)

max_disp_x:	-5.945448e-04	0.4%
max_disp_y:	1.345624e-03	0.8%
max_disp_z:	1.538635e-04	0.0%
max_prin_mag:	-2.295273e+04	6.7%
max_rot_mag:	0.000000e+00	0.0%
max_rot_x:	0.000000e+00	0.0%
max_rot_y:	0.000000e+00	0.0%
max_rot_z:	0.000000e+00	0.0%
max_stress_prin:	2.028103e+04	15.4%
max_stress_vm:	2.038053e+04	16.4%
max_stress_xx:	-9.037661e+03	7.7%
max_stress_xy:	-9.476953e+03	16.2%
max_stress_xz:	3.849938e+03	14.3%
max_stress_yy:	-1.616673e+04	9.1%
max_stress_yz:	7.891967e+03	8.7%
max_stress_zz:	-1.577741e+04	7.2%
min_stress_prin:	-2.295273e+04	6.7%
strain_energy:	2.873992e-01	0.7%

Analysis "IH_and_BB_vert_sym" Completed (16:44:45)

Memory and Disk Usage:

Machine Type: Windows NT/x86
RAM Allocation for Solver (megabytes): 128.0

Total Elapsed Time (seconds): 352.93
Total CPU Time (seconds): 218.97
Maximum Memory Usage (kilobytes): 225768
Working Directory Disk Usage (kilobytes): 509952

Appendix I: (Continued)

Results Directory Size (kilobytes):
12331 .\IH_and_BB_vert_sym

Maximum Data Base Working File Sizes (kilobytes):
300032 .\IH_and_BB_vert_sym.tmp\kblk1.bas
188416 .\IH_and_BB_vert_sym.tmp\kel1.bas
21504 .\IH_and_BB_vert_sym.tmp\oel1.bas

Run Completed
Fri Mar 23, 2007 16:44:45

Appendix J: Outer Hub and Spoke Analysis

This is the “run status” out-put file for the Pro-Mechanica analysis of the Outer Hub and Spoke analysis. A camber of 3 degrees was used, 5 times the static load was applied, and the convergence was set to 10%.

Mechanica Structure Version K-01-41:spg
Summary for Design Study "oh_five_x_static"
Mon Jan 15, 2007 17:15:32

Run Settings
Memory allocation for block solver: 128.0
Checking the model before creating elements...
These checks take into account the fact that AutoGEM will automatically create elements in volumes with material properties, on surfaces with shell properties, and on curves with beam section properties.

Generate elements automatically.
Checking the model after creating elements...

No errors were found in the model.

Mechanica Structure Model Summary

Principal System of Units: Inch Pound Second (IPS)

Length: in
Force: lbf
Time: sec
Temperature: F

Model Type: Three Dimensional

Appendix J: (Continued)

Points: 453
Edges: 1994
Faces: 2559

Springs: 0
Masses: 0
Beams: 0
Shells: 0
Solids: 1036

Elements: 1036

Standard Design Study

Description:
287 lbs on top spoke hole
bottom spoke hole fixed

Static Analysis "oh_five_x_static":

Convergence Method: Multiple-Pass Adaptive
Plotting Grid: 4

Convergence Loop Log: (17:15:41)

>> Pass 1 <<
Calculating Element Equations (17:15:41)
Total Number of Equations: 1300
Maximum Edge Order: 1
Solving Equations (17:15:41)
Post-Processing Solution (17:15:41)
Calculating Disp and Stress Results (17:15:41)

Appendix J: (Continued)

```
      Checking Convergence              (17:15:44)
        Elements Not Converged:      1036
        Edges Not Converged:         1994
        Local Disp/Energy Index:    100.0%
        Global RMS Stress Index:    100.0%
      Resource Check                    (17:15:44)
        Elapsed Time    (sec):      13.30
        CPU Time        (sec):      10.69
        Memory Usage    (kb):      195558
        Wrk Dir Dsk Usage (kb):      8192

  >> Pass  2 <<
      Calculating Element Equations     (17:15:45)
        Total Number of Equations:   7164
        Maximum Edge Order:             2
      Solving Equations                 (17:15:45)
      Post-Processing Solution          (17:15:45)
      Calculating Disp and Stress Results  (17:15:46)
      Checking Convergence              (17:15:49)
        Elements Not Converged:      937
        Edges Not Converged:         1858
        Local Disp/Energy Index:    100.0%
        Global RMS Stress Index:     93.4%
      Resource Check                    (17:15:49)
        Elapsed Time    (sec):      17.91
        CPU Time        (sec):      13.66
        Memory Usage    (kb):      195558
        Wrk Dir Dsk Usage (kb):      8192

  >> Pass  3 <<
      Calculating Element Equations     (17:15:49)
        Total Number of Equations:  26635
        Maximum Edge Order:             4
```

Appendix J: (Continued)

Solving Equations (17:15:50)
Post-Processing Solution (17:15:53)
Calculating Disp and Stress Results (17:15:54)
Checking Convergence (17:15:57)
Elements Not Converged: 442
Edges Not Converged: 1001
Local Disp/Energy Index: 100.0%
Global RMS Stress Index: 17.4%
Resource Check (17:15:57)
Elapsed Time (sec): 26.32
CPU Time (sec): 19.66
Memory Usage (kb): 197546
Wrk Dir Dsk Usage (kb): 26624

>> Pass 4 <<
Calculating Element Equations (17:15:58)
Total Number of Equations: 46833
Maximum Edge Order: 5
Solving Equations (17:16:03)
Post-Processing Solution (17:16:07)
Calculating Disp and Stress Results (17:16:10)
Checking Convergence (17:16:14)
Elements Not Converged: 6
Edges Not Converged: 0
Local Disp/Energy Index: 15.7%
Global RMS Stress Index: 7.3%
Resource Check (17:16:15)
Elapsed Time (sec): 43.63
CPU Time (sec): 31.41
Memory Usage (kb): 201314
Wrk Dir Dsk Usage (kb): 56320

Appendix J: (Continued)

```
>> Pass  5 <<
     Calculating Element Equations          (17:16:15)
       Total Number of Equations:   75896
       Maximum Edge Order:            6
     Solving Equations                    (17:16:25)
     Post-Processing Solution             (17:16:39)
     Calculating Disp and Stress Results  (17:16:44)
     Checking Convergence                 (17:16:48)
       Elements Not Converged:        0
       Edges Not Converged:           0
       Local Disp/Energy Index:     5.9%
       Global RMS Stress Index:     6.1%

     RMS Stress Error Estimates:

     Load Set         Stress Error  % of Max Prin Str
     ---------------  ------------  -----------------
     LoadSet1          2.12e+03      5.8% of  3.69e+04

     Resource Check                       (17:16:54)
       Elapsed Time     (sec):     82.37
       CPU Time         (sec):     62.50
       Memory Usage     (kb):    230358
       Wrk Dir Dsk Usage (kb):    283648

The analysis converged to within 10% on
edge displacement, element strain energy,
and global RMS stress.

Total Mass of Model:  8.107128e-04

Total Cost of Model:  0.000000e+00
```

Appendix J: (Continued)

Mass Moments of Inertia about WCS Origin:

Ixx: 2.59612e-03
Ixy: -1.28562e-08 Iyy: 2.59612e-03
Ixz: 1.54412e-09 Iyz: -1.78294e-09 Izz: 4.49841e-03

Principal MMOI and Principal Axes Relative to WCS Origin:

Max Prin	Mid Prin	Min Prin
4.49841e-03	2.59613e-03	2.59611e-03

WCS X:	8.11724e-07	8.09053e-01	5.87735e-01
WCS Y:	-9.37261e-07	-5.87735e-01	8.09053e-01
WCS Z:	1.00000e+00	-1.20759e-06	2.81216e-07

Center of Mass Location Relative to WCS Origin:
(-4.91346e-06, 3.44632e-06, 5.73958e-01)

Mass Moments of Inertia about the Center of Mass:

Ixx: 2.32905e-03
Ixy: -1.28562e-08 Iyy: 2.32904e-03
Ixz: -7.42185e-10 Iyz: -1.79315e-10 Izz: 4.49841e-03

Principal MMOI and Principal Axes Relative to COM:

Max Prin	Mid Prin	Min Prin
4.49841e-03	2.32906e-03	2.32903e-03

WCS X:	-3.42121e-07	8.09053e-01	5.87735e-01
WCS Y:	-8.26556e-08	-5.87735e-01	8.09053e-01
WCS Z:	1.00000e+00	2.28215e-07	2.67949e-07

Appendix J: (Continued)

Constraint Set: ConstraintSet1

Load Set: LoadSet1

Resultant Load on Model:
in global X direction: 3.711114e-10
in global Y direction: 2.870000e+02
in global Z direction: 7.662270e-11

Measures:

Name	Value	Convergence
max_beam_bending:	0.000000e+00	0.0%
max_beam_tensile:	0.000000e+00	0.0%
max_beam_torsion:	0.000000e+00	0.0%
max_beam_total:	0.000000e+00	0.0%
max_disp_mag:	2.280043e-02	0.3%
max_disp_x:	-1.085224e-02	0.3%
max_disp_y:	2.280042e-02	0.3%
max_disp_z:	-1.281594e-03	1.0%
max_prin_mag:	3.688925e+04	5.2%
max_rot_mag:	0.000000e+00	0.0%
max_rot_x:	0.000000e+00	0.0%
max_rot_y:	0.000000e+00	0.0%
max_rot_z:	0.000000e+00	0.0%
max_stress_prin:	3.688925e+04	5.2%
max_stress_vm:	3.723139e+04	0.3%
max_stress_xx:	3.561172e+04	5.6%
max_stress_xy:	1.198523e+04	3.4%
max_stress_xz:	-8.956634e+03	13.9%
max_stress_yy:	-2.155031e+04	2.9%
max_stress_yz:	-3.738425e+03	9.2%

Appendix J: (Continued)

```
    max_stress_zz:      1.253873e+04      5.3%
    min_stress_prin:   -2.176151e+04      2.4%
    strain_energy:      3.205368e+00      0.3%

Analysis "oh_five_x_static" Completed  (17:16:54)

------------------------------------------------------------

Memory and Disk Usage:

  Machine Type: Windows NT/x86
  RAM Allocation for Solver (megabytes): 128.0

  Total Elapsed Time (seconds): 82.95
  Total CPU Time     (seconds): 62.92
  Maximum Memory Usage (kilobytes): 230358
  Working Directory Disk Usage (kilobytes): 283648

  Results Directory Size (kilobytes):
  17814 .\oh_five_x_static

  Maximum Data Base Working File Sizes (kilobytes):
  169984 .\oh_five_x_static.tmp\kblk1.bas
  100352 .\oh_five_x_static.tmp\kel1.bas
  13312 .\oh_five_x_static.tmp\oel1.bas

------------------------------------------------------------
Run Completed
Mon Jan 15, 2007   17:16:54
```